

Republic of Iraq

Ministry of Higher Education and

Scientific Research

University of Misan/Collage of

Engineering

Department of Electrical Engineering



# Mathematical Modeling of High-Speed Solid Rotor Induction Motor Based On 3D Electromagnetic Field Analysis

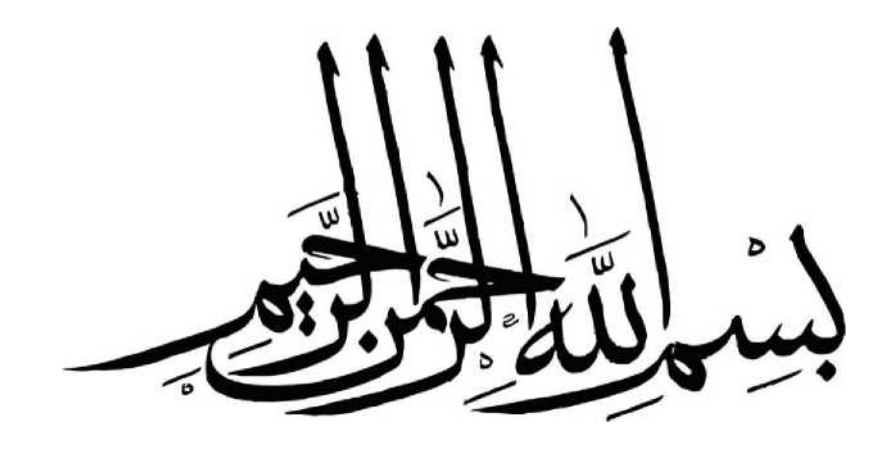
Ву

## Abdullah Maya Fazaa

**A THESIS** 

Submitted in Partial Fulfillment of the Requirements for the Degree of Master of Electrical Engineering

Supervisor Name: Asst.Prof.Dr. Ahmed Thamer Radhi



((وَقُلْ رَبِّ زِدْنِي كِلْمًا))

سورة طه: رقم الاية 114

# Statement of Authorship

This thesis was completed as part of the MSc. (Electrical Engineering) at the College of Engineering -University of Misan. This is my own unaided work. Where the work of others has been used or drawn on then has been fully attributed to the relevant source.

Signature

Name: Abdullah Maya Fazaa

Date:1/ 7 /2025

# Certification of the Examining Committee

We certify that we have read the thesis entitled "Mathematical Modeling of High-Speed Solid Rotor Induction Motor Based On 3D Electromagnetic Field Analysis" which is being submitted by Abdullah Maya Fazaa and as the Examining Committee, examined the student in its content. In our opinion, the thesis is adequate for the award of the degree of Master of Science in Electrical Engineering.

Signature:	المستسملل
------------	-----------

Name: Asst.Prof.Dr. Ahmed Thamer

Radhi

(Supervisor)

Date:5/ 10 /2025

Signature:

Name: Assist Prof. Dr.Osama Yaseen

Khudair

(Member) 5/10/2025

Signature:

Name: Assist Prof. Dr. Mohammed Kh.

AL-NUSSAIRI

(Member)

Date 5 / 10 /2025

Signature:

Name: Prof. Dr. Adel Manaa Dakhil

(Chairman)

Date 5 / 10 /2025

Signature:

Name: Prof. Dr. Abbas Oda Dawood

Dean of the College of Engineering

Date o / 10 /2025

# Supervisor Certification

I certify that this thesis which is entitled "Mathematical Modeling of High-Speed Solid Rotor Induction Motor Based on 3D Electromagnetic Field Analysis" which is being submitted by "Abdullah Maya Fazaa" was prepared under my supervision at College of Engineering, University of Misan, as a partial fulfilment of the requirements for the degree of Master of Science in Electrical Engineering.

Signature:

Supervisor: Asst.Prof.Dr. Ahmed Thamer Radhi

Date: 3/ 9 / 2025

I forward this thesis for debate by exam committee

Signature:

Name: Assist Prof. Dr. Mohammed Kh. AL-NUSSAIRI

Head of Electrical Engineering Department

Date: 10/2015

#### Dedication

To my beloved family, your unwavering support and unconditional love have been the driving force behind my educational journey.

This graduation is not only a celebration of my accomplishments but a testament to your sacrifices and belief in me. From late-night study sessions to comforting words during moments of doubt, you have been my rock.

I am forever grateful for the opportunities you have given me and the unwavering encouragement that has propelled me forward.

This achievement is as much yours as it is mine.

With heartfelt appreciation, I dedicate my graduation to you, my family, for being the wind beneath my wings.

# Acknowledgment

I extend my sincere gratitude to my supervisor, Asst.Prof.Dr. Ahmed Thamer Radhi for his invaluable guidance throughout this research.

Special thanks to the Department of Electrical Engineering at the University of Misan and the Ministry of Higher Education and Scientific Research for their support. I am grateful to my family for their endless encouragement and patience during my academic journey.

#### **ABSTRACT**

This thesis presents a comprehensive study on the mathematical modeling of high-speed solid rotor induction motors, with the application of three-dimensional (3D) electromagnetic field analysis. High-speed induction motors are increasingly utilized in various industrial applications due to their superior power density and efficiency. However, the accurate prediction of their performance under different operating conditions remains a significant challenge due to the complex interactions between electromagnetic fields and rotor dynamics at high speeds.

The research begins by developing a detailed mathematical model that captures a simplified 3D electromagnetic field within the motor. Then extracting the rotor impedance. The study then extends to the direct-quadrature model (dq-model), where the derived equations are used to simplify the dynamic behavior of the motor.

Furthermore, the thesis demonstrates the application of the developed model in MATLAB Simulink, enabling the simulation and analysis of the motor under various operating conditions.

Lastly, the modelling of harmonics circuit is simulated in MATLAB by using inverter contraction to generate 5 level ac waveform from dc source and notifying its effect.

The results provide valuable insights into the design optimization of high-speed induction motors, contributing to enhanced performance and reliability.

# **List of Contents**

Dedication		vi
Acknowledgme	ent	vii
ABSTRACT		viii
List of Figures		xi
List of Tables		xiv
List of Abbrevia	ations	xv
List of Symbols		xvi
Chapter One		1
Introduction		1
1.1.	Overview of High-Speed Induction Motors (HS-IMs)	1
1.2. Solid Rot	tor Induction Motors (SRIMs)	3
1.3. Aim of St	tudy	5
1.4. Thesis O	Organization	6
Chapter Two		8
Literature Reviev	W	8
2.1. Introduct	tion	8
2.2. Topologie	es Of SRIM	8
2.2.1. Overvie	ew of solid rotor Induction Motor topologies	8
2.2.2. Smooth	h solid-rotor IM	10
2.2.3. Axially s	slitted solid-rotor IM	11
2.2.4. Copper	r coated solid-rotor IM	13
2.2.5 Solid-rot	otor Induction Motor with radial rotor surface grooves	14
2.2.6 Squirrel	cage solid rotor IM	14
2.3.Designs &	k modeling studies	16
2.3. Mechanic	cal Limitations	28
2.3.1. Rotor D	Diameter	28
2.3.2. Rotor Le	ength	28
2.3.3. Air Gap	D	29

	2.3.4. Winding Factors	30
	2.4. Applications of Solid-Rotor IM	30
С	hapter Three	32
	3.1. Introduction	32
	3.2. Analytical Methods	33
	3.2.1 Saturation and Hysteresis	34
	3.2.2 Electromagnetic Fields in Solid Rotor	35
	3.2.3 Rotor Impedance	43
	3.2.4 End Effect	48
	3.3. DQ Model and Simulation	51
	3.3.1. DQ Model	51
	3.3.2. Detailed Explanation	57
	3.3.2.1 Stator and Rotor Voltage Equations	57
	3.3.2.2 Stator Voltage Equations	58
	3.3.2.3 Rotor Voltage Equations	59
	3.4. Summary of Modelling Equations and MATLAB Simulation	60
	3.5. Time Harmonic Analysis and Simulation	68
	3.5.1. Effect of Harmonics	68
	3.5.2. Inverter Feeding the Motor	70
	3.5.3. Fourier Steady-State Analysis	72
	3.5.4. Harmonic Circuits Simulation	74
C	hapter Four	80
R	esults	80
	4.1. Results for Fundamental with Sinusoidal Input	80
	4.2. Results for Harmonics Non-Sinusoidal Input	88
C	hapter Five	92
C	onclusion and Recommendations	92
	References	95
_	uhlisation	110

# List of Figures

Fig. 2.1. Conventional compressor (a) Integrated compressor (direct drive) (s	<u>)).</u>
	21
Fig. 2.2. High-speed high-power IM for an integrated compressor. Cut view of	of a
squirrel-cage rotor (a) and detail of a high-speed solid rotor	22
Fig.2.3. Construction of a smooth SRIM	22
Fig.2.4. axially slitted solid-rotor	23
Fig.2.5. output torque vs the number of rotor slits	23
Fig. 2.6. ASSR with axial slits skewed in tangential and axial	
<u>directions</u>	23
Fig.2.7. Construction of an axially slitted solid-rotor for an IM: I	24
Fig. 2.8. Per unit output torque as a function of the number of rotor slits,	24
Fig. 2.9. Construction of axially slitted solid-rotor with radial grooves for an IN	<u> </u>
	24
Fig.3.1 coordinate system for analyzing	34
Figure 3.2 the consistent layers of solid ferromagnetic rotor covered with a	
copper	35
Fig.3.3. Equivalent Circuit Per Phase.	51
Fig.3.4. the three reference frames.	55
Fig. 3.5. Simulation of $\lambda d$ and $\lambda q$ equations (3.97a $-$ 3.97b)	60
Fig. 3.6. simulation of $\lambda f$ and $\lambda g$ equations (3.97c – 3.97d).	61
Fig.3.7. simulation of Eqs. (3.98) did/dt.	61
Fig.3.8. Simulation of Eqs. (3.99) diq/dt.	62
Fig.3.9. Simulation of Eqs. (3.100) dif/dt.	62
Fig.3.10. Simulation of Eqs. (3.101) dig/dt.	63
Fig.3.11. Simulation of eqations (3.103-3.104) torque and rotor speed	64

Fig.3.12. Simulation of eqations (3.105-3.106) slip and electromagnetic pov	ver.
	64
Fig.3.13. Input voltage convertions of SRIM part	65
Fig.3.14. Output current conversions part.	66
Fig.3.15. Simulation of SRIM motor block.	67
Fig. 3.16. simulation of overall operation parts of HS- SRIM	67
Fig.3.17. Source voltage waveform.	72
Fig.3.18. Inverter construction to get voltage source.	74
Fig.3.19. The inverter source voltage waveform	
Fig.3.20. Three phase inverter source formation.	
Fig.3.21. Inverter output 3-phase voltage waveform.	76
Fig.3.22. simulation of fundamental harmonic circuit.	
Fig.3.23. Clark-Park transformation stages	77
Fig.3.24. Dirction of rotation of 5 <sup>th</sup> and 7 <sup>th</sup>	78
Fig.3.25. Simulation of resultant (5 <sup>th</sup> and 7 <sup>th</sup> harmonics) circuits with the	
<u>fundamental one.</u>	79
Fig.3.26. simulation of 5th (upper one) with 7th (lower one) combination	
<u>circuits</u>	79
Fig.4.1. Torque and power at no load.	81
Fig.4.2. At NO Load (without end factor).	81
Fig.4.3. At full load (without end factor).	82
Fig 4.4. At full load (without end factor).	82
Fig.4.5. At no load (with end factor).	83
Fig.4.6. At No load (with end factor).	83
Fig.4.7. At full load (with end factor).	84
Fig.4.8. At full load (with end factor).	84
Fig.4.9. At no load (with copper coating).	85
Fig.4.10. At No load (with copper coating).	
Fig.4.11. At full load (with copper coating).	86
Fig.4.12. At full load ( with copper coating ).	86

Fig.4.13. FFT of the steady state of the 1 <sup>st</sup> harmonic.	. 88
Fig.4.14. Current of 1st harmonic.	. 88
Fig.4.15.Torque of 1st harmonic.	. 89
Fig.4.16. FFT of the steady state of the 1 <sup>st</sup> with 5 <sup>th</sup> and 7 <sup>th</sup> harmonic	. 89
Fig.4.17. current of 1 <sup>st</sup> with 5 <sup>th</sup> and 7 <sup>th</sup> harmonic	. 90
Fig.4.18. Torque of 1 <sup>st</sup> with 5 <sup>th</sup> and 7 <sup>th</sup> harmonic.	. 90

# List of Tables

List of Contentsvii
List of Figuresix
List of Tablesxi
List of Abbreviationsxii
List of Sympolesxiii
Table.2.1. Power and speed requirements of selected applications,
Table.2.2. An overview of possible and suitable materials for solid rotors, along with their characteristic properties
Table .2.3. An overview of possible and suitable copper alloys for explosive coating of solid rotor surfaces and their characteristic properties. The percentage value of electrical conductivity is related to the maximum conductivity value of pure copper, respectively 58 MSm <sup>-1</sup>
Table.4.1. speed , slip and Torque ripple at no load no end factor conditions
Table.4.2. torque and efficiency at full load with end factor conditions
Table.4.3. torque and efficiencyat full load with end factor and copper coating conditions
Table.4.4. THD comparison (fundamental vs addition of 5th and 7th harmonics)91
Table 4.1 Motor Parameters 100

# List of Abbreviations

Abbreviation	Full Term
3D	Three-Dimensional
2D	Two-Dimensional
ASSR	Axially Slitted Solid Rotor
dq-model	Direct-Quadrature model
EMF	Electromotive Force
FEA	Finite Element Analysis
FESSs	Flywheel Energy Storage Systems
FFT	Fast Fourier Transform
HS-IMs	High-Speed Induction Motors
HS-SRIMs	High-speed solid-rotor induction machines
IM	Induction Machine
SRIMs	Solid Rotor Induction Motors
RNM	Reluctant Networks Method
SCSRs	Squirrel Cage Solid Rotors
SRIMs	Solid Rotor Induction Motors
THD	Total harmonic distortion

# List of Symbols

a, b, c	Phases in a three-phase system.
α, β	Orthogonal stationary reference frame components.
$a_R$	Neyman's constant coefficient of resistance
$a_{x}$	Neyman's constant coefficient of reactance
α	complex propagation constant
a <sub>1h</sub>	linecurrent density of the stator
A: <sub>m</sub>	complex amplitudes of the line-current density
В	Magnetic flux density.
С	Constat related to stress factor
c	Constant for material properties.
$C_1, C_2, C_3, C_4$	complex constants
Cu	copper
d, q	Direct and quadrature axis components in the rotating
	reference frame.
d1	Thickness of iron layer
d2	Thickness of copper layer
Dr	Rotor outer diameter.
Е	Electric field strength.
f	Fundamental frequency.
fh	Harmonic frequency.
Fe	iron
g	Air gap (mechanical clearance)
Н	Magnetic field strength.
h	Harmonic sequence number.
hslit	Slit depth on the rotor.
I <sub>1</sub>	Stator current
I	Current.
if	Field winding current.
Js	Surface current density.
k	General correction factor or The ratio of the nominal angular
	velocity to the nth critical frequency

kh       Attenuation coefficient of electromag netic field for the harmonic,         Ksafe       Safety factor.         kt       transformation coefficient         kw       winding factor         Ld       Directaxis synchronous inductance.         Lq       Quadratureaxis synchronous inductance.         Lm       Magnetizing inductance.         Lm       Magnetizing inductance.         Lm       Rotor length.         Nr       Rotor length.         Nr       Rotor speed.         Ns       Synchronous speed.         n       Exponent in magnetic material equations.         n       intrinsic impedance         p       Number of pole pairs         P       Power.         P Isoad       Load power.         Pf       Power factor.         p       Resistivity.         Rr       Rotor resistance.         Rs       Stator resistance.         Rs       Stator resistance.         s       Slip.         sh       Slip of harmonic wave.         ST       Stress factor         T       Torque.         t       Time.         Te       Electromagnetic torque.      <	Ke	Endregion correction factor.
Ksafe       Safety factor.         kt       transformation coefficient         kw       winding factor         Ld       Directaxis synchronous inductance.         Lq       Quadratureaxis synchronous inductance.         Lm       Magnetizing inductance.         Lg2       Saliency related inductance.         Ir       Rotor length.         Nr       Rotor speed.         Ns       Synchronous speed.         n       Exponent in magnetic material equations.         η       intrinsic impedance         p       Number of pole pairs         P       Power.         P Power       Power.         P Power factor.       Resistivity.         Rr       Rotor resistance.         Rs       Stator resistance.         Rs       Stator resistance.         R Radius of the rotor.       Stip.         Sh       Slip of harmonic wave.         ST       Stress factor         T       Torque.         t       Time.         Te       Electromagnetic torque.         To       Pole pitch.         V       Voltage.         v       relevant material's Poisson's coefficient	kh	Attenuation coefficient of electromag netic field for the h
kt       transformation coefficient         kw       winding factor         Ld       Directaxis synchronous inductance.         Lq       Quadratureaxis synchronous inductance.         Lm       Magnetizing inductance.         Lg2       Saliency related inductance.         lr       Rotor length.         Nr       Rotor speed.         Ns       Synchronous speed.         n       Exponent in magnetic material equations.         η       intrinsic impedance         p       Number of pole pairs         P       Power.         P power.       Power factor.         ρ       Resistivity.         Rr       Rotor resistance.         Rs       Stator resistance.         r       Radius of the rotor.         S       cylinder's cross-section         s       Slip         sh       Slip of harmonic wave.         ST       Stress factor         T       Torque.         t       Time.         Te       Electromagnetic torque.         T       Pole pitch.         V       Voltage.         v       relevant material's Poisson's coefficient         V1		harmonic,
kw         winding factor           Ld         Directaxis synchronous inductance.           Lq         Quadratureaxis synchronous inductance.           Lm         Magnetizing inductance.           Lg2         Saliency related inductance.           lr         Rotor length.           Nr         Rotor speed.           Ns         Synchronous speed.           n         Exponent in magnetic material equations.           η         intrinsic impedance           p         Number of pole pairs           P         Power.           P Power.         Power.           Pr         Power factor.           ρ         Resistivity.           Rr         Rotor resistance.           Rs         Stator resistance.           r         Radius of the rotor.           S         cylinder's cross-section           s         Slip.           sh         Slip of harmonic wave.           ST         Stress factor           T         Torque.           t         Time.           Te         Electromagnetic torque.           τ         Pole pitch.           V         Voltage.           v	Ksafe	Safety factor.
Ld       Directaxis synchronous inductance.         Lq       Quadratureaxis synchronous inductance.         Lm       Magnetizing inductance.         Lg2       Saliency related inductance.         lr       Rotor length.         Nr       Rotor speed.         Ns       Synchronous speed.         n       Exponent in magnetic material equations.         η       intrinsic impedance         p       Number of pole pairs         P       Power.         P Power.       Power.         Pr       Power factor.         p       Resistivity.         Rr       Rotor resistance.         Rs       Stator resistance.         r       Radius of the rotor.         S       cylinder's cross-section         s       Slip.         sh       Slip of harmonic wave.         ST       Stress factor         T       Torque.         t       Time.         Te       Electromagnetic torque.         τ       Pole pitch.         V       Voltage.         v       relevant material's Poisson's coefficient         V1       Fundamental component of voltage.         Van <td>k<sub>t</sub></td> <td>transformation coefficient</td>	k <sub>t</sub>	transformation coefficient
Lq       Quadratureaxis synchronous inductance.         Lm       Magnetizing inductance.         Lg2       Saliency related inductance.         Ir       Rotor length.         Nr       Rotor speed.         Ns       Synchronous speed.         n       Exponent in magnetic material equations.         η       intrinsic impedance         p       Number of pole pairs         P       Power.         P Power.       Power.         Pf       Power factor.         p       Resistivity.         Rr       Rotor resistance.         Rs       Stator resistance.         r       Radius of the rotor.         S       cylinder's cross-section         s       Slip.         sh       Slip of harmonic wave.         ST       Stress factor         T       Torque.         t       Time.         Te       Electromagnetic torque.         T       Pole pitch.         V       Voltage.         v       relevant material's Poisson's coefficient         V1       Fundamental component of voltage.         Va, vb, vc       Stator terminal voltages (phases a, b, and c). <td>k<sub>w</sub></td> <td>winding factor</td>	k <sub>w</sub>	winding factor
Lm       Magnetizing inductance.         Lg2       Saliency related inductance.         lr       Rotor length.         Nr       Rotor speed.         Ns       Synchronous speed.         n       Exponent in magnetic material equations.         η       intrinsic impedance         p       Number of pole pairs         P       Power.         P       Power.         P       Power.         P       Power factor.         ρ       Resistivity.         Rr       Rotor resistance.         R       Ratios of the rotor.         S       Stator resistance.         r       Radius of the rotor.         S       cylinder's cross-section         s       Slip.         sh       Slip of harmonic wave.         ST       Stress factor         T       Torque.         t       Time.         Te       Electromagnetic torque.         τ       Pole pitch.         V       Voltage.         v       relevant material's Poisson's coefficient         V1       Fundamental component of voltage.         Va       Voltage of the nth harmonic.	Ld	Directaxis synchronous inductance.
Lg2       Saliency related inductance.         Ir       Rotor length.         Nr       Rotor speed.         Ns       Synchronous speed.         n       Exponent in magnetic material equations.         η       intrinsic impedance         p       Number of pole pairs         P       Power.         P       Power.         Pf       Power factor.         ρ       Resistivity.         Rr       Rotor resistance.         r       Radius of the rotor.         S       cylinder's cross-section         s       Slip.         sh       Slip of harmonic wave.         ST       Stress factor         T       Torque.         t       Time.         Te       Electromagnetic torque.         τ       Pole pitch.         V       Voltage.         v       relevant material's Poisson's coefficient         Vn       Voltage of the nth harmonic.         va, vb, vc       Stator terminal voltages (phases a, b, and c).	Lq	Quadratureaxis synchronous inductance.
Ir Rotor length.  Nr Rotor speed.  Ns Synchronous speed.  n Exponent in magnetic material equations.  η intrinsic impedance  p Number of pole pairs  P Power.  P load Load power.  Pf Power factor.  ρ Resistivity.  Rr Rotor resistance.  Rs Stator resistance.  r Radius of the rotor.  S cylinder's cross-section  s Slip.  sh Slip of harmonic wave.  ST Torque.  t Time.  Te Electromagnetic torque.  τ Pole pitch.  V Voltage.  v relevant material's Poisson's coefficient  V1 Fundamental component of voltage.  Va, Vb, Vc Stator terminal voltages (phases a, b, and c).	Lm	Magnetizing inductance.
Nr       Rotor speed.         Ns       Synchronous speed.         n       Exponent in magnetic material equations.         η       intrinsic impedance         p       Number of pole pairs         P       Power.         P load       Load power.         Pf       Power factor.         ρ       Resistivity.         Rr       Rotor resistance.         r       Radius of the rotor.         S       cylinder's cross-section         s       Slip.         sh       Slip of harmonic wave.         ST       Stress factor         T       Torque.         t       Time.         Te       Electromagnetic torque.         τ       Pole pitch.         V       Voltage.         v       relevant material's Poisson's coefficient         V1       Fundamental component of voltage.         Vn       Voltage of the nth harmonic.         va, vb, vc       Stator terminal voltages (phases a, b, and c).	Lg2	Saliency related inductance.
Ns Synchronous speed.  n Exponent in magnetic material equations.  η intrinsic impedance  p Number of pole pairs  P Power.  P load Load power.  Pf Power factor.  ρ Resistivity.  Rr Rotor resistance.  Rs Stator resistance.  r Radius of the rotor.  S cylinder's cross-section  s Slip.  sh Slip of harmonic wave.  ST Stress factor  T Torque.  t Time.  Te Electromagnetic torque.  τ Pole pitch.  V Voltage.  v relevant material's Poisson's coefficient  Vu Voltage of the nth harmonic.  va, vb, vc Stator terminal voltages (phases a, b, and c).	lr	Rotor length.
n Exponent in magnetic material equations.  η intrinsic impedance  p Number of pole pairs  P Power.  Pload Load power.  Pf Power factor.  ρ Resistivity.  Rr Rotor resistance.  Rs Stator resistance.  r Radius of the rotor.  S cylinder's cross-section  s Slip.  sh Slip of harmonic wave.  ST Stress factor  T Torque.  t Time.  Te Electromagnetic torque.  τ Pole pitch.  V Voltage.  v relevant material's Poisson's coefficient  V1 Fundamental component of voltage.  Va, vb, vc Stator terminal voltages (phases a, b, and c).	Nr	Rotor speed.
η       intrinsic impedance         p       Number of pole pairs         P       Power.         P load       Load power.         Pf       Power factor.         ρ       Resistivity.         Rr       Rotor resistance.         Rs       Stator resistance.         r       Radius of the rotor.         S       cylinder's cross-section         s       Slip.         sh       Slip of harmonic wave.         ST       Stress factor         T       Torque.         t       Time.         Te       Electromagnetic torque.         τ       Pole pitch.         V       Voltage.         v       relevant material's Poisson's coefficient         V1       Fundamental component of voltage.         Vn       Voltage of the nth harmonic.         va, vb, vc       Stator terminal voltages (phases a, b, and c).	Ns	Synchronous speed.
p       Number of pole pairs         P       Power.         P load       Load power.         Pf       Power factor.         ρ       Resistivity.         Rr       Rotor resistance.         Rs       Stator resistance.         r       Radius of the rotor.         S       cylinder's cross-section         s       Slip.         sh       Slip of harmonic wave.         ST       Stress factor         T       Torque.         t       Time.         Te       Electromagnetic torque.         T       Pole pitch.         V       Voltage.         v       relevant material's Poisson's coefficient         V1       Fundamental component of voltage.         Vn       Voltage of the nth harmonic.         va, vb, vc       Stator terminal voltages (phases a, b, and c).	n	Exponent in magnetic material equations.
P Power.  Pload Load power.  Pf Power factor.  ρ Resistivity.  Rr Rotor resistance.  Rs Stator resistance.  r Radius of the rotor.  S cylinder's cross-section  s Slip.  Sh Slip of harmonic wave.  ST Stress factor  T Torque.  t Time.  Te Electromagnetic torque.  τ Pole pitch.  V Voltage.  v relevant material's Poisson's coefficient  Vu Voltage of the nth harmonic.  va, vb, vc Stator terminal voltages (phases a, b, and c).	η	intrinsic impedance
Pf       Power factor.         ρ       Resistivity.         Rr       Rotor resistance.         Rs       Stator resistance.         r       Radius of the rotor.         S       cylinder's cross-section         s       Slip.         sh       Slip of harmonic wave.         ST       Stress factor         T       Torque.         t       Time.         Te       Electromagnetic torque.         τ       Pole pitch.         V       Voltage.         v       relevant material's Poisson's coefficient         V1       Fundamental component of voltage.         Vn       Voltage of the nth harmonic.         Va, vb, vc       Stator terminal voltages (phases a, b, and c).	р	Number of pole pairs
Pf Power factor.  ρ Resistivity.  Rr Rotor resistance.  Rs Stator resistance.  r Radius of the rotor.  S cylinder's cross-section  s Slip.  sh Slip of harmonic wave.  ST Stress factor  T Torque.  t Time.  Te Electromagnetic torque.  τ Pole pitch.  V Voltage.  v relevant material's Poisson's coefficient  V1 Fundamental component of voltage.  Va, vb, vc Stator terminal voltages (phases a, b, and c).	P	Power.
ρResistivity.RrRotor resistance.RsStator resistance.rRadius of the rotor.Scylinder's cross-sectionsSlip.shSlip of harmonic wave.STStress factorTTorque.tTime.TeElectromagnetic torque.τPole pitch.VVoltage.vrelevant material's Poisson's coefficientV1Fundamental component of voltage.VnVoltage of the nth harmonic.Va, Vb, VcStator terminal voltages (phases a, b, and c).	P load	Load power.
Rr Rotor resistance.  Rs Stator resistance.  r Radius of the rotor.  S cylinder's cross-section  S Slip.  Sh Slip of harmonic wave.  ST Stress factor  T Torque.  t Time.  Te Electromagnetic torque.  T Pole pitch.  V Voltage.  v relevant material's Poisson's coefficient  V1 Fundamental component of voltage.  Va, Vb, Vc Stator terminal voltages (phases a, b, and c).	Pf	Power factor.
Rs Stator resistance.  r Radius of the rotor. S cylinder's cross-section S Slip. Sh Slip of harmonic wave.  ST Stress factor T Torque. t Time. Te Electromagnetic torque.  T Pole pitch. V Voltage. v relevant material's Poisson's coefficient V1 Fundamental component of voltage. Va, vb, vc Stator terminal voltages (phases a, b, and c).	ρ	Resistivity.
r Radius of the rotor.  S cylinder's cross-section  S Slip.  Sh Slip of harmonic wave.  ST Torque.  T Torque.  t Time.  Te Electromagnetic torque.  T Pole pitch.  V Voltage.  v relevant material's Poisson's coefficient  V1 Fundamental component of voltage.  Va, vb, vc Stator terminal voltages (phases a, b, and c).	Rr	Rotor resistance.
S cylinder's cross-section  Slip. Sh Slip of harmonic wave.  ST Stress factor  T Torque.  t Time.  Te Electromagnetic torque.  V Voltage.  v relevant material's Poisson's coefficient  V1 Fundamental component of voltage.  Va, Vb, Vc Stator terminal voltages (phases a, b, and c).	Rs	Stator resistance.
Slip.  Sh Slip of harmonic wave.  ST Stress factor  Torque.  t Time.  Te Electromagnetic torque.  T Pole pitch.  V Voltage.  v relevant material's Poisson's coefficient  V1 Fundamental component of voltage.  Vn Voltage of the nth harmonic.  Va, Vb, Vc Stator terminal voltages (phases a, b, and c).	r	Radius of the rotor.
Sh Slip of harmonic wave.  ST Stress factor  T Torque.  t Time.  Te Electromagnetic torque.  Voltage.  v relevant material's Poisson's coefficient  V1 Fundamental component of voltage.  Va, vb, vc Stator terminal voltages (phases a, b, and c).	S	cylinder's cross-section
ST Stress factor  T Torque.  t Time.  Te Electromagnetic torque.  T Pole pitch.  V Voltage.  v relevant material's Poisson's coefficient  V1 Fundamental component of voltage.  Vn Voltage of the nth harmonic.  va, vb, vc Stator terminal voltages (phases a, b, and c).	S	Slip.
T Torque.  t Time.  Te Electromagnetic torque.  τ Pole pitch.  V Voltage.  v relevant material's Poisson's coefficient  V1 Fundamental component of voltage.  Vn Voltage of the nth harmonic.  va, vb, vc Stator terminal voltages (phases a, b, and c).	Sh	Slip of harmonic wave.
t Time.  Te Electromagnetic torque.  T Pole pitch.  V Voltage.  v relevant material's Poisson's coefficient  V1 Fundamental component of voltage.  Vn Voltage of the nth harmonic.  Va, vb, vc Stator terminal voltages (phases a, b, and c).	ST	Stress factor
Te Electromagnetic torque.  τ Pole pitch.  V Voltage.  v relevant material's Poisson's coefficient  V1 Fundamental component of voltage.  Vn Voltage of the nth harmonic.  Va, vb, vc Stator terminal voltages (phases a, b, and c).	T	Torque.
<ul> <li>τ Pole pitch.</li> <li>V Voltage.</li> <li>v relevant material's Poisson's coefficient</li> <li>V1 Fundamental component of voltage.</li> <li>Vn Voltage of the nth harmonic.</li> <li>Va, vb, vc Stator terminal voltages (phases a, b, and c).</li> </ul>	t	Time.
V     Voltage.       v     relevant material's Poisson's coefficient       V1     Fundamental component of voltage.       Vn     Voltage of the nth harmonic.       va, vb, vc     Stator terminal voltages (phases a, b, and c).	Te	Electromagnetic torque.
v relevant material's Poisson's coefficient  V1 Fundamental component of voltage.  Vn Voltage of the nth harmonic.  Va, vb, vc Stator terminal voltages (phases a, b, and c).	τ	Pole pitch.
V1 Fundamental component of voltage.  Vn Voltage of the nth harmonic.  va, vb, vc Stator terminal voltages (phases a, b, and c).	V	Voltage.
Vn Voltage of the nth harmonic.  Va, Vb, Vc Stator terminal voltages (phases a, b, and c).	V	relevant material's Poisson's coefficient
Va, Vb, Vc Stator terminal voltages (phases a, b, and c).	V <sub>1</sub>	Fundamental component of voltage.
	Vn	Voltage of the nth harmonic.
vd Voltage in the daxis.	Va, Vb, Vc	Stator terminal voltages (phases a, b, and c).
	vd	Voltage in the daxis.

vq	Voltage in the qaxis.
Vf	Field winding voltage.
Vh	Harmonic voltage amplitudes.
wd	Conduction period.
ω	Angular velocity.
ωs	Stator angular frequency.
x, y, z	Coordinate system axes.
Zr	Rotor impedance.
Z	Impedance.
Z <sub>c</sub>	rotor impedance constant value which is independent on the
	values of slip
Zs	Stator impedance.
$z_0$	characteristic impedance
σ	Conductivity.
λ	Flux linkage.
μ	Permeability of material.
μr	Relative permeability.
θ	Electrical angle.
$\theta$ 5, $\theta$ 7	Phase angles for 5th and 7th harmonics.
φ	Phase angle.
$\sigma_{\delta}$	leakage factor
∇	Nabla operator (gradient operator in vector calculus).
ð	Partial derivative.
ſ	Integral.
Σ	Summation.
±	Plus-minus operator.

### **Chapter One**

#### Introduction

High-speed solid rotor induction motors have grown to become an essential part in various industrial applications, especially in high-speed drives, aeronautics, and electric propulsion[1]. The demands for efficiency and power density of such systems require deep understanding of electromagnetic phenomena taking place within the motor [2]. The traditional 2D analysis methods usually cannot capture the complexity of the electromagnetic field in HS-SRIM at high frequencies and rotational speeds[3]. Developing direct-quadrature model (dq- model) of a three-dimensional electromagnetic mathematical model and analyzing the influences of harmonics on High-speed solid rotor induction motors (HS-SRIMs) are the focuses of this thesis.

### 1.1. Overview of High-Speed Induction Motors (HS-IMs)

Industries have adopted high-speed solid rotor induction motors for applications demanding rapid rotation, including sectors such as high-speed drive systems, aerospace, and electric propulsion technologies.

There has been a notable surge in the implementation of swift electrical machinery within industrial settings, as confirmed by a growing body of literature over recent years. For evaluating rotor robustness, a high-speed system often implies a velocity surpassing 3000 RPM [4].

One approach to achieving elevated rotational velocities is to pair a conventional electric motor with a gearbox [5]. Alternatively, a direct-drive high-speed electrical machine can be used, which allows for direct coupling of the motor to the load the impeller, for example thereby improving both reliability and efficiency across the whole system [6] compared with setups that utilize gearboxes.

Contrary to (synchronous permanent-magnet machines) [7] [8] which are generally favored for situations requiring both high speeds and low power, induction machines are often deployed in lower speed yet higher power scenarios [6]. Synchronous machines commonly provide advantages, including increased power density, a better power factor, and enhanced overall operating efficiency relative to equivalent IMs.

Employing a solid rotor without a squirrel cage empowers induction machines to withstand substantial mechanical forces at a lower manufacturing cost. Such designs also present specific benefits, like simplified control mechanisms and increased tolerance to elevated temperatures[9].

Finland has emerged as an important hub for innovation related to high-speed electric machines. For instance, research documented in [10] focused on studying ferromagnetic core materials in solid rotors with sleek surfaces. Lähteenmäki [11] investigated rotor designs and voltage sources that are appropriate for high-speed applications Machines. Saari [12] conducted research on thermal analysis of high-speed induction machines, whereas Kuosa [13] examined the air-gap friction in high-speed machines. Antila [14] and Lantto [15] conducted research on the utilization of active magnetic bearings in high-speed induction machines. Interestingly, these investigations all targeted devices running beyond 400 Hz.

Operating an electrical motor at high speeds offers key advantages, chief among them being a reduction in physical size and the ability to forgo mechanical couplings like gearboxes. If optimal materials are used, there is a nearly inverse relationship between the motor's power-to-weight and power-to-volume ratios [16], tightly linked to rotational velocity over the high-speed operational spectrum.

At speeds nearing 10,000 RPM, the motor's mass and dimensions may drop to as little as one-third of their size at 3000 rpm, depending on the cooling method. This holds true for open-frame designs; however, the benefit of size minimization is lost in cases where a fully enclosed motor construction is adopted.

#### 1.2. Solid Rotor Induction Motors (SRIMs)

For IMs, the solid rotor is a nonlaminated rotor kind that provides excellent resistance to temperature, centrifugal force, and environmental factors. Thus, solid rotors provide electrical machinery with exceptional durability and dependability. Probably the most distinctive feature of the HS-SRIM is the solid rotor configuration-in contrast to conventional induction motors that almost invariably use laminated rotors. Benefits include robustness of the mechanical construction[17], the possibility to operate at higher speeds than normally allowed by rotor centrifugal forces without a risk of rotor damage [18], and a more uniform distribution of magnetic flux in the rotor. On the other hand, a solid rotor shows peculiar criticalities, especially related to the electromagnetic phenomena that take place during operation[19]. In these applications, the relentless drive for more efficiency, higher power density, and better reliability has put an increased burden on understanding the nature of electromagnetic behavior within HS-SRIM. With the increase in operation speed of such motors, the complexity of the electromagnetic field in the motor increases, leading to skin effects, eddy currents, and saturation effects that can seriously affect performance.

A single, solid piece of ferromagnetic material serves as the rotor core for solid-rotor induction motors [20], The simplest type of solid rotor is a smooth steel cylinder. Since the solid rotor is usually quite large, numerous adjustments must be made. The existence of a solid core material that is always utilized to build the rotor's electric and magnetic circuits is a defining trait of rotors, also referred to as solid rotors. By carefully splitting the rotor's cross section, better flux penetration is made possible, which results in the first performance boost of a solid rotor [21].

Another improvement is accomplished by welding electrically conductive nonmagnetic short-circuit rings to the rotor's edge faces [22]. A proper squirrel cage must be installed on the rotor in order to achieve the maximum improvement for a solid rotor. During these enhancements, it is most efficient to weld all extra

parts to the rotor's solid core in order to guarantee its longevity. It is also possible to apply a highly conductive coating to smooth solid-steel rotors [23].

The smooth solid-rotor is the most straightforward option and hence the most convenient and cost-effective to produce. Additionally, it possesses superior mechanical and fluid dynamic characteristics, while exhibiting the least favorable electrical qualities. Manufacturing a smooth solid rotor is not easily achieved in practice.

The rotor can be made more powerful, with a little greater power factor and higher efficiency, by milling axial slits into it [24]. This method is also cost-effective as the machine expenses are moderate. Coating the rotor, end ring, and squirrel-cage structure increases the production requirements and expenses. However, these structures significantly enhance the motor's torque and characteristics [25].

The solid rotor induction motor construction gives many advantages ,such as Excellent mechanical strength[24], stiffness, and long-lasting performance[25]. The solid rotor is the most stable and has superior balance retention compared to other rotor types., Exceptional heat resistance. Easy to safeguard against corrosive substances., Exceptional dependability. The construction is uncomplicated, making it straightforward and cost-effective to produce. Highly scalable across a wide range of power and speed levels [26]. Minimal noise and vibrations at low levels (when the surface is smooth).

This study supposes the simplest solid rotor type, it is the smooth-steel rotor which is easy to manufacture with low-cost while providing the best mechanical and fluid-dynamical properties due to low air friction.

The fully three-dimensional nature of the field phenomena in a purely solid rotor makes the field solution is too difficult so many authors suggest modifying end effect factors for smooth solid rotors In two-dimensional calculations to tackle the problem like Trickey [27]. Russell [28], Yee [29], O'Kelly [30], and Woolley [31]. The main goal of this thesis is to develop a mathematical model of a high-

speed SRIM based on simplified 3D electromagnetic field analysis using dq-axis model to capture dynamic performance characteristics.

### 1.3. Aim of Study

The development of a mathematical model of High-Speed Solid Rotor Induction Motors (HS-SRIMs) based on 3D electromagnetic field analysis represents a significant step forward in the field of electric machine design and analysis. Traditional two-dimensional approaches are unable to capture the complexity of electromagnetic interactions in high-speed motors, whereas the 3D analysis ensures a more precise and comprehensive representation of the electromagnetic field [32]. Such insight is indispensable for optimizing HS-SRIMs to achieve highly efficient and robust machines capable of meeting the demanding requirements of aerospace, automotive, and energy-related applications.

This study also employs the dq- model which provides a simplified yet powerful mathematical representation of motor dynamics. While the 3D electromagnetic field analysis offers detailed spatial accuracy, the dq- model allows efficient analysis of transient and steady-state performance, rotor impedance behavior, and control strategies in the time domain. This complementary use of the dq- model improves understanding of motor operation, reduces computational effort in control-oriented studies, and facilitates the optimization of design parameters with respect to torque, losses, and efficiency.

Among the prime contributions of this study are improvements in motor performance, particularly by reducing losses in applications where both speed and efficiency are critical. The 3D electromagnetic field analysis enables accurate prediction of rotor impedance distribution and harmonic effects, while the dq-model provides valuable data for system-level studies and controller design. Together, they allow optimization to minimize eddy current losses, mitigate heat generation, and extend the operational life of motors.

Ultimately, the 3D model combined with the dq-framework provides a strong basis for future investigations into electric machine design. This includes assessing the influence of rotor geometry, material properties, and advanced cooling techniques on motor performance. The versatility of these models makes them indispensable tools for engineers and researchers striving to push the boundaries of electric machine design, not only for HS-SRIMs but also for other machine types such as synchronous and permanent magnet motors.

### 1.4. Thesis Organization

Chapter Two provides a thorough literature review of previous work and developments related to solid rotor induction motors. It outlines the historical context and applications of SRIMs in modern industries such as flywheel energy storage systems, compressors, high speed spindles and turbo molecular pumps. This chapter also discusses various rotor topologies—such as smooth, axially slitted, and squirrel-cage designs—and evaluates materials suitable for rotor construction. Mechanical limitations including rotor diameter, air gap, and winding factors are explored, along with the challenges posed by edge effects and high-speed operation.

Chapter Three explains the materials and methods used in the study. It begins by analyzing the electromagnetic field distribution in solid rotors and the complexity added by their nonlinear magnetic properties and three-dimensional structure. Various analytical approaches are discussed, including linear, nonlinear, and multi-layer methods. The chapter then derives the electromagnetic field equations and rotor impedance, ultimately leading to the development of an equivalent circuit. A mathematical model in the d-q reference frame is formulated, and simulation methods are introduced to evaluate the dynamic behavior of the motor.

Chapter Four presents the results obtained from simulations and analytical modeling. Time harmonic analysis is used to examine the effects of different harmonic orders on motor performance. The chapter also investigates the behavior of the motor when supplied by a multi-level inverter and performs Fourier

analysis to assess the harmonic content of voltage and current waveforms. These results offer insights into the electromagnetic response, torque generation, and losses under various operating conditions.

Chapter Five concludes the thesis by summarizing the key findings and contributions of the study. It highlights the effectiveness of the proposed 3D analytical modeling approach and its potential for accurately predicting rotor impedance and harmonic effects. The chapter also offers recommendations for future research, such as exploring other rotor geometries, enhancing thermal models, or integrating advanced control strategies to further improve the design and performance of HS-SRIMs

### **Chapter Two**

#### Literature Review

#### 2.1. Introduction

Solid-rotor machines have been extensively examined in earlier studies and dissertations, as documented in [6], [33], [34] and doctoral theses [35], [36], [37], [38] However, these works, though informative, It is difficult to determine the electromagnetic parameters of the electrical machine with a solid-rotor because of the non-linear rotor material features. Such a machine's multi-physical model, which has been the focus of several papers [17], [39], [40] must be considered in its design. These high-speed machine models usually incorporate mechanical, thermal, and electromagnetic computations.

One of the initial stages in the multi-physics design of high speed electrical motor is electromagnetic computation and design [41]. A appropriate machine topology and a list of requirements are typically known or chosen in advance. Depending on the impedance that result in the electromagnetic field analysis in the rotor , the mathematical modeling can be derived by direct and quadrature parameters for solid rotor .

# 2.2. Topologies Of SRIM

## 2.2.1. Overview of solid rotor Induction Motor topologies

A piece of ferromagnetic material or a combination of ferromagnetic and non-magnetic materials are typically used to create HSSRIMs. This machine's primary benefit is its strong rotor construction, which allows it to reach extremely high speeds. The choice of building type in high-speed applications is mostly determined by circumferential speed and centrifugal forces. Because of its higher rotational or circumferential speeds and megawatt range power, that type of rotor is typically chosen instead of a laminated rotor. [38] lists the following benefits of HSSRIM: great reliability, ease of protection from strong chemicals, high

stiffness, durability, and mechanical integrity; generally straightforward, affordable, and simple to manufacture; good thermal durability; simple scaling for a broad range of power and speed; and minimal vibration and noise (for smooth solid rotors).

Therefore, HSSRIMs are widely employed for high-speed and high-power-density applications in the industrial sector. The following are the most important rotor topologies that are mostly discussed or used, though any of the above rotor topologies may be combined.

Incorporating non-magnetic, highly conductive end rings into the solid steel rotor (SSR) enhances both torque density and electromagnetic characteristics, as highlighted in [36], [38], [11]. These end rings enable greater current flow within the steel—predominantly in the direction parallel to the axis which in turn amplifies the Lorentz force. Studies show that the two-pole SSR fitted with copper end rings is capable of producing double the torque of a conventional SSR under equivalent slip conditions [38], [42], [43]. The structure of this rotor is shown in Fig. 2.3(b).

Another notable modification to SSRs involves the copper-coated smooth solid-rotor (CCSSR), shown in Fig. 2.3(c). In this configuration, a conductive copper layer is applied over the rotor's exterior, creating a path that connects one end ring to the other, as described in [34], [44]. The thickness of this copper coating may either increase near the end rings or remain uniform along the length of the rotor.

The rotor's conductivity is enhanced by a larger layer of copper at the end rings, which also enhances the rotor's internal electrical current flow. Numerous articles state that a non-magnetic material with low or high conductivity should be used for the coating [38], [42][43].

A material with excellent electrical conductivity, such as copper, effectively replicates the function of countless end rings and rotor bars. Thanks to its superior conductivity, it primarily channels the rotor currents. Additionally, it acts as a

shield against high-frequency disturbances caused by air-gap and stator slot harmonics, which are unable to penetrate the coating [45], [11] This shielding effect diminishes eddy currents within the rotor iron and helps lower losses in the stator windings.

#### 2.2.2. Smooth solid-rotor IM

A smooth solid-rotor (SSR) is the most basic solid-rotor design [38], [42] Although they do not work well in electromagnetic fields, SSRs are the most mechanically resilient. This kind of machine frequently experiences large slip and losses, and a low power factor is usually the consequence of inadequate penetration of flux [37] into the rotor because of the high rotor slip and low electrical rotor material conductivity. As a result of its low magnetization inductance, high apparent resistance, and over-saturated solid-rotor surface, SSRs have an extremely low electromagnetic torque density [39]. The best mechanical and fluid-dynamical properties for low air friction are provided by an SSR, which also has the benefits of being very simple to manufacture and reasonably priced. Fig. 2.3(a) shows its layout. Many authors deals with this kind of rotor like the following:

The paper [46] is a foundational work on smooth solid rotors with end effects in. It introduced the "Russell correction factor," a crucial analytical tool for modifying the equivalent conductivity of the rotor material to account for 3D current paths at the rotor ends, improving the accuracy of 2D models.

The Paper [29] is Another classic study on the finite-length (end-effect) problem in smooth solid rotors. It provides an alternative analytical method to Russell's for calculating the correction factor needed to accurately predict the performance of a real, finite-length rotor from a 2D model.

The paper [30] is A comprehensive theoretical treatment of smooth solid rotors. It covers the electromagnetic field analysis, derives equivalent circuits, and explores the performance characteristics, serving as a key reference for understanding the fundamental operation of SSRs.

The paper [47] Investigates the impact of end regions on the impedance and performance of smooth solid rotors. It contributes to the body of work on endeffect correction factors, considering factors like the rotor's aspect ratio and material properties.

The paper [48] Provides a detailed analysis of the electromagnetic field distribution within a smooth solid rotor. This work is fundamental for understanding phenomena like skin effect and flux penetration depth, which govern the rotor's impedance and loss behavior.

The study [49] Focuses on the influence of the rotor material's properties (electrical conductivity and magnetic permeability) on the performance of a smooth solid rotor machine. It provides methods for incorporating material non-linearity into performance calculations.

The paper [50] is an early work that addresses two critical complexities in SRIMs: magnetic saturation of the rotor steel and the finite length of the rotor. It proposes methods to account for these effects in analytical models.

In the paper [51] one of the earlier applications of 3D Finite Element Analysis (FEA) to study end effects in smooth solid rotors. It validates and refines the simpler analytical correction factors proposed by Russell and Yee.

## 2.2.3. Axially slitted solid-rotor IM

Compared to SSRs, axially slitted solid rotors (ASSRs) offer a noticeably better electromagnetic performance. By cutting the rotor's cross-section axially, this simple rotor modification is achieved. Axial slits are crucial for pushing the flux's fundamental component further into the solid rotor [52], [42]. Additionally, the rotor's low-frequency impedance is reduced by axially slitting it, increasing torque and efficiency. Furthermore, it lowers the rotor's eddy-current Additionally, the rotor's low-frequency impedance is reduced by axially slitting it, increasing torque and efficiency. Furthermore, it lowers the rotor's eddy-current losses of

undesirable harmonics by raising the rotor's high-frequency surface impedance [53]. This kind of rotor find its way to be studied by many researches like:

In the study [35] the impact of axial slits and eddy-current phenomena in solid rotors were thoroughly examined in this seminal thesis. It illustrated how slit number, depth, and layout affect torque, efficiency, and slip using mathematical derivations and 2D/3D FEM. Additionally, it suggested workable slit geometries and cautioned against mechanical weakness caused by excessive slitting. Later SRIM studies used this study as their reference baseline.

In the paper [54] a specific experimental and analytical study demonstrating that output torque increases with the number of rotor slits, but also highlighting the risk of increased torque ripple and mechanical weakening. It helps define the optimal range for the number of slits per pole pair.

The paper [55] examines the critical trade-off between electromagnetic performance (which improves with deeper slits) and mechanical integrity (which deteriorates). It establishes that a slit depth of 40-50% of the rotor radius is often an optimal compromise.

The paper [56] focuses on the systematic optimization of slit geometry (width and depth) to maximize electromagnetic performance while adhering to mechanical constraints. It likely uses techniques like response surface methodology or genetic algorithms.

The paper [57] explore an advanced manufacturing technique (EDM) to create very thin and precise slits, which are difficult to achieve with conventional milling. This allows for better electromagnetic performance by minimizing the slit width, thus increasing the effective conductive area.

The paper [58] investigates the combination of axial slits with copper end rings. The end rings help guide axial currents, further improving torque density and efficiency by reducing the impedance to current flow along the rotor length.

The paper [59] proposes a novel rotor design where the slits are skewed, similar to skewing in a conventional cage rotor. This design is shown to significantly reduce torque ripple (to around 1%), albeit at the cost of increased manufacturing complexity.

The study [53] created and evaluated a variety of rotor designs, such as caged, copper-coated, and slitted models. Measurements of torque, losses, and temperature increase demonstrated real-world trade-offs between efficiency and manufacturability while also validating theoretical predictions. Rotor modification techniques were validated in the actual world by the study

# 2.2.4. Copper coated solid-rotor IM

As for the SSR, Fig. 2.4(d) illustrates how an ASSR's surface can be modified to include either a resistive non-magnetic substance or a highly conductive material. The optimum electromagnetic performance is demonstrated by an ASSR covered with a highly conductive material, such as copper [37], which also has the advantage of axial slits. Similar behavior is exhibited by the machine when coated with a resistive non-magnetic substance [54]. In addition to creating high surface impedance, the resistive coat serves as a high-frequency shield.

In the paper [60] the copper coatings on solid rotors change current pathways and lower surface losses. Efficiency increased when paired with axial slits, but manufacturing complexity went up according to this early experimental study. These findings connected analytical research with practical implementation by providing the first experimental confirmation of theoretical predictions..

The paper [44] focuses on the design and manufacturing challenges of applying a copper coating to a solid rotor, such as ensuring a strong bond between the coating and the rotor core. It discusses the electromagnetic and thermal advantages of this approach.

The study [61] explores the interaction between a copper-coated rotor and advanced control strategies. It shows that the improved characteristics of the

coated rotor can be leveraged by control algorithms to enhance overall system performance.

The paper [45] includes methodologies for calculating the performance of coated rotors, while covering solid rotors in general treating the coating as a separate layer in the electromagnetic model and analyzing its shielding effect.

In the paper [62] copper coatings on solid rotors change current pathways and lower surface losses, according to this early experimental study. Efficiency increased when paired with axial slits, but manufacturing complexity went up. These findings connected analytical research with practical implementation by providing the first experimental confirmation of theoretical predictions.

## 2.2.5 Solid-rotor Induction Motor with radial rotor surface grooves

This is a unique instance of solid rotor arrangement where the rotor surface is coated with shallow radial grooves. The radial grooves provide the same characteristics as a high-resistive coating by increasing the rotor's surface impedance and functioning as a highly resistive material layer, also known as a high-frequency filter. The active rotor length's groove width and inter-groove distance need to be properly constructed in order to provide the intended effect. Figure 2. 8 displays an ASSR with radial grooves.

The paper [63] demonstrates that radial grooves act as a high-resistive layer on the rotor surface, increasing the impedance to harmonic fields. This can reduce rotor surface eddy current losses by 30-60% with a relatively simple and mechanically sound modification.

# 2.2.6 Squirrel cage solid rotor IM

Laminated rotors are unable to endure intense centrifugal forces and high tensile stress[64], making them unsuitable for certain demanding conditions. As a result, solid rotor designs that feature drilled holes or machined slots into which copper bars are inserted and then connected with a short circuit copper ringare

often favored. These squirrel-cage solid rotors (SCSRs) closely resemble conventional squirrel-cage rotors used in induction machines.

Rectangular open slots and a brazed squirrel cage characterize the most basic SCSR design (Fig.2.9(a)). From a mechanical perspective, a SCSR with an isostatic pressure-embedded squirrel cage is marginally superior (Fig. 2.9(b)).

The paper [65] addresses the primary challenge of SCSRs: the mechanical connection between the copper bars and the end rings under extreme centrifugal forces. It explores manufacturing techniques like brazing and isostatic pressing to ensure reliability.

The study [66] gives a direct comparison of various SCSR constructions (e.g., open slots, embedded bars) for large machines. It evaluates their electromagnetic performance, mechanical strength, and manufacturability, providing a guide for selecting the best design for a given application.

The paper [67] details the electromagnetic design process for a high-power, high-efficiency SCSR motor. It focuses on optimizing the bar and slot geometry to minimize losses and leakage inductance while maximizing torque.

The study [68] shows that SCSRs can achieve the best electromagnetic performance (highest efficiency, lowest slip) among all solid rotor types, but confirms that this comes with the highest manufacturing complexity and cost.

The research [69] develops algorithms to accurately calculate eddy current losses in the solid iron portions of an SCSR. This is critical for thermal management, as these losses can be significant even though most current flows in the cage.

The paper [70] discusses the selection of the base iron material for an SCSR. It argues for using iron with higher resistivity to minimize eddy current losses in the iron itself, since the cage carries the majority of the useful current.

### 2.3. Designs & modeling studies

The right iron material must be carefully chosen for each solid rotor topology. Compared to laminated rotors, pure solid rotors have the drawbacks of low power factors and large eddy-current losses. By adding a layer of copper, copper ends, or sometimes, a squirrel cage, these drawbacks can be somewhat mitigated. It is favorable to choose a material with good conductivity for a purely solid rotor. This will allow rotor currents to flow without significant resistance and enable the creation of high torque at low slip.

The paper [37] systematically evaluates different ferromagnetic materials for solid rotors, balancing electromagnetic properties (conductivity, permeability) with mechanical properties (tensile strength) for a given operational speed and power level.

The study [71] a comprehensive account of a large-scale industrial project, covering the integrated design of electromagnetics, cooling, rotor-dynamics, and manufacturing for a multi-MW SRIM. It includes valuable experimental data from prototype testing.

The study [40] emphasizes the tight coupling between electromagnetic, thermal, and mechanical design in ultra-high-speed machines. It discusses how the rotor's dimensions (diameter, length) are constrained by mechanical stress and critical speed limits.

The paper [41] is a case study of a very high-speed (120,000 rpm) SRIM design, highlighting the extreme mechanical challenges and the specialized design choices required for such applications, including material selection and rotor dynamics analysis.

The paper [72] provides a practical application of the dq-model for induction motors, demonstrating its implementation in software like MATLAB/Simulink for analyzing dynamic behavior, which is directly relevant to the simulation work in your thesis.

The study [73] systematically categorizes rotor topologies (smooth, slitted, coated, caged), details analytical and numerical modeling techniques, discusses manufacturing processes, and identifies future challenges, particularly in thermal management for multi-megawatt machines. It serves as a perfect starting point for understanding the state of the art.

The paper [6] provides a broad comparative analysis of various high-speed machine technologies, including permanent magnet and induction machines. It clearly articulates the advantages of SRIMs, such as mechanical robustness and cost-effectiveness, especially in high-power applications where traditional laminated rotors would fail, thus establishing the context for their use.

The study [43] focused on large-scale MW-class machines, demonstrated the need to integrate electromagnetic design with mechanical stress and temperature control. The authors emphasized how designs that appear to be good electromagnetically can be invalidated by centrifugal forces, vibrations, and heating. The foundation for transdisciplinary SRIM design processes was laid by their efforts.

The paper [42] directly compares the performance of different high-speed induction motor rotors, likely including laminated, solid, and possibly slitted designs. It provides valuable empirical data on the trade-offs between efficiency, torque density, and mechanical strength, helping to guide the selection of rotor type for a specific application.

**The study** [74] focused on large-scale MW-class machines, demonstrated the need to integrate electromagnetic design with mechanical stress and temperature control. The authors emphasized how designs that appear to be good electromagnetically can be invalidated by centrifugal forces, vibrations, and heating. The foundation for transdisciplinary SRIM design processes was laid by their efforts.

**The study** [75] created a quick analytical technique that does not require timedomain FEM to compute eddy-current losses from stator harmonics. The technique worked well for optimization studies that needed a lot of iterations and was accurately tested against FEM. It enabled the incorporation of harmonic loss into realistic design processes.

The study [2] presents an advanced analytical method that models the rotor as multiple layers (e.g., a coating and the base iron), providing a more accurate calculation of the magnetic field distribution and complex rotor impedance than single-layer models.

In the paper [76] the magnetic diffusion equations were solved to give closed-form mathematical solutions for torque and air-gap power in slotless solid rotors. It made it clearer how much input power turns into useful torque in relation to losses. Early design studies and validation benefited from this little model's ability to provide fast estimates without requiring complex simulations

The study [77] suggested a hybrid simulation technique in which more targeted 3D FEM investigations are started using the results of 2D FEM. This process significantly decreased computing time without sacrificing precision. It provided engineers with a useful method for balancing cost and accuracy in SRIM rotor research..

The study [78] created a quick analytical technique that does not require time-domain FEM to compute eddy-current losses from stator harmonics. The technique worked well for optimization studies that needed a lot of iterations and was accurately tested against FEM. It enabled the incorporation of harmonic loss into realistic design processes.

**The paper** [79] proposes a novel equivalent circuit model that uses fractional-order calculus to more accurately represent the frequency-dependent behavior of the solid rotor's impedance, improving the precision of dynamic simulations.

The paper [80] develops a quasi-3D analytical model for disk-type (axial flux) SRIMs. This method offers a good compromise between the simplicity of 2D analysis and the accuracy of full 3D FEA for a specific machine geometry.

**This paper** [81] presents a detailed 2D analytical model for predicting eddy currents, equivalent circuit parameters, and steady-state performance, accounting for material saturation and the finite length of the machine.

The study [82] documents an investigation into the operation of a solid-rotor induction motor with a rectilinear inverter excitation in order to determine the impact of the related temporal harmonics, the study. The theoretical results correlate well with measured results and the significant harmonic effects are identified

The paper [83] describes a hybrid modeling technique that combines analytical solutions for the electromagnetic fields in the rotor with numerical methods, aiming to achieve high accuracy with lower computational effort than pure FEA.

**This paper** [84] uses 3D FEA to quantify "additional losses" in induction motors, which are particularly relevant for SRIMs due to the solid rotor's susceptibility to eddy currents from various sources like slot harmonics and endregion fields.

According to [37].the main drawbacks of axial slits in a solid rotor are that they significantly raise the rotating rotor's air friction and compromise the ASSR's resilience at higher circumferential speeds. Nonetheless, the axial slitting improves cooling since it expands the rotor's surface. Figure 2.4(a) shows this arrangement.

As shown in Fig. 2.5, research has shown that the machine output-torque rises as the number of rotor slits increases [36], [85], In order to minimize imbalanced magnetic force (which could be more than the weight of the rotor) and the rotor mechanical vibration, only equal numbers of rotor slits were taken into consideration in [36]. Using an odd number of rotor slits lessen the

electromagnetic torque ripple, even though there is a chance of a highly imbalanced magnetic pull. The optimal number of slits per pole pair has been proposed to be between 5 and 15 [86].

Slit width and depth are two crucial factors. Machine performance is greatly impacted by the slit depth [43],and the optimal machine electromagnetic parameters can be generated at a depth of 60% of the radius of the rotor. Such depth, however, jeopardizes an ASSR's overall strength and integrity, perhaps leading to rotor disintegration or a shorter lifespan. For this reason, depths ranging from 40% to 50% of the rotor's radius are commonly selected, taking into account the machine's dimensions, circumferential speed, and the rotor mechanical integrity of [55]. Ideally, the slit width should be kept to a minimum due to the mechanical stress that accumulates at the base and rotor slits inner corners. Significantly, that stress can be reduced by rounding off the bottom ends of the slits, though it is important to note that this solution may not be applicable or effective for all cases.

The ideal slit width, as determined by [87], [56], [57] is between 9% and 15% of tooth pitch of the rotor in order to obtain the best electromagnetic machine parameters. But the manufacturer's technological prowess has a significant impact on the slit width. The rotor tooth pitch is 13.47% composed of the tiniest slits created and documented thus far [57] . Typically, rotor slits should be as thin and deep as feasible.

By altering the slit depths, it is possible to slightly modify the ASSR, as illustrated in Fig. 2.4(b). This approach is intended to lower the material's high saturation at the narrow sections between the slits and enhance the machine's torque output. Nevertheless, the design is still bordered by the Maximum slit depth, which remains within the 40–50% range. Even after considering ASSR with slits of different depths—while adhering to the maximum permissible depth specified in [36] the machine's electromagnetic performance did not show any notable improvement.

As seen in Fig. 2.4(c), copper rings can be introduced to ASSRs, just like they can to SSRs. Axial slits, which aid in aligning the current flow in the axis-parallel direction, are an additional benefit of this design, which incorporates all the benefits listed in Section 2.2. As a result, the machine's torque and efficiency are enhanced [88].

In Fig. 2.1, a compressor drive types works with solid rotor are shown. Active magnetic bearings are advised in order to increase the compressor drive's lifespan, performance, and efficiency [16]. IM, which range in size from 3 MW to 15 MW and have corresponding speeds of 20 krpm to 5 krpm, are widely used in this industry [44], [102] .An integrated compressor's high-speed, high-power IM is seen in Fig. 2.2.

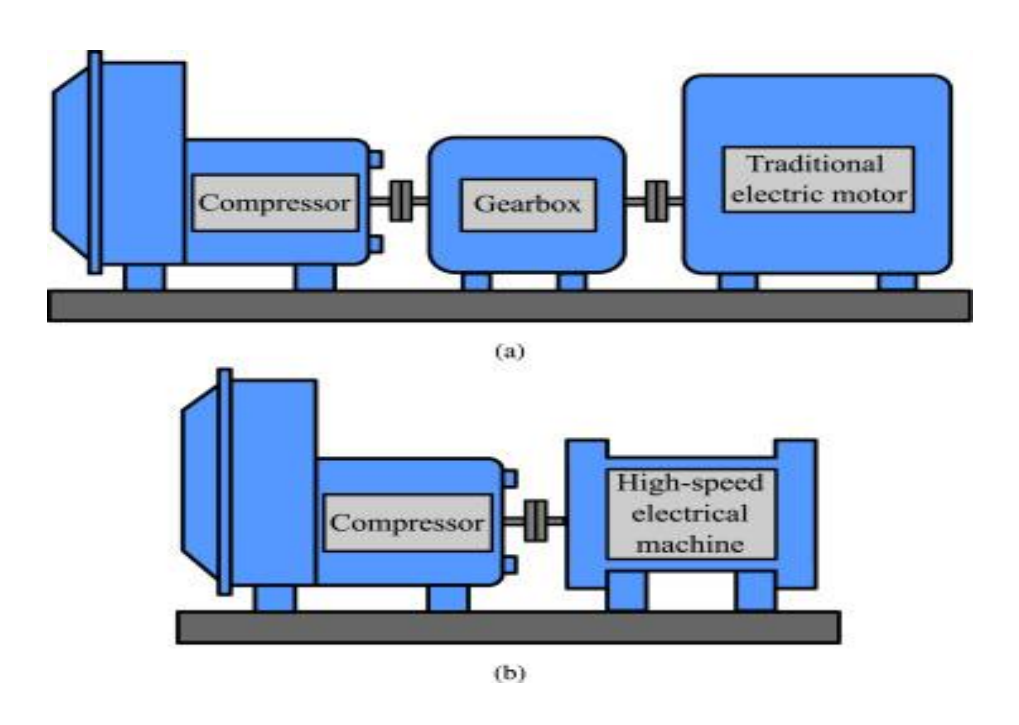


Fig.2.1. compressor working with SR (a), integrated compressor (b), [6].

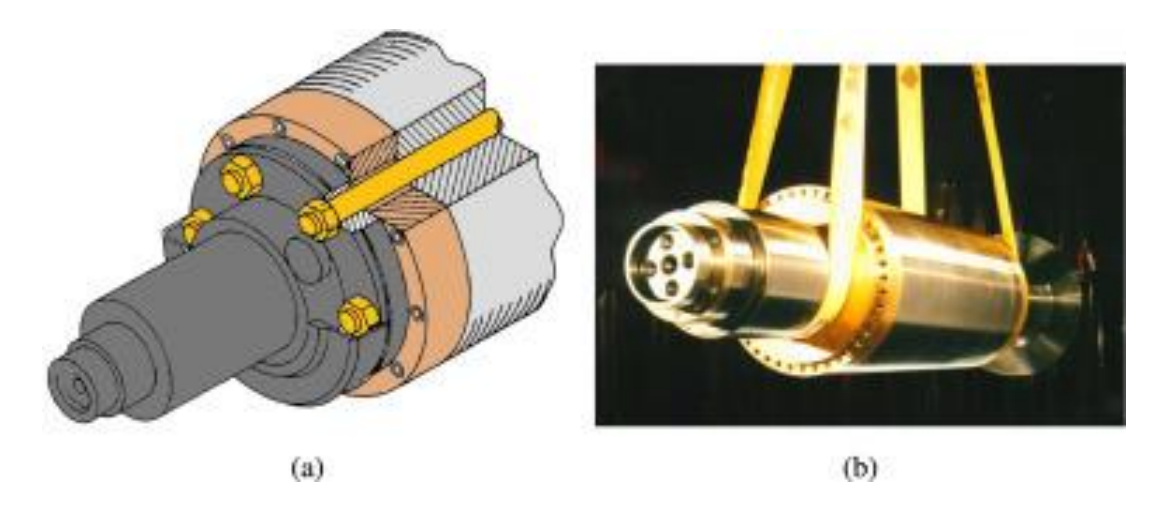


Fig. 2.2. High speed high power for an integrated compressor. squirrel-cage rotor (a) detail of a high speed solid rotor(b) [90].

axial slits were skewed by 30° tangentially and 26° axially, resulting in a significant reduction of torque ripple to just 1% of the machine's output torque [59]. This type of rotor modification offers the benefit of enhanced machine torque, but it comes with the downside of considerable manufacturing complexity.

The shielded axial slitted solid-rotor (SASSR), depicted in Figure 2.7, is a rotor topology that combines the advantages of all the designs discussed above. The components of an SASSR are an ASSR, copper end- rings, and a copper covering, and they resemble squirrel cage solid-rotors [52][87].

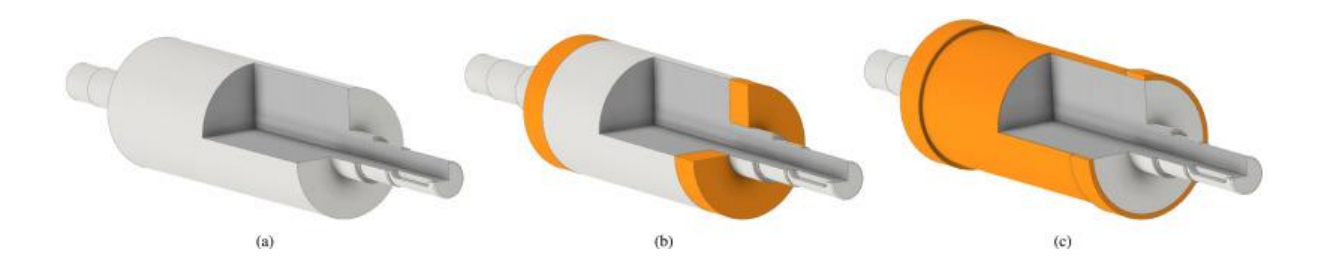


Fig.2.3. Construction of a smooth SRIM: (a) simple smooth solid rotor, (b) smooth solid rotor with copper end rings, and (c) copper coated smooth solid-rotor, [36], [37], [45].



Fig.2.4. axially slitted solid-rotor(ASSR) construction for an IM: (a) ASSR, (b) ASSR with slit of various depth, (c) ASSR with copper end rings, and (d) ASSR coated with conductive or resistive material, [37].

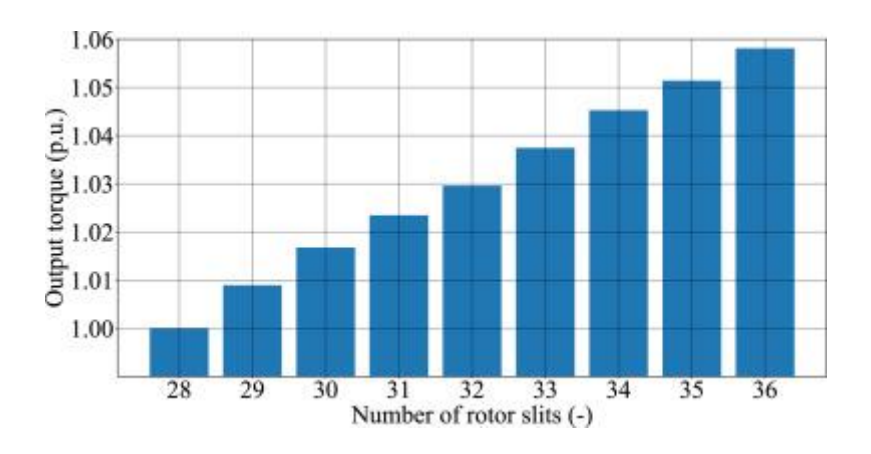


Fig.2.5. output torque vs the number of rotor slits, according to [36], [85].



Fig.2.6. ASSR with axial slits skewed in tangential and axial directions: (a) equal slits depth and (b) various depths of slits, [59].

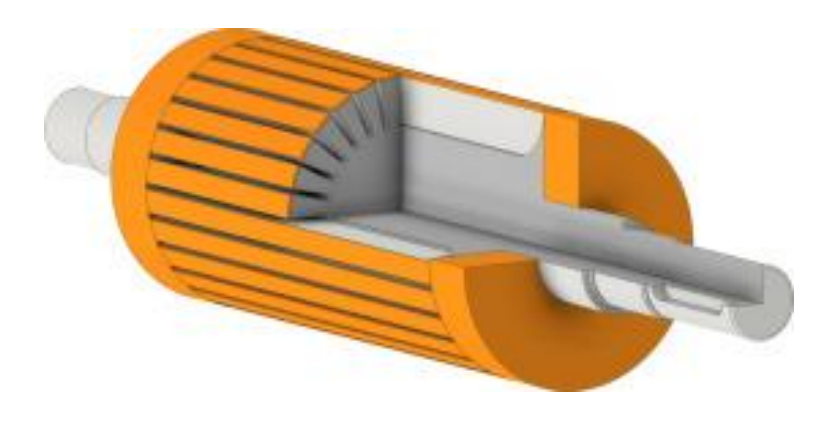


Fig.2.7. SASSR for an IM, [52][87].



Fig.2.8. Construction of ASSR with radial grooves for an IM, [63].

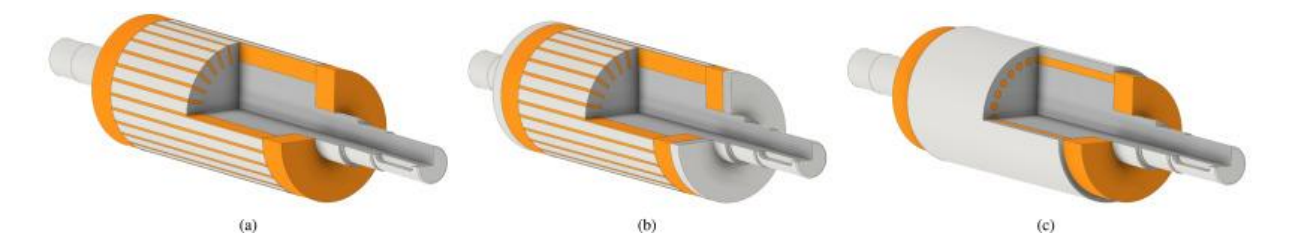


Fig.2.9. a solid-rotor with squirrel cage for an SRIM: (a) rectangular opened slots with brazed squirrel cage, (b) squirrel cage embedded by isostatic pressure, and (c) insert a round embedded copper bars into a solid rotor with holes [66].

Table 2.1 (as referenced in [89] )outlines the main uses for high-speed electrical machines. The focus of that study includes high-speed spindles, flywheel energy storage, compressors and turbines for oil, gas, and air, as well as turbomolecular pumps.

Table.2.1. Power & speed requirements of the applications, [89].

Application	Power	Speed	
Oil & gas	3–15 MW	5–15 krpm	
Spindles	300 W-60 kW	15–300 krpm	
Turbocharger	1–3 kW/10 kW	150 krpm/80 krpm	
Air compressor	4 kW-500 kW	15–80 krpm	
Micro-turbines	30–400 kW	15–120 krpm	
Turbomolecular			
Pumps	50 W-3 kW	70–100 krpm	

Power inverters combined with high speed electric machines have begun to replace traditional gearbox-based machines in recent years, thanks to advancements in power electronics [90], [91], This method has the obvious benefits of being smaller, lighter, and having a greater power density and efficiency [92], [93], [94]

Table.2.2. a suitable materials for solid rotors, with their characteristic properties. [70] .

Name	Material	Tensile	Resistivity	Saturation
		strength	$[\mu\Omega\ cm]$ at 20	flux density
		[MPa]	°C (at 200 °C)	[T]
Imacro M	4CrMn16-4	1100	25 (37.3)	1.63-1.95
AISI430	X6Crl7	600	25.7 (38)	1.66–1.74
Maraging	Fe-Ni-Co-	2200	49	1.9
	Mo-Ti			
C15	_	440	15.9 (30)	1.9
Supermendur	Fe-V-Co	800	40	2.4
S355	-	520	25.7 (38)	1.9–2.1
Fe-Ni	Fe-Ni	545	48.2	1.5
Fe-Cu	Fe-Cu	_	11	1.6
ARNOKRO	Fe-Cr-Co	_	69	_
ME III				
Vicalloy	Fe-Co-V	880	61.5	1.3
HyMu 80	Ni-Fe-Mo	930	58	_
Consument	_	345	13	2.15
Vim Var (AISI	C-Si-Mn-Cr-	315	13	2.15
M50)	Mo-V			
MuShield	_	620	58	1.9
AISI H13	Cr-Mo-V	1820	52 (63)	1.9
(Orvar)				
X20Cr13	_	880	55 (66)	1.7–1.9
MoCN315M	34CrNiMo6	345	19 (33)	1.97-1.99

In addition to electromagnetic factors, the material's mechanical qualities and ability to withstand the machine's heat requirements must be taken into account. The material must have a high enough tensile-strength in high-speed applications so that the rotor can meet the rotor dynamic requirements and endure high circumferential speeds. Table 2.2 provides a list of selected materials along with the properties that qualify them for use in solid-rotors.. For use in an IM with a solid rotor and squirrel cage here, five materials with rated speed of 12,000 rpm and rated power of 1 MW were selected and compared [95], In a comparable study, an IM with an ASSR with a rated power of 180 kW and a speed of 10,000 rpm used seven different materials [70].

The elongation value of the solid rotor's iron and copper alloy serves as the last criteria. Both materials should have an elongation of at least 10%. All of the appropriate copper alloys that are suitable for explosive plating are listed in Table 2.3. conductivity, tensile-strength, and material cost are all trade-offs when choosing an alloy; no single alloy offers the best qualities.

Table .2.3. suitable copper-alloys for coating of solid rotor surfaces and their properties.  $MSm^{-1}$ .

Name	EN code	USN code	Tensile	Electrical
			strength [MPa]	conductivity [%]
Cu-OF	CW008A	_	240–360	100
CuNi2SiCr	CW111C	C18000	650–780	40
CuCr1Zr	CW106C	C18150	400–600	75
CuCr1	CW105C	C18200	400–500	80
GlidCop AL-15	_	C15715	500-700	55

#### 2.3. Mechanical Limitations

#### 2.3.1. Rotor Diameter

If the tangential tension remains constant, increasing the rotor diameter has the advantage of producing more torque. However, the rotor's tangential stress mechanical strength sets a limit on rotor diameter. The circumferential force rises in tandem with the rotor diameter.

According to Ylinen [37], a cylindrical solid rotor's mechanical stress can be calculated as

$$ST_{\text{max}} = C\rho r^2 \Omega^2$$
 (2.1)

For smooth rotor

$$C = \frac{3+v}{8}, \qquad (2.2)$$

For cylinder with small bore

$$C = \frac{3+v}{4} \qquad (2.3)$$

For thin cylinder

$$C \approx 1$$
 (2.4)

where v is the relevant material's Poisson's coefficient. For rotor steel, the applied Poisson's coefficient (v) is 0.29; for copper, which is utilized in the rotor end rings, it is 0.34. Aho [19], [20], asserts that a variety of elements, including the width, depth, and number of slits, significantly impact the motor's mechanical and performance characteristics.

# 2.3.2. Rotor Length

The machine may vibrate dangerously due to the rotor's natural frequency. The solid rotor's critical frequencies are high due to its single ferromagnetic material construction. Two primary determinants of the rotor's stiffness are geometry and

elasticity.

The core material's elasticity is described by its Young's modulus E. Wiart states that the critical rotor length, or l crit, can be determined as[98]

$$l_{\rm crit}^2 = n^2 \frac{\pi^2}{k\Omega} \sqrt{\frac{EI}{\rho S}} \qquad (2.5),$$

where S is the cylinder's cross-section, I is the modulus of inertia, and n is the ordinal of the critical speed. The ratio of the nominal angular velocity to the nth critical frequency is the definition of the variable k.

$$k = \frac{W_{c}}{W_{n}} \qquad (2.6)$$

It is important to consider the safety factor ksafe for the maximum mechanical stress.

Thus, it is possible to measure the ratio of the rotor length (lr) to the radius (r).

$$\frac{l_{\rm r}}{r} = n\pi \sqrt{\frac{k_{\rm safe}}{k}} \sqrt[4]{\frac{CE}{4\sigma}}$$
 (2.7)

To accomplish high speeds without vibrations, a short, thick rotor structure would be preferable from the perspective of mechanical rigidity.

## 2.3.3. Air Gap

The properties of the machine are greatly impacted by the choice of air gap length g.

For an induction motor, the long air gap is a problem because the rotor needs to get magnetized from the side of the stator. That means a higher magnetization current, which increased the ohmic losses in stator windings and minimize the power factor.

Minimal possible air gap is approximately 0.2 mm Small air gap leads to low magnetizing current and the high eddy current surface losses [99].

### 2.3.4. Winding Factors

The winding factor shows the properties of the winding that cause harmonics. It has an impact on the electromotive force (emf) and current linkage, which in turn affects the motor's performance. Conversely, the winding factor explains the relationship between the magnetizing inductance and the harmonic current linkage force. It might be stated as

$$k_{wh} = \frac{\sin\left(\frac{hq_5\alpha_s}{2}\right)\sin\left(\frac{hy\pi}{2}\right)}{q_s\sin\left(\frac{h\alpha_s}{2}\right)}$$
(2.8)

here h is the number of harmonic ( h=1 for fundamental). he symmetrical m-phase stator winding creates current li (Richter 1954)[100]

$$h = 2km + 1, k = 0, \pm 1, \pm 2, \pm 3, ...$$
 (2.9)

According to research by Huppunen [35], the optimal winding pitch from the perspective of the detrimental effect of air-gap harmonics is 5/6 since it provides the lowest value for the leakage factor  $\sigma\delta$ , which Richter [99] defines.

$$\sigma_{\delta} = \sum_{n \neq 1} \left( \frac{k_{\text{wh}}}{n k_{\text{w1}}} \right)^2 \tag{2.10}$$

here  $k_{w1}$  is the fundamental winding factor.

# 2.4. Applications of Solid-Rotor IM

According to [89] ongoing advancements in power electronic technology, inverter systems, manufacturing techniques, and material engineering [95], [70] have significantly boosted the use of high-speed solid-rotor electrical machines in rapid-rotation applications throughout the past ten years. Engineering these high-speed machines tends to be highly intricate, demanding optimization that spans multiple disciplines [89]

High-speed electrical machines are categorized based on their rotor's peripheral velocity. In various industrial high-speed settings, these machines have either

supplanted or supplemented traditional mechanical setups, which typically involve a gearbox paired with a slower electric motor [6]

Integrating a high-speed machine with a power inverter brings notable benefits such systems are generally more compact, lighter in weight, and exhibit increased reliability compared to arrangements that rely on a gearbox and a lower-speed motor. Thanks to their robust rotor structure, affordability, precision, and ease of production, high speed solid-rotor induction machines have become a common solution in these applications [101]

In Fig. 2.1, a compressor drive types works with solid rotor are shown. Active magnetic bearings are advised in order to increase the compressor drive's lifespan, performance, and efficiency [16]. IM, which range in size from 3 MW to 15 MW and have corresponding speeds of 20 krpm to 5 krpm, are widely used in this industry [44], [102] .An integrated compressor's high-speed, high-power IM is seen in Fig. 2.2.

## **Chapter Three**

## Mathematical Modeling

#### 3.1. Introduction

The magnetically nonlinear rotor material and the three-dimensional character of the electromagnetic fields make it difficult to calculate the magnetic and electric fields of a smooth solid rotor, even though its manufacture is straightforward [29]. Accurately and swiftly solving these fields is a difficult task. The electric and magnetic circuits in the stator and rotor of a traditional laminated squirrel-cage rotor induction motor can be thought of as distinct circuits. The electric circuit passes via the coils, while the magnetic circuit mostly passes through the steel components and the air-gap[84]. This division makes it possible to investigate these phenomena independently. Additionally, in traditional induction motors, the magnetic circuit is combinations of laminated electric sheets, and end-rings are included in the squirrel cage, enabling accurate twodimensional analysis and separate study of non-dominant end effects. Because the steel in a solid rotor creates a channel for both electric current and magnetic flux, non-linearity and three-dimensional effects must be taken into account[103]. Standard linear analysis techniques that solely take lumped parameters into account are therefore no longer appropriate.

Three-dimensional FEM computations might be used to solve the rotor field problem, however this method is too laborious for routine motor design procedures. Furthermore, FEM computations become even more challenging when rotating movement is modeled[104]. As a result, the rotor fields need to be solved analytically in three dimensions. Solving Maxwell's field equations under the assumptions of a smooth solid rotor and magnetically linear rotor material is the ultimate simplification.

### 3.2. Analytical Methods

Significant machine simplifications are typically taken into account in analytical design. When compared to actual machine data, the modeling accuracy of an unsaturated rotor with constant permeability was quite low in the past [49]. Then, in order to improve the accuracy of analytical methodologies, researchers began to take into account the 3D aspect of solid-rotors [49].

Solid-rotor saturation is taken into account by contemporary analytical techniques [105], and some researchers even divide the rotor into multiple layers to produce more precise results: For example, the transfer matrix method was integrated with three-dimensional linear methods in [49]. Despite producing good results, this method is only applicable to SSRs and is somewhat complex. Even better and more accurate results are the goal of more recent analytical techniques, some of which were introduced in [31], [48], [83], [106], [107], [108], [109], [110], [111], however they are all restricted to SSRs.

For calculating the performance of steady-state machines, electrical circuits (EECs), whose main benefit is their ease of use, are comparable to far more straightforward and adaptable analytical techniques. To guarantee the greatest outcomes, more modern techniques put forth in [81],employ T-shaped EECs with empirical formulas. Additional calculation parameters, including the solid-rotor's resistance and end-region leaking reactance, were provided in [112]. In order to solve electromagnetic fields in solid-steel rotors, a unique instance of single-phase CCSSR Induction Motor analysis employing an EEC was developed in [61]. In this work, the machine was analyzed using d-q axes modeling

In this section, only the smooth solid rotors of and copper coated solid rotor are considered (as shown in figure 3.2).

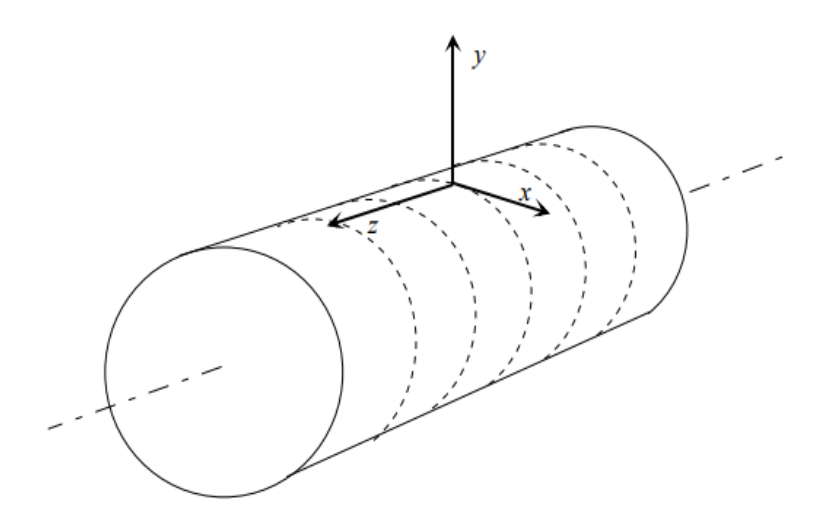


Fig.3.1 coordinate system for analyzing the field in SR

### 3.2.1 Saturation and Hysteresis

Many authors employ the well-known approximate Neyman's technique to take hysteresis and saturation in solid ferromagnetic rotors into consideration [113], Neyman showed that a constant coefficient,  $a_R \approx 1.45$ ., should be multiplied by the active power and resistance losses for continuous permeability. In a similar manner, a constant coefficient, approximately  $a_x \approx 0.85$ ., should be applied to the reactance and reactive power losses when the permeability remains unchanged. Neyman's approach considers both the fundamental harmonic of the electromagnetic wave and the changes in permeability along the direction of wave propagation.

It is important to note that the coefficients  $a_R$  and  $a_x$  are not fixed values; rather, they depend on the intensity of the magnetic field at the surface of the ferromagnetic material, as demonstrated in [12]

For a one-dimensional analysis of a ferromagnetic half-space, the complex propagation constant which accounts for both magnetic saturation and hysteresis—can be expressed as follows:

$$\alpha = (a_R + ja_x)k_{\text{Fe}} \tag{3.1}$$

where the coefficients are  $a_R = f_1(H)$  and  $a_x = f_2(H)$ . The surface relative permeability attenuation coefficient

 $v_{\rm rs}$  is equal to:

$$k_{\rm Fe} = (\pi f s \mu_0 \mu_{\rm rs} \sigma_{\rm Fe})^{1/2}$$
 (3.2)

where s is the fundamental harmonic slip and  $\sigma_{Fe}$  is the steel conductivity.

From Eq. 3.2, one can obtain equivalent complex magnetic permeability:

$$\mu_{\rm re} = \mu_{\rm rs}(\mu' - j\mu'')$$
 (3.3)

where:

$$\mu' = a_R a_x \tag{3.4}$$

$$\mu' = a_R a_x \tag{3.4}$$

$$\mu'' = 0.5(a_R^2 - a_x^2) \tag{3.5}$$

As a result, the corresponding complex permeability's real part ( $\mu' \mu_{rs}$ ) and imaginary part  $(j\mu''\mu_{rs})$  depend on the strength of the magnetic field. Electromagnetic fields in a ferromagnetic media can also be analyzed in two or three dimensions using the equivalent permeability from Eq. 3.5.

# 3.2.2 Electromagnetic Fields in Solid Rotor

Figure 3.2 illustrates the design of a double-layer rotor which are used in this study . Typically, the outermost layer referred to as the high-conductivity cap is composed of:

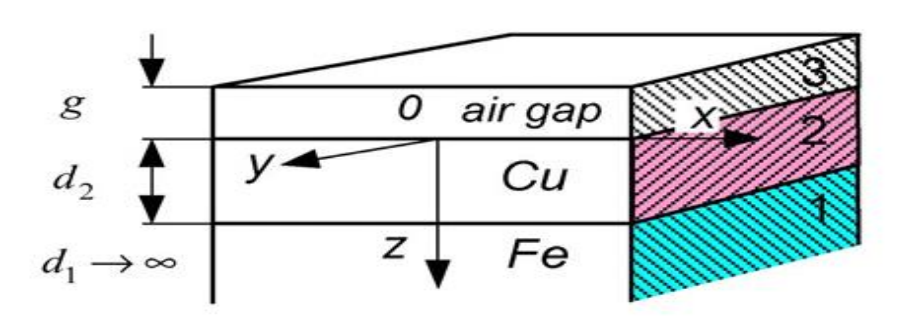


Figure 3.2 the consistent layers of solid ferromagnetic rotor covered with a copper

The system under consideration features a structure composed primarily of copper, providing an efficient path for electrical conduction. In this design, the solid back iron serves a dual function, forming both the electric and magnetic circuits essential for device performance. The interaction between these elements is governed by a set of foundational starting points that facilitate calculation of electromagnetic field distribution within the air gap and through the double-layer rotor.

To simplify and model the complex behavior of the machine, several key hypotheses are adopted. First, the stator core is constructed from thin laminations, which are assumed to possess infinite magnetic permeability and resistivity. This essentially directs all magnetic flux within the stator while eliminating any eddy current losses. The stator's active surface, defined in terms of its physical dimensions and pole pitch, is modeled as an unslotted region, ensuring an even magnetic field distribution.

The windings of stator themselves are idealized as an infinitely thin current sheet. This current sheet, distributed in uniform along the core surface, produces a consistent line-current density across the entire active area. On the rotor side, the configuration assumes a smooth cylindrical core with an exterior sheath of highly conductive, isotropic, nonmagnetic material and an interior of isotropic ferromagnetic material. The magnetic properties of the core of the ferromagnetic rotor are defined quantitatively by a specific permeability relation (given by Equation 3.5 in the reference material).

Furthermore, the rotor core is assumed to have a defined axial length, remaining precisely aligned and concentric with the stator cylinder. For analytical tractability, the curvature radius of the rotor is posited to be much larger than the penetration depth of any propagating electromagnetic waves, permitting the use of a simplified rectangular coordinate system in field calculations. Additional assumptions smooth the mathematical treatment: the rotor core equivalent magnetic permeability is considered uniform even for higher harmonics, matching

the response to the fundamental harmonic field component. Both rotor and stator are conceptually "unwrapped" into flat bodies, and the rotor core is further modeled as a half space to streamline boundary condition handling. The electromagnetic field's spatial variation is set to repeat over each pole pitch with perfect periodicity.

For the sake of analysis, the entire structure is treated as two-dimensional, postulating that both the rotor and stator are extended axially into infinity. Any effects due to their actual finite length are to be considered in a subsequent, more detailed study. Finally, all involved electromagnetic quantities, including fields and currents, are assumed to vary sinusoidally over time, aligning with typical alternating current (AC) operation.

when the coordinate system is fixed to the stator and two waves are traveling in opposite directions. Eq. 3.6 provides the stator's linecurrent density after differentiating with regard to x, which is:

$$a_{1h}(x,t) = A_{mh}^{+} e^{j\left(h\omega t - \frac{\pi x}{\tau} - \frac{\pi}{2}\right)} + A_{mh}^{-} e^{j(h\omega t + \pi x/\tau + \pi/2)}$$
(3.6)

neglecting  $e^{(jh\omega t \pm \pi/2)}$ :

$$a_{1h}(x) = A_{mh}^{+} e^{-j\pi x/\tau} + A_{mh}^{-} e^{j\pi x/\tau}$$
(3.7)

where the complex amplitudes of the line-current density are

$$A_{mh}^{+} = \frac{3\sqrt{2}N_1K_{\omega 1}}{\tau p}I_{1h}^{+} \tag{3.8a}$$

$$A_{mh}^{-} = \frac{3\sqrt{2}N_1K_{\omega 1}}{\tau p}I_{1h}^{-} \tag{3.8b}$$

The higher-order time harmonics summation (h) in Equation 3.7 has been excluded. Thus, Equations 3.7 and 3.8 represent sinusoidal waveforms for the line-current density at the frequency (hf).

A two-dimensional electromagnetic field distribution inside the air gap and the rotor can be found by integrating Maxwell's equations, the line-current density found in Equation 3.7, and the pertinent boundary conditions.

Maxwell's equations, which allow for the omission of displacement and convection currents, describe the electromagnetic field in electrical machines. The following Laplace's (for air layer) and Helmholtz (for a conductor layers) equations are obtained following standard vector analysis operations.

1. For  $0 \le y \le g$  and  $y \ge g + d1 + d2$ :

$$\nabla^2 \overline{\mathbf{H}}_h = 0 \tag{3.9a}$$

$$\nabla^2 \overline{\mathbf{E}}_h = 0 \tag{3.9b}$$

2. For nonmagnetic layer  $(g \le y \le g + d2)$ :

$$\nabla^2 \overline{H}_{Cuh} = \alpha_{Cuh}^2 \overline{H}_{Cuh} \tag{3.10a}$$

$$\nabla^2 \overline{\mathbf{E}}_{\mathrm{Cu}h} = \alpha_{\mathrm{Cu}h}^2 \overline{\mathbf{E}}_{\mathrm{Cu}h} \tag{3.10b}$$

3. For the ferromagnetic layer  $(g + d2 \le y \le g + d1 + d2)$ :

$$\nabla^2 \overline{H}_{Feh} = \alpha_{Feh}^2 \overline{H}_{Feh} \tag{3.11a}$$

$$\nabla^2 \overline{\mathcal{E}}_{\mathrm{Fe}h} = \alpha_{\mathrm{Cu}hl}^2 \overline{\mathcal{E}}_{\mathrm{Fe}h} \tag{3.11b}$$

The constants of complex propagation are expressed as follows:

1. for forward rotating fields (h = 1,7,13,19,):

$$\alpha_{\text{Cu}h}^{+} = (j\omega_{h}^{+}\mu_{0}\sigma_{\text{Cu}})^{1/2} = (1+j)(\pi h f s_{h}^{+}\mu_{0}\sigma_{\text{Cu}})^{\frac{1}{2}}$$
(3.12a)

$$\alpha_{\text{Fe}h}^+ = (j\omega_h^+ \mu_0 \mu_{\text{re}} \sigma_{\text{Fe}})^{1/2}$$
  
=  $(a_R + ja_x) \times (\pi h f s_h^+ \mu_0 \mu_{\text{rs}} \sigma_{\text{Fe}})^{1/2} (3.12b)$ 

2. for backward rotating fields (h = 5,11,17,23):

$$\alpha_{\text{Cu}h}^- = (j\omega_h^- \mu_0 \sigma_{\text{Cu}})^{1/2} = (1+j)(\pi h f s_h^- \mu_0 \sigma_{\text{Cu}})^{\frac{1}{2}}$$
 (3.13a)

$$\alpha_{\text{Fe}h}^- = (j\omega_h^- \mu_0 \mu_{\text{re}} \sigma_{\text{Fe}})^{1/2} \tag{3.13b}$$

$$= (a_R + ja_X) \times (\pi h f s_h^- \mu_0 \mu_{rs} \sigma_{Fe})^{1/2}$$
 (3.13c)

$$s_h^+ = 1 - \frac{1}{h}(1 - s) \tag{3.14a}$$

$$s_h^- = 1 + \frac{1}{h}(1 - s) \tag{3.14b}$$

Thus the rotor's magnetic flux and eddy currents have the following angular frequencies:

$$\omega_h^+ = 2\pi f h s_h^+ = \omega h s_h^+ \tag{3.15a}$$

$$\omega_h^+ = 2\pi f h s_h^+ = \omega h s_h^+$$
 (3.15a)  
 $\omega_h^- = 2\pi f h s_h^- = \omega h s_h^-$  (3.15b)

where  $\omega = 2\pi f$  is the angular frequency of the fundamental harmonic for the stator current:

The electric field intensity components in the y direction do not exist, that is,  $E_{\rm Cuhy} = 0$  and  $E_{\rm Fehy} = 0$ 

Using separation of variables, the general solutions for Eqs. 3.9a to 3.15b is

1. For  $0 \le y \le g$  and  $y \ge g + d1 + d2$ :

$$F_h = \left(C_{1h}e^{-jcx} + C_{2h}e^{jcx}\right)\left(C_{3h}e^{-cy} + C_{4h}e^{cxy}\right) \tag{3.16}$$

2. For  $g \leq y \leq g + d2$ :

$$F_{\text{Cu}h} = \left(C_{1\text{Cu}h}e^{-jcx} + C_{2\text{Cu}h}e^{jcx}\right) \times \left(C_{3\text{Cu}h}e^{-\kappa_{\text{Cu}h}^2 + C_{4\text{Cu}h}e^{\kappa_{\text{Cu}h}^2}}\right) (3.17)$$

3. For  $g + d2 \le y \le g + d2 + d1$ :

$$F_{\text{Fe}h} = \left(C_{1\text{Fe}h}e^{-jcx} + C_{2\text{Fe}h}e^{jcx}\right) \times \left(C_{3\text{Fe}h}e^{-\kappa_{\text{Fe}h}y} + C_{4\text{Fe}h}e^{\kappa_{\text{Fe}h}y}\right) (3.18)$$

where  $F_h$  stands for the air's electric and magnetic field intensity components,  $F_{\text{Cuh}}$  " for the nonmagnetic layer's components, and  $F_{\text{Feh}}$  " for the ferromagnetic material's components.

If  $F_h = X_h y_h$ ,  $F_{\text{Cu}h} = X_{\text{Cu}h} y_{\text{Cu}h}$ , and  $F_{\text{Fe}h} = X_{\text{Fe}h} y_{\text{Fe}h}$ , the propagation constants  $\kappa_{\text{Cuh}}$  and  $\kappa_{\text{Feh}}$  dependent on the polepitch  $\tau$  are equal to:

$$\kappa_{\text{Cu}h} = (\alpha_{\text{Cu}h}^2 + c^2)^{1/2} \tag{3.19}$$

$$\kappa_{\text{Fe}n}^2 = (\alpha_{\text{Fe}h}^2 + c^2)^{1/2}$$
(3.20)

where:

$$c = \frac{\pi}{\tau} \tag{3.21}$$

The constants  $C_{ih}C_{iCuh}$  and  $C_{iFeh}$  where i = 1,23,4 in Eqs. 3.16, 3.17, and 3.18 can be got from the following boundary conditions:

$$H_{xh}(x,0) = -a_{1h}(x) (3.22)$$

$$H_{xh}(x,g) = H_{xCuh}(x,g) \tag{3.23}$$

$$H_{x\text{Cu}h}(x, g + d1) = H_{x\text{Fe}h}(x, g + d1)$$
 (3.24)

$$H_{xFeh}(x, g + d1 + d2) = H_{xh}(x, g + d1 + d2)$$
 (3.25)

$$H_{\nu h}(x,g) = H_{\nu Cuh}(x,g)$$
 (3.26)

$$H_{\nu \text{Cu}h}(x, g + d1) \approx \mu_{\text{re}} H_{\nu \text{Fe}h}(x, g + d1) \tag{3.27}$$

$$\mu_{\text{re}} H_{\text{yFe}h}(x, g + d1 + d2) \approx H_{\text{y}h}(x, g + d1 + d2)$$
 (3.28)

and from the fundamental equation of electromagnetic fields,

In other words, ignoring displacement and convection current, curl  $\overline{H} = \sigma \overline{E}$ , div  $\overline{B} = 0$ , and div  $\overline{E} = 0$ . Eq. 3.17 provides the line-current density  $a_{1n}(x)$   $C_{4h} = 0$  for  $y \ge g + d1 + d2$  because the electromagnetic field decays fully for  $y \rightarrow \infty$ . The solution of the electromagnetic field equations is finished once the complex constants  $C_{ih}$ ,  $C_{iCuh}$  and  $C_{iFeh}$ , have been determined.

### 1. For $0 \le y \le g$ :

$$H_{xh}^{+} = \frac{1}{M_{4h}^{+}} (-A_{mh}^{+}) e^{-jcx} \left[ \frac{\kappa_{\text{Cu}h}^{+}}{c} M_{3h}^{+} \cosh c(y - g) - W_{3n}^{+} \sinh c(y - g) \right] (3.29a)$$

$$H_{xh}^{-} = \frac{1}{M_{4h}^{-}} (-A_{mh}^{-}) e^{jcx} \left[ \frac{\kappa_{Cuh}^{-}}{c} M_{3h}^{-} \cosh c(y - g) - W_{3h}^{-} \sinh c(y - g) \right]$$

$$-W_{3h}^{-} \sinh c(y - g)$$

$$H_{yh}^{+} = \frac{1}{M_{4h}^{+}} j A_{mh}^{+} e^{-jcx} [W_{3h}^{+} \cosh c(y - g) - \frac{\kappa_{Cuh}^{-}}{c} M_{3h}^{+} \sinh c(y - g) \right]$$

$$-\frac{\kappa_{Cuh}^{-}}{c} M_{3h}^{-} \sinh c(y - g)$$

$$-\frac{\kappa_{Cuh}^{-}}{c} M_{3h}^{-} \sinh c(y - g)$$

$$E_{zh}^{+} = \frac{1}{M_{4h}^{+}} \frac{jn\omega\mu}{c} A_{mh}^{-} e^{-jcx} [W_{3h}^{+} \cosh c(y - g) - \frac{\kappa_{Cuh}^{-}}{c} M_{3h}^{+} \sinh c(y - g)$$

$$-\frac{\kappa_{Cuh}^{-}}{c} M_{3h}^{+} \sinh c(y - g)$$

$$E_{zh}^{-} = \frac{1}{M_{4h}^{-}} \frac{jh\omega\mu}{c} A_{mh} e^{-jcx} [W_{3h}^{-} \cosh c(y - g) - \frac{\kappa_{Cuh}^{-}}{c} M_{3h}^{-} \sinh c(y - g) ]$$

$$(3.31a)$$

$$E_{zh}^{-} = \frac{1}{M_{4h}^{-}} \frac{jh\omega\mu}{c} A_{mh} e^{-jcx} [W_{3h}^{-} \cosh c(y - g) - \frac{\kappa_{Cuh}^{-}}{c} M_{3h}^{-} \sinh c(y - g) ]$$

$$(3.31b)$$

## 2. For $g \le y \le g + d$ :

$$H_{x\text{Cu}h}^{+} = \frac{1}{M_{h4}^{+}} \frac{\kappa_{\text{Cu}h}^{+}}{c} (-A_{mh}^{+}) e^{-jcx} \left[ \frac{\kappa_{\text{Fe}h}^{+}}{\kappa_{\text{Cu}h}^{+}} M_{2h}^{+} \times \cosh \kappa_{\text{Cu}h}^{+} (y - g - d2) - \mu_{\text{re}} W_{2h}^{+} \sinh \kappa_{\text{Cu}h}^{+} (y - g - d2) \right] (3.32a)$$

$$H_{x\text{Cu}h}^{-} = \frac{1}{M_{h4}^{-}} \frac{\kappa_{\text{Cu}h}^{-}}{c} (-A_{mh}^{-}) e^{jcx} \left[ \frac{\kappa_{\text{Fe}h}^{-}}{\kappa_{\text{Cu}h}^{-}} M_{2h}^{-} \times \cosh \kappa_{\text{Cu}h}^{-} (y - g - d2) - \mu_{\text{re}} W_{2h}^{-} \sinh \kappa_{\text{Cu}h}^{-} (y - g - d2) \right] (3.32b)$$

$$H_{y\text{Cu}h}^{+} = \frac{1}{M_{h4}^{+}} j A_{mh}^{+} e^{-jcx} [\mu_{\text{re}} W_{h2}^{+} \cosh \kappa_{\text{Cu}h}^{+} (y - g - g)]$$

$$d2)] - \frac{\kappa_{\text{Fe}h}^{+}}{\kappa_{\text{Cu}h}^{+}} M_{2h}^{+} \sinh \kappa_{\text{Cu}h}^{+} (y - g - d2) \bigg] (3.33a)$$

$$\begin{split} &H_{y\text{Cuh}}^{-} = \frac{1}{M_{h4}^{-}} \left( -jA_{tmh}^{-}e^{jcx} \right) [\mu_{\text{re}}W_{h2}^{-}\cosh\kappa_{\text{Cuh}}^{-}(y-g-d2) \\ &- \frac{\kappa_{\text{Feh}}^{+}}{\kappa_{\text{Cuh}}^{+}} M_{2h}^{-}\sinh\kappa_{\text{Cuh}}^{-}(y-g-d2) \right] \\ &E_{z\text{Cuh}}^{+} = \frac{1}{M_{h4}^{+}} \frac{j\omega_{h}^{+}\mu}{c} A_{mh}^{+}e^{-jcx} [\mu_{\text{re}}W_{h2}^{+}\cosh\kappa_{\text{Cuh}}^{+}(y-g-d2) \\ &- \frac{\kappa_{\text{Feh}}^{+}}{\kappa_{\text{Cuh}}^{+}} M_{2h}^{+}\sinh\kappa_{\text{Cuh}}^{+}(y-g-d2) \right] \\ &E_{z\text{Cuh}}^{-} = \frac{1}{M_{h4}^{-}} \frac{j\omega_{h}^{-}\mu}{c} A_{mhl}^{-}e^{jcx} [\mu_{\text{re}}W_{h2}^{-}\cosh\kappa_{\text{Cuh}}^{-}(y-g-d2) \\ &- \frac{\kappa_{\text{Feh}}^{-}}{\kappa_{\text{Cuh}}^{-}} M_{2h}^{-}\sinh\kappa_{\text{Cuh}}^{-}(y-g-d2) \right] \\ &3. \text{ For } g + d2 \leqslant z \leqslant g + d1 + d2) : \\ &H_{x\text{Feh}}^{+} = \frac{1}{M_{h4}^{+}} \frac{\kappa_{\text{Feh}}^{+}}{c} \left( -A_{mh}^{+}\right) e^{-jcx} \left[ \frac{c}{\kappa_{\text{Feh}}^{+}}\cosh\kappa_{\text{Feh}}^{+}(y-g-d1-d2) \\ &- \frac{1}{\mu_{\text{re}}}\sinh\kappa_{\text{Feh}}^{+}(y-g-d1-d2) \right] \\ &H_{x\text{Feh}}^{-} = \frac{1}{M_{h4}^{-}} \frac{\kappa_{\text{Feh}}^{-}}{c} \left( -A_{mh}^{-}\right) e^{jcx} \left[ \frac{c}{\kappa_{\text{Feh}}^{+}}\cosh\kappa_{\text{Feh}}^{-}(y-g-d1-d2) \\ &- \frac{1}{\mu_{\text{re}}}\sinh\kappa_{\text{Feh}}^{-}(y-g-d1-d2) \right] \\ &H_{y\text{Feh}}^{+} = \frac{1}{M_{h4}^{+}} jA_{mh}^{+}e^{-jcx} \left[ \frac{1}{\kappa_{\text{Feh}}^{+}}\cosh\kappa_{\text{Feh}}^{-}(y-g-d1-d2) \\ &- \frac{c}{\kappa_{\text{Feh}}^{+}}\sinh\kappa_{\text{Feh}}^{+}(y-g-d1-d2) \right] \\ &H_{y\text{Feh}}^{-} = \frac{1}{M_{h4}^{+}} \left( -jA_{mh}^{+}\right) e^{jcx} \left[ \frac{1}{\mu_{\text{re}}}\cosh\kappa_{\text{Feh}}^{-}(y-g-d1-d2) \\ &- \frac{c}{\kappa_{\text{Feh}}^{+}}\sinh\kappa_{\text{Feh}}^{+}(y-g-d1-d2) \right] \\ &E_{z\text{Feh}}^{+} = \frac{1}{M_{h4}^{+}} \frac{j\omega_{h}^{+}\mu_{\text{Fe}}}{c} A_{mh}^{+}e^{-jcx} \left[ \frac{1}{\mu_{\text{re}}}\cosh\kappa_{\text{Feh}}^{-}(y-g-d1-d2) \\ &- \frac{c}{\kappa_{\text{Feh}}^{+}}\sinh\kappa_{\text{Feh}}^{+}(y-g-d1-d2) \right] \\ &G_{x\text{Feh}}^{-} = \frac{1}{M_{h4}^{+}} \frac{j\omega_{h}^{+}\mu_{\text{Fe}}}{c} A_{mh}^{+}e^{-jcx} \left[ \frac{1}{\mu_{\text{Fe}}}\cosh\kappa_{\text{Feh}}^{-}(y-g-d1-d2) \\ &- \frac{c}{\kappa_{\text{Feh}}^{+}}\sinh\kappa_{\text{Feh}}^{+}(y-g-d1-d2) \right] \\ &- \frac{c}{\kappa_{\text{Feh}}^{+}}\sinh\kappa_{\text{Feh}}^{+}(y-g-d1-d2) \right] \\ &G_{x\text{Feh}}^{-} = \frac{1}{M_{h4}^{+}} \frac{j\omega_{h}^{+}\mu_{\text{Fe}}}{c} A_{mh}^{+}e^{-jcx} \left[ \frac{1}{\mu_{\text{Fe}}}\cosh\kappa_{\text{Feh}}^{-}(y-g-d1-d2) \\ &- \frac{c}{\kappa_{\text{Feh}}^{+}}\sinh\kappa_{\text{Feh}}^{-}(y-g-d1-d2) \right] \\ &- \frac{c}{\kappa_{\text{Feh}}^{+}}\sinh\kappa_{\text{Feh}}^{-}(y-g-d1-d2) \right] \\ &- \frac{c}{\kappa_{\text{Feh}}^{+}}\sinh\kappa_{\text{Feh}}^{-}(y-g-d1-d2) \right] \\ &- \frac{c}{\kappa_{\text{F$$

$$E_{z\text{Fe}h}^{-} = \frac{1}{M_{h4}^{-}} \frac{j\omega_{h}^{-}\mu\mu_{\text{re}}}{c} A_{mhl}^{-} e^{jcx} \left[ \frac{1}{\mu_{\text{re}}} \cosh \kappa \overline{\text{Fe}h} (y - g - d1 - d2) - \frac{c}{\kappa \overline{\text{Fe}h}} \sinh \kappa \overline{\text{Fe}h} (y - g - d1 - d2) \right] (3.37b)$$

where:

$$M_{4h} = \frac{\kappa_{\text{Cu}h}}{c} M_{3h} \cosh cg + W_{3h} \sinh cg$$
 (3.38)

$$W_{4h} = W_{3h} \cosh cg + \frac{\kappa_{\text{Cu}h}}{\beta} M_{3h} \sinh cg \qquad (3.39)$$

$$M_{3h} = \frac{\kappa_{\text{Fe}h}}{\kappa_{\text{Cu}h}} M_{2h} \cosh \kappa_{\text{Cu}h} d2 + \mu_{\text{re}} W_{2h} \sinh \kappa_{\text{Cu}h} d2 \qquad (3.40)$$

$$W_{3h} = \mu_{\rm re} W_{2h} \cosh \kappa_{\rm Cu} d2 + \frac{\kappa_{\rm Fe} h}{\kappa_{\rm Cu} h} M_{2h} \sinh \kappa_{\rm Cu} d2 \qquad (3.41)$$

$$M_{2h} = \frac{c}{\kappa_{\text{Fe}h}} \cosh \kappa_{\text{Fe}h} d1 + \frac{1}{\mu_{\text{re}}} \sinh \kappa_{\text{Fe}h} d1$$
 (3.42)

$$W_{2h} = \frac{1}{\mu_{re}} \cosh \kappa_{Feh} d1 + \frac{c}{\kappa_{Feh}} \sinh \kappa_{Feh} d1$$
 (3.43)

The equations for  $y \ge g + d1 + d2$  are not important.

### 3.2.3 Rotor Impedance

For the nth time harmonic, the intrinsic impedance of the air half-space (  $\geq g + d + h_{Fe}$ ), as determined by two-dimensional electromagnetic field analysis, is:

$$\eta_{0n} = -\frac{\mathrm{j}n\omega\mu_0}{c} \tag{3.44}$$

Equations 3.35a, 3.35b, 3.37a, and 3.37b gives the intrinsic impedance of the ferromagnetic layer  $(g + d2 \le y \le g + d2 + d1)$  and the air  $(y \ge g + d1 + d2)$ 

$$\eta_{(\text{Fe+0})h} = |E_{z\text{Fe}h}/H_{x\text{Fe}h}|_{y=g+d2}$$

$$= -\frac{j\omega_h \mu_0 \mu_{\text{re}}}{\kappa_{\text{Fe}h}} \frac{(1/\mu_{\text{re}}) + (c/\kappa_{\text{Fe}h}) \tanh \kappa_{\text{Fe}h} d1}{(c/\kappa_{\text{Fe}h}) + (1/\mu_{\text{re}}) \tanh \kappa_{\text{Fe}h} d1} (3.45)$$

Inserting Eq. 3.44 into Eq. 3.45

$$\eta_{(\text{Fe+0})h} = \frac{j\omega_{h}\mu_{0}\mu_{\text{re}}}{\kappa_{\text{Fe}h}} \times \frac{(\omega_{h}/n_{\omega})(-\eta_{0h})(j\omega_{h}\mu_{0}\mu_{\text{re}}/\kappa_{\text{Fe}h})\tanh\kappa_{\text{Fe}h}d1}{(j\omega_{h}\mu_{0}\mu_{\text{re}}/\kappa_{\text{Fe}h})(\omega_{h}/n_{\omega})(-\eta_{0h})\tanh\kappa_{\text{Fe}h}d1} (3.46)$$

Denoting  $z_{0h} = j\omega_h \mu_0 \mu_{re} / \kappa_{Feh}$  and  $z_{Lh} = [\omega_h / (n\omega)] / (-\eta_{0h})$ 

$$\eta_{(\text{Fe+0})h} = -z_{0n} \frac{1 + \left(\frac{z_{oh}}{z_{Lh}}\right) \tanh \kappa_{\text{Fe}h} d1}{\left(\frac{z_{oh}}{z_{Lh}}\right) + \tanh \kappa_{\text{Fe}h} d1}$$
(3.47)

when analogy with transmission line The characteristic impedance of a transmission line is denoted by  $z_{0h}$ , while the load impedance is denoted by  $z_{Lh}$ . The input impedance of an open-circuited line or the impedance of a ferromagnetic cylinder alone can be obtained using Equation 3.47 by substituting  $z_{Lh} \rightarrow \infty$ :

$$\eta_{(\text{Fe}h+0)h} = \eta_{\text{Fe}h} = z_{0h} \frac{1}{\tanh \kappa_{\text{Fe}h} d1}$$

$$= -\frac{j\omega_h \mu_0 \mu_{\text{re}}}{\kappa_{\text{Fe}h}} \frac{1}{\tanh \kappa_{\text{Fe}h} d1}$$
(3.48a)

A similar method can be used to determine the intrinsic impedance of the copper layer for the nth time harmonic.:

$$\eta_{\text{Cu}h} = \frac{j\omega_h \mu_0 \mu_{\text{re}}}{\kappa_{\text{Cu}h}} \frac{1}{\tanh \kappa_{\text{Cu}h} d2}$$
(3.48b)

If, $d_1 \to \infty$ ,  $\tanh(\kappa_{h1}d_1) \to 1$ , and

$$\eta_{\mathrm{Cu}h} = j\omega_h \mu_1 / \kappa_{h1}$$

The complex propagation constant for a ferromagnetic rotor material in a balanced three-phase system with a fundamental magnetic field can be written as:

$$\alpha_{\text{Fe}} = \sqrt{jw\mu_0\mu_{\text{rs}}\sigma_{\text{Fe}}} = (a_{\text{R}} + ja_{\text{x}})k_{\text{Fe}}$$
 (3.49)

The conductivity of the rotor (S/m) is represented by  $\alpha_{Fe}$ , the resistance coefficient  $a_R$  .that accounts for hysteresis losses and nonlinear magnetic permeability . the reactance coefficient  $a_x$  that accounts for hysteresis losses and nonlinear magnetic permeability, the electromagnetic field attenuation coefficient (1/m) by  $k_{Fe}$  the angular frequency (rad/s) by w, the free space magnetic permeability (H/m), and the relative magnetic permeability of the surface (H/m) by  $\mu_0$ ...:

$$z_{\text{Cu}h}(s_n) = \frac{k_{\text{tr}}L_2}{\tau\eta_{\text{Cu}h}}$$
 (3.50)

$$z_{\text{Cu}h}(s_n) = \frac{k_{\text{tr}}L_2}{\tau\eta_{\text{Cu}h}}$$

$$z_{\text{Fe}h}(s_n) = \frac{k_{\text{tr}}L_2}{\tau\eta_{\text{Fe}h}}$$
(3.50)
$$(3.51)$$

The winding factor  $k_{w2} = 1$ , the number of phases  $m_2 = 2p$ , and the number of turns  $N_2 = 1/2$  for a solid rotor, so that

$$k_{\rm tr} = \frac{m_1 (N_1 k_{w1})^2}{m_2 (N_2 k_{w2})^2} = \frac{6(N_1 k_{w1})^2}{p}$$
(3.52)

where p is the number of pole pairs.

Therefore, the rotor impedance for a balanced, three-phase system under fundamental field conditions successfully derived: has been

$$Z_{r} = \frac{jw\mu_{Fe}}{k_{Fe}} \frac{L}{\tau} = \frac{jw\mu_{Fe}\sigma_{Fe}}{k_{Fe}\sigma_{Fe}} \frac{L}{\tau} \approx \frac{\alpha_{Fe}}{\sigma_{Fe}} \frac{L}{\tau}$$
(3.53a)

By substituting the expressions for rotor length (L) in meters and pole pitch ( $\tau$ ) in meters from equations (1) and (2) into equation (3), we arrive at the following new expression for the rotor impedance, Zr:

$$Z_{r} = (a_{R} + ja_{x}) \frac{L}{\tau} \sqrt{\frac{w\mu_{0}\mu_{rs}}{2\sigma_{Fe}}}$$
(3.53b)

for positive sequence rotating fields, fr += sf, and for rotating fields of negative sequence, fr=(2-s)f, are as follows:

$$Z_{r} = (a_{R} + ja_{x}) \frac{L}{\tau} \sqrt{\frac{\pi f_{r} \mu_{0} \mu_{rs}}{\sigma_{Fe}}}$$
(3.54)

To find the stator referred rotor impedance, we multiply the impedance from equation (3.25) by the transformation coefficient. The resulting expression is:

$$k_{t} = \frac{2 m_{1} (N_{1} k_{w1})^{2}}{p}$$
 (3.55)

The rotor impedance referred to the stator is given by:

$$Z_r' = (a_R + ja_x)k_t k_z \frac{L}{\tau} \sqrt{\frac{\pi f \mu_0 \mu_{rs}}{\sigma_{Fe}}}$$
(3.56)

For positive rotating field  $f_r^+ = sf$ , rotor impedance stator referred is given by:

$$Z'_{r+} = (a_R + ja_x)k_tk_z \frac{L}{\tau} \sqrt{\frac{\pi sf\mu_0\mu_{rs}}{\sigma_{Fe}}}$$
(3.57)

$$R'_{r+} = a_R k_t k_z \frac{L}{\tau} \sqrt{\frac{\pi s f \mu_0 \mu_{rs}}{\sigma_{Fe}}} = a_R Z_c \sqrt{\mu_{rs}} \sqrt{s}$$
 (3.58)

$$X'_{r+} = a_X k_t k_z \frac{L}{\tau} \sqrt{\frac{\pi s f \mu_0 \mu_{rs}}{\sigma_{Fe}}} = a_X Z_c \sqrt{\mu_{rs}} \sqrt{s}$$
 (3.59)

For negative sequence rotating field  $f_r^- = (2 - s)f$ , rotor impedance referred to stator is given by:

$$Z'_{r-} = (a_R + jja_x)k_tk_z \frac{L}{\tau} \sqrt{\frac{\pi(2-s)f\mu_0\mu_{rs}}{\sigma_{Fe}}}$$
 (3.60)

$$R'_{r-} = a_R k_t k_z \frac{L}{\tau} \sqrt{\frac{\pi (2-s) f \mu_0 \mu_{rs}}{\sigma_{Fe}}} = a_R Z_c \sqrt{\mu_{rs}} \sqrt{2-s}$$
 (3.61)

$$X'_{r-} = a_X k_t k_z \frac{L}{\tau} \sqrt{\frac{\pi (2-s) f_0 \mu_{rs}}{\sigma_{Fe}}} = a_X Z_c \sqrt{\mu_{rs}} \sqrt{2-s}$$
 (3.62)

where  $Z_c = k_t k_z \frac{L}{\tau} \sqrt{\frac{\pi f \mu_0}{\sigma_{Fe}}}$ . is the constant value of rotor impedance which is not dependent on the values of slip s and the surface relative magnetic permeability  $\mu_{rs}$ .

$$R_{\rm r}' = \frac{R_{2s}'}{s} = a_R Z_c \sqrt{\frac{\mu_{rs}}{s}}$$
 (3.63)

$$X_{\rm r}' = \frac{X_{2s}'}{s} = a_{x} Z_{c} \sqrt{\frac{\mu_{rs}}{s}}$$
 (3.64)

in which

$$a_{Rh} = \frac{1}{\sqrt{2}} \left\{ \left[ 4a_R^2 a_X^2 + \left( a_R^2 - a_X^2 + \frac{c^2}{k_h^2} \right) \right]^{\frac{1}{2}}$$
 (3.65)

$$a_{Xh} = \frac{1}{\sqrt{2}} \left\{ \left[ 4a_R^2 a_X^2 + \left( a_R^2 - a_X^2 + \frac{c^2}{k_h^2} \right) \right]^{\frac{1}{2}}$$
 (3.66)

or

$$a_{Rh} = \frac{1}{\sqrt{2}} \sqrt{\left\{ \left[ 4a_R^2 a_X^2 + \left( a_R^2 - a_X^2 + \frac{c^2}{k_h^2} \right) \right]^{\frac{1}{2}} + \left( a_R^2 - a_X^2 + \frac{c^2}{k_h^2} \right) \right\}}$$
 (3.67a)

$$a_{Xh} = \frac{1}{\sqrt{2}} \sqrt{\left\{ \left[ 4a_R^2 a_X^2 + \left( a_R^2 - a_X^2 + \frac{c^2}{k_h^2} \right) \right]^{\frac{1}{2}} + \left( -a_R^2 + a_X^2 + \frac{c^2}{k_h^2} \right) \right\}}$$
 (3.67b)

Where

$$c_h = \frac{h\pi}{\tau}$$

The resultant impedance of a solid rotor covered with a copper layer is:

$$Z'_{2h}(s_h) = \frac{Z'_{Cuh}(s_h)Z'_{Feh}(s_h)}{Z'_{Cuh}(s_h)Z'_{Feh}(s_h)}$$
(3.68a)

$$= R'_{2h}(s_h) + jX'_{2h}(s_h) \tag{3.68b}$$

where  $R'_{2h}(s_h = \text{Re}[Z'_{2h}(s_h)], X'_{2h}(s_h) = \text{Im}[Z'_{2h}(s_h)], s_h = s_h^+$  for h = 1,7,13,19,... is according to Eq. 3.14a, and  $s_h = s_h^-$  for h = 5,11,17,23,... is according to Eq. 3.14b.

#### 3.2.4 End Effect

The performance of the motor is greatly affected by the end fields when the rotor is made of ferromagnetic material without high conductive end rings[22]. An excessively optimistic estimate of the motor's output power will result from underestimating the rotor impedance due to the end-area effects of a solid steel rotor.

One of the biggest challenges in solid rotors is the end effects problem[84]. If the current routes are nearly axial due to the rotor's thick end rings and extremely low impedance, then ignoring the issue can be acceptable[2]. However, even solid rotors with copper end rings do not operate under this premise. The torque at a given slip is 10–30% higher than the measured values when a solid-rotor with copper end rings is used without taking end effects into account [96].

In his analysis, Wood [114]created an approximation whose validity is called into question. A complex factor that can be used for the rotor impedance was proposed by Angst [115] and was obtained by solving the three-dimensional field problem under constant permeability. 3D field problem with constant permeability was similarly resolved by Yee [29], Ducreux [51] calculated the end effects using 2D and 3D FEM programs, comparing the 3D results with 2D results corrected by factors from Yee and Russell [46]

An analogous conductivity for the rotor material can be used to make precise calculations for solid rotors with end rings. When taking into consideration the conductivity of the rotor, this equivalent conductivity takes into account the resistivity of the end rings.

The rotor impedance should be calculated using a sophisticated corrective endeffect factor that accounts for the three-dimensional rotor end effects.

$$\underline{Z}_{corr} = \underline{k}_{er} \underline{Z}_{r}$$
 (3.69)

Since the end-effect factor (ker) must take into consideration the end-region's inductance, it is basically a complex number. This is significant because the impedance angle in the rotor's active regions may be different from that at the end-region. Consequently, the rotor impedance's phase angle is:

$$\cos \varphi_{t} = \frac{R_{s}}{Z_{t}} = \frac{R_{t}}{\sqrt{R_{t}^{2} + (\omega_{t} L_{to})^{2}}} = \frac{R_{t}}{\sqrt{R_{t}^{2} + (s\omega_{s} L_{ro})^{2}}}$$
(3.70)

According to Trickey, Russell, Yee, O'Kelly, and Woolley, the 3D rotor end effects are usually taken into consideration by modifying the rotor's conductivity with end-factor. The rotor phase angle is not taken into account by these end-factors, which are only applied to the resistive portion of the rotor impedance.

It was thought that the resistivity adjustment by an end-effect factor k might be used to modify the rotor material equivalent conductivity  $\sigma$  in the case of numerical computations of a solid iron rotor.

$$\sigma_{\rm corf} = k\sigma \tag{3.71}$$

The Russell correction factor is [96]

$$k_{\text{Russell}} = 1 - \frac{2\tau_{\text{p}}}{\pi l} \tanh\left(\frac{\pi l}{2\tau_{\text{p}}}\right)$$
 (3.72)

where  $t_p$  is the pole pitch and  $l_r$  is the rotor length.

According to Yee, the end-factor for a smooth solid rotor is defined as

$$k_{\text{Yee}} = \frac{\frac{\pi}{\tau_{\text{p}}} l_{\text{r}} \left( 1 + \coth\left(\frac{\pi l_{\text{r}}}{2\tau_{\text{p}}}\right) \right)}{\frac{\pi}{\tau_{\text{p}}} l_{\text{r}} \left( 1 + \coth\left(\frac{\pi l_{\text{r}}}{2\tau_{\text{p}}}\right) \right) - 2}$$
(3.73)

According to Trickey[27], the end-factor depends on the inner and outer diameters and the pole pair number of the rotor, and is defined as

$$k_{\text{Trickey}} = \frac{p}{2} \left[ \frac{1 + \left(\frac{D_{\text{in}}}{D_{\text{r}}}\right)^{p}}{1 - \left(\frac{D_{\text{in}}}{D_{\text{r}}}\right)^{p}} \right] \left(1 - \frac{D_{\text{in}}}{D_{\text{r}}}\right)$$
 (3.74)

where *p* is the number of pole pairs and Dr is the rotor's outer diameter. The slit depth can be used to define the inner diameter Din in the case of a slitted solid rotor:

$$D_{\rm in} = D_{\rm r} - 2h_{\rm slit} \tag{3.75}$$

where hslit stands for the rotor slitting depth. It should be mentioned that the rotor length is not taken into account by Eq. (3.72). The End correction factor is a constant value for all rotor lengths in accordance with Trickey's formula.

An expression defining the end factor that lowers the rotor equivalent conductivity was put out by O'Kelly [30]. The end effect correction factor k was proposed to be expressed as

$$k_{\text{O'Kelly}} = \frac{l_{\text{r}}}{l_{\text{r}} + \frac{\pi r_{\text{ave}}}{p}}$$
 (3.76)

where  $r_{ave}$  is the average radius of the rotor.

Woolley[47] determined the end factor k as

$$k_{\text{Woolley}} = \left[ \frac{1}{2} \left( Q_1 + \sqrt{Q_1^2 + 4k_1 \cdot \tanh\left(\frac{pl_r}{D_r}\right)} \right) \right]$$
(3.77)

The variables Q1 and k1 are defined as

$$Q_{1} = 1 - \left(\frac{D_{r}}{pl_{t}} + k_{1}\right) \tanh\left(\frac{pl_{t}}{D_{r}}\right).$$

$$where: k_{1} = \frac{z_{er}\rho_{c}}{h_{slit}\rho_{er}}$$
(3.78)

where hslit is the slit depth,  $\rho c$  is the cylindrical shell region resistivity, and zer and  $\rho er$  stand for the end region thickness and resistivity, respectively. The square of the edge factor reciprocal  $k_z$  must be multiplied by the solid steel conductivity  $\sigma_{Fe}$  in the  $k_{Fe}$  parameter in order to incorporate the end effect.:

$$\sigma_{\rm Fe} = \frac{\sigma_{\rm Fe}}{k_z^2} \tag{3.79}$$

Where: $k_z = 1 + \frac{2}{\pi} \frac{\tau}{L}$ 

substituting (3.79) into (3.60), yields:

$$Z_{r} = (a_{R} + jax_{x})k_{z} \frac{L}{\tau} \sqrt{\frac{\pi f_{r} \mu_{0} \mu_{rs}}{\sigma_{Fe}}}$$
(3.80)

For simplicity The Russell correction factor (eq 3.72) is used in this study.

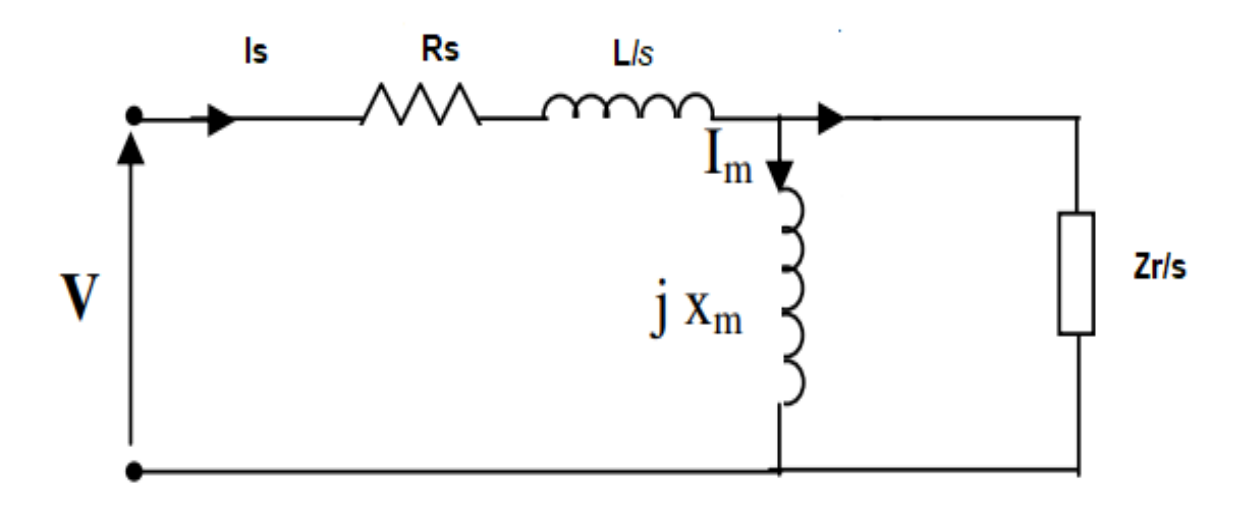


Fig.3.3. Equivalent Circuit Per Phase of SRIM.

### 3.3. DQ Model and Simulation

### 3.3.1. DQ Model

In fact, the dq model is a fundamental method for the dynamic performance analysis of an induction motor and is specifically applied to HS-SRIMs. This model allows the stator and rotor quantities of the three-phase system to be transformed into a two-axis orthogonal system-namely, the direct axis 'd' and

quadrature axis 'q', which simplify the analysis of the motor's behavior under various operating conditions.

An electrical model of the machine based on dq0 quantities is presented in this section.

By studying the equivalency between three-phase and two-phase machines, the dynamic model of an induction motor may be constructed. Based on the amount of MMF generated in two-phase and three-phase windings with similar current magnitudes, the equivalency is determined.

The two-phase winding will have 3,-s/2 turns per phase for MMF equality if each of the three-phase windings has N-s. turns per phase and equal current magnitudes. Resolving the MMF of the three-phase along the d and q axes yields the MMF of the d and q axes. The existing equalities remain once the common term, the number of turns, is cancelled on both sides of equations. Under balanced circumstances, the three-phase stator voltages of an induction machine can be written as [116][117].

$$V_a = \sqrt{2}V_{rms}\sin(\omega t) \qquad (3.81a)$$

$$V_b = \sqrt{2}V_{rms}\sin(\omega t - 2\pi/3) \qquad (3.81b)$$

$$V_c = \sqrt{2}V_{rms}\sin(\omega t + 2\pi/3) \qquad (3.81c)$$

$$\begin{bmatrix}
\lambda_{a} \\
\lambda_{b} \\
\lambda_{c} \\
\lambda_{f}
\end{bmatrix} = \begin{bmatrix}
\ell_{aa} & \ell_{ab} & \ell_{ac} & \ell_{af} \\
\ell_{ba} & \ell_{bb} & \ell_{bc} & \ell_{bf} \\
\ell_{ca} & \ell_{cb} & \ell_{cc} & \ell_{cf} \\
\ell_{ma} & \ell_{mb} & \ell_{mc} & \ell_{ff}
\end{bmatrix} \begin{bmatrix}
-i_{a} \\
-i_{b} \\
-i_{c} \\
i_{f}
\end{bmatrix}$$
(3.82)

where  $V_a$ .  $V_b$ .  $V_c$  are the three line voltage

λa, λb, and λc represent the flux linkages of the stator.

ia, ib, and ic are the stator currents, which are also the output currents from the generator. The negative signs indicate that the currents are considered positive when they flow out of the generator.

λf corresponds to the flux linkage analogous to the field winding.

if is the current analogous to the current flowing through the field winding. Based on these definitions, we have:

$$v_{a} = R_{a}i_{a} \frac{d}{dt}\lambda_{a} \qquad (3.83a)$$

$$v_{b} = -R_{a}i_{b} + \frac{d}{dt}\lambda_{b} \qquad (3.83b)$$

$$v_{c} = -R_{a}i_{c} + \frac{d}{dt}\lambda_{c} \qquad (3.83c)$$

$$v_{f} = R_{f}i_{f} + \frac{d}{dt}\lambda_{f} \qquad (3.83d)$$

Where:

 $v_a$ ,  $v_b$ ,  $v_c$  denote the stator terminal voltages (generator output voltages);

 $v_f$  denotes the field winding voltage.

 $R_a$  denotes the resistance of each winding on the stator.

 $R_f$  denotes the field winding resistance.

The position of the rotor affects the mutual and self-inductances in (3.81). The self-inductances of the stator are provided by

$$\ell_{ab} = \ell_{ba} = L_{ab} + L_{g2} \cos(2\theta - 120^{\circ}) \quad (3.84)$$

$$\ell_{bc} = \ell_{cb} = L_{ab} + L_{g2} \cos(2\theta) \quad (3.84b)$$

$$\ell_{ac} = \ell_{ca} = L_{ab} + L_{g2} \cos(2\theta + 120^{\circ}) \quad (3.84c)$$

$$\ell_{ff} = L_{ff} \quad (3.84d)$$

and the stator to stator mutual inductances are:

$$\ell_{aa} = L_{aa} + L_{g2}\cos(2\theta) \tag{3.84e}$$

$$\ell_{bb} = L_{aa} + L_{g2}\cos(2\theta + 120^{\circ}) \tag{3.84}f$$

$$\ell_{cc} = L_{aa} + L_{a2}\cos(2\theta - 120^{\circ}) \tag{3.84g}$$

These inductances consist of a sinusoidal term that varies with  $2\theta$  and a constant term. In the event that the rotor is not exactly round, which results in "saliency effects," this extra term is necessary. Furthermore, depending on the rotor position, the stator-to-rotor mutual inductances change and are determined by

$$\ell_{am} = \ell_{ma} = L_m \cos(\theta)$$
 (3.85a)  
 $\ell_{bm} = \ell_{mb} = L_m \cos(\theta - 120^\circ)$  (3.85b)  
 $\ell_{cm} = \ell_{mc} = L_m \cos(\theta + 120^\circ)$  (3.85c)

and the self-inductance of the field winding is the same (3.84d), which is an equilibrium point because the inductances change over time due to the rotor angle  $\theta$ , now it can be created an equivalent model based on dq0 as a result. The Clarke-Park transform is the name of such a model [118].

Balanced three-phase values can be transformed into balanced two-phase quadrature quantities using Clarke's transformation. The Park Transformation Vectors of a balanced two-phase orthogonal stationary system are transformed into an orthogonal rotating reference frame by applying this transformation. In this implementation, three reference frames are essentially considered: Threephase co-planar quantities A three-phase reference frame consists of Ia, Ib, and Ic, which positioned 120-degree are at angle another. to one Despite being in the same plane as the three-phase reference frame, I $\alpha$  (along the  $\alpha$  axis) and I $\beta$  (along the  $\beta$  axis) are perpendicular to one another in an orthogonal stationary reference frame.

An orthogonal rotating reference frame in which Id is at an angle  $\theta$  (rotation angle) to the  $\alpha$  axis and Iq is perpendicular to Id along the q axis. The three reference frames are displayed in Figure 1.

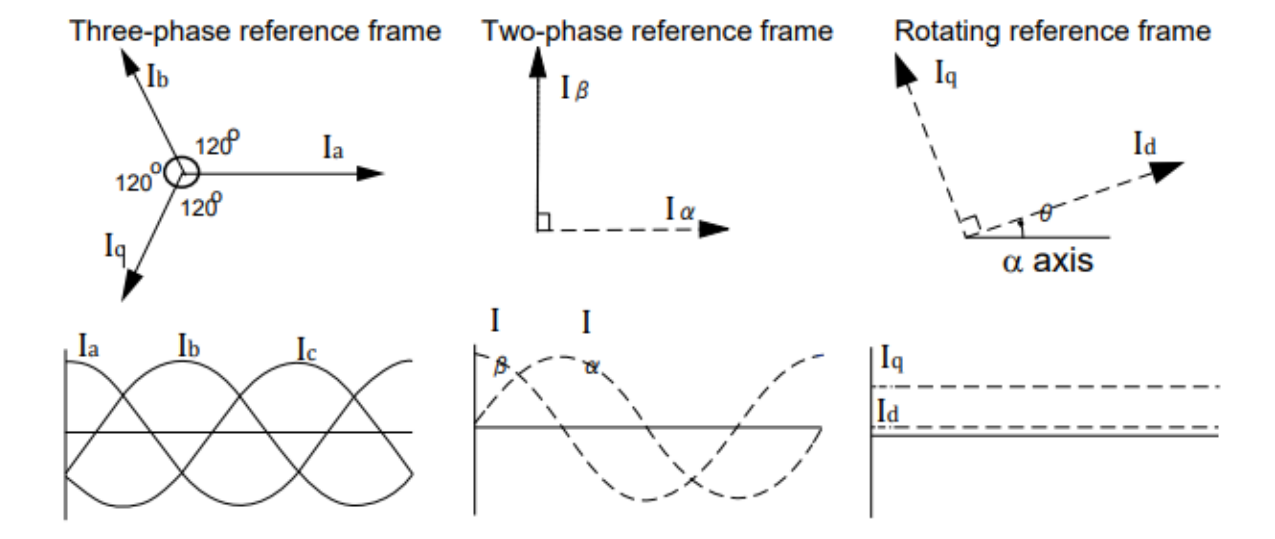


Fig.3.4. the three reference frames.

The relationship between  $\alpha\beta$  and abc is as follows [119]:

$$\begin{bmatrix} V_{\alpha} \\ V_{\beta} \end{bmatrix} = \frac{2}{3} \begin{bmatrix} 1 & \frac{1}{2} & -\frac{1}{2} \\ 0 & \frac{\sqrt{3}}{2} & -\frac{\sqrt{3}}{2} \end{bmatrix} \begin{bmatrix} V_{a} \\ V_{b} \\ V_{c} \end{bmatrix}$$
(3.86)

Then, the direct and quadrature axes voltages are:

$$\begin{bmatrix} V_d \\ V_q \end{bmatrix} = \begin{bmatrix} \cos \theta & \sin \theta \\ -\sin \theta & \cos \theta \end{bmatrix} \begin{bmatrix} V_{\alpha} \\ V_{\beta} \end{bmatrix}$$
 (3.87)

$$\begin{bmatrix} i_{\alpha} \\ i_{\beta} \end{bmatrix} = \begin{bmatrix} \cos \theta & -\sin \theta \\ \sin \theta & \cos \theta \end{bmatrix} \begin{bmatrix} i_{d} \\ i_{q} \end{bmatrix}$$
 (3.88)

The instantaneous values of the stator and rotor currents in the three-phase system are ultimately calculated using the following transformation.

$$\begin{bmatrix} i_a \\ i_b \\ i_c \end{bmatrix} = \frac{2}{3} \begin{bmatrix} 1 & 0 \\ -\frac{1}{2} & -\frac{\sqrt{3}}{2} \\ -\frac{1}{2} & -\frac{\sqrt{3}}{2} \end{bmatrix} \begin{bmatrix} i_\alpha \\ i_\beta \end{bmatrix}$$
(3.89)

That yeld equations:

$$v_d = R_a i_d + \frac{d}{dt} \lambda_d - \omega \lambda_q \qquad (3.90a)$$

$$v_q = R_a i_q + \frac{d}{dt} \lambda_q + \omega \lambda_d \qquad (3.90b)$$

$$v_0 = -R_a i_0 + \frac{d}{dt} \lambda_0 \qquad (3.90c)$$

$$v_f = R_f i_f + \frac{d}{dt} \lambda_f \qquad (3.90d)$$

The dq0 transformation of va, vb, and vc (stator terminal voltages) is represented by vd, vq, and v0.

The dq0 transformation of  $\lambda a$ ,  $\lambda b$ , and  $\lambda c$  (stator flux connections) is represented by  $\lambda d$ ,  $\lambda q$ , and  $\lambda 0$ .

$$L_{d} = L_{aa} - L_{m} + \frac{3}{2}L_{g2}$$

$$L_{q} = L_{aa} - L_{m} - \frac{3}{2}L_{g2}$$

$$L_{0} = L_{aa} + 2L_{m}$$
(3.91a)
$$(3.91b)$$

$$(3.91c)$$

The solid rotor have no field winding ,so , According to kimpark 111[120] two circuits called (f ) analogouse of (Ldr) , and (g) for (Lqr ) are placed .

To make these equations compatable with the solid round rotor motor, these considerations will be taken:

The circulation of zero-sequence current harmonics is null because the IM is usually Delta or isolated Wye connected[121]

The rotor is round, so  $L_{g2} = 0$  (no "saliency effects"), and Ld=Lq

Also, the rotor resistance and leakage inductance will be a function of slip as mentioned before.

Lm, the typical magnetizing inductance in this case, is equal in each phase and may be computed as [122]

$$L_m = \mu_0 \frac{2m\tau_{\rm p}}{p\pi^2 {\rm g}} l'(k_{\rm w} {\rm N})^2$$
 (3.92)

Lr is rotor equivalent inductance

Ld is the direct-axis inductance.

Lq is the quadrature-axis inductance.

#### L0 is the zero inductance

So the following equations will be similar to that usual induction machine [72] except that the above modifications will be taken into consideration:

$$Ld = Lq = L_{\rm s} = L_{\rm m} + L_{\rm ls}$$
 (3.93*a*)

$$Lf = Lg = L_{\rm r} = L_{\rm m} + \frac{L_{\rm lr}}{s}$$
 (3.93b)

$$L_{md} = L_{mq} = L_m \tag{3.93c}$$

$$\lambda_d = L_d i_d + L_{m_f} i_f \tag{3.94a}$$

$$\lambda_q = L_q i_q + L_{m_q} i_q \tag{3.94b}$$

$$\lambda_f = L_{ff} i f_f + L_{m_f} i_d \tag{3.94c}$$

$$\lambda_g = L_{gg}i_g + L_{m_g}i_g \tag{3.94d}$$

$$v_d = ri_d + \frac{d\lambda_d}{dt} - \omega \lambda_q \tag{3.95a}$$

$$v_q = ri_q + \frac{d\lambda_q}{dt} + \omega\lambda_d \tag{3.95b}$$

$$v_f = R_f i_f + \frac{\mathrm{d}}{\mathrm{d}t} \lambda_g - (\omega - \omega r) \lambda_g \qquad (3.95c)$$

$$v_g = R_g i_g + \frac{\mathrm{d}}{\mathrm{d}t} \lambda_f + (\omega - \omega r) \lambda_f \qquad (3.95d)$$

## 3.3.2. Detailed Explanation

## 3.3.2.1 Stator and Rotor Voltage Equations

The stator and rotor voltage equations form the backbone of the dq model used to analyze the dynamic performance of high speed solid rotor induction motors (HS-SRIMs). These equations describe how the voltages, currents, and flux linkages in the motor's windings interact in the dq reference frame, which simplifies the analysis by transforming the three-phase system into two orthogonal axes: direct axis (d) and quadrature axis (q).

## 3.3.2.2 Stator Voltage Equations

In the dq reference frame, the stator voltage equations govern the relationship between the applied stator voltages and the resulting currents and flux linkages. These equations are derived from Faraday's Law of Electromagnetic Induction and Kirchhoff's Voltage Law (KVL), applied to the stator winding of the motor.

The stator voltage equations are expressed as:

$$V_d = R_s I_d + \frac{d\lambda_d}{dt} - \omega \lambda_q \quad (3.96a)$$

$$V_q = R_s I_q + \frac{d\lambda_q}{dt} + \omega \lambda_d \quad (3.96b)$$

Where:

- $V_{ds}$  stator voltage along the d-axis
- $V_{qs}$  stator voltage along the q-axis
- $R_s$  stator resistance
- $I_{ds}$  stator current in the d-axis.
- $I_{qs}$  stator current in q-axis
- $\lambda_{ds}$  and  $\lambda_{qs}$  are stator flux linkages in d-axis and q-axis, respectively.
- $\omega$  is the angular velocity of the rotor

## • Resistive Drop ( $R_s I_{ds}$ and $R_s I_{qs}$ ):

 $I_{dq}V_f$  and  $I_qX_e$  represent the voltage drops across the stator resistance from d-axis and q-axis currents, respectively. In other words, these terms are for the energy losses within the stator windings due to their resistive nature.

# • Induced EMF $(\frac{d\lambda_{ds}}{dt} \ and \frac{d\lambda_{qs}}{dt})$ :

These terms represent the EMF induced in the stator windings due to the time rate of change of the magnetic flux linkage. According to Faraday's Law, a time-varying magnetic flux induces a voltage in the winding, which these terms represent.

## • Rotational EMF $(-\omega \lambda_{qs} \ and + \omega \lambda_{ds})$ :

These terms account for the voltages induced due to the motion of the rotor relative to the magnetic field. In the dq frame, the motion of the rotor induces additional voltages, which are proportional to the product of the rotor speed  $\omega$  and the flux linkages in the perpendicular axis (i.e., d-axis flux induces voltage in the q-axis and vice versa). The sign difference between these terms reflects the 90-degree phase difference between the d and q components.

## 3.3.2.3 Rotor Voltage Equations

The rotor voltage equations are similar in structure to the stator voltage equations but include additional terms to account for the relative motion between the rotor and the stator fields, commonly referred to as the slip speed  $\omega_s = \omega - \omega_r$ , where  $\omega_r$  is the rotor angular velocity relative to the stator.

The rotor voltage equations are given by:

$$V_f = (R_r/s) I_f + \frac{d\lambda_f}{dt} - (\omega - \omega_r) \lambda_g \quad (3.97a)$$

$$V_g = (R_r/s)I_g + \frac{d\lambda_g}{dt} + (\omega - \omega r)\lambda_f \quad (3.97b)$$

Where:

- $V_f$  and  $V_g$  are the rotor direct and quadrature voltages respectively.
- $R_r$  means rotor resistance, which is the resistance of rotor winding to current flow.
- $I_f$  and  $I_g$  are the d-axis and q-axis rotor currents respectively.
- the rotor flux linkages in the d-axis and q-axis respectively are denoted by  $\lambda_f$  and  $\lambda_g$ .
- $\omega_r$  is the rotor angular velocity relative to the stator, and  $\omega$  - $\omega$ r gives the slip speed.
- Resistive Drop  $(\frac{R_r}{s}) I_f$  and  $(\frac{R_r}{s}) I_g$ :

These terms are analogous to the stator resistive drops and represent the voltage losses due to the resistance of the rotor it dependent.

# - Induced EMF $(\frac{d\lambda_f}{dt} and \frac{d\lambda_g}{dt})$ :

Like the stator these terms capture the EMF induced in the rotor windings due to the changing flux link over time.

- Slip-Induced EMF 
$$(-(\omega - \omega_r)\lambda_g \ and + (\omega - \omega_r)\lambda_f)$$
:

These terms reflect the additional voltages induced in the rotor due to the relative motion between the stator's rotating magnetic field and the rotor.

## 3.4. Summary of Modelling Equations and MATLAB Simulation

 $V_f$  and  $V_g$  are the direct and quadrature voltages of rotor.  $R_r$  is rotor resistance, which is dependent on slip value, it the equations below it will be denoted as small  $r(\frac{R}{s} = r_f = r_g)$ .  $I_f$  is the d-axis rotor current while  $I_g$  is the q-axis rotor current.  $\lambda_f$  and  $\lambda_g$  give the rotor flux linkages in d-axis and q-axis.

Simulation of direct and quadrature of stator flux linkage of equations (3.94) is:

$$\lambda_d = L_d i_d + L_{m_f} i_f \qquad (3.94a)$$

$$\lambda_q = L_q i_q + L_{m_q} i_g \qquad (3.94b)$$

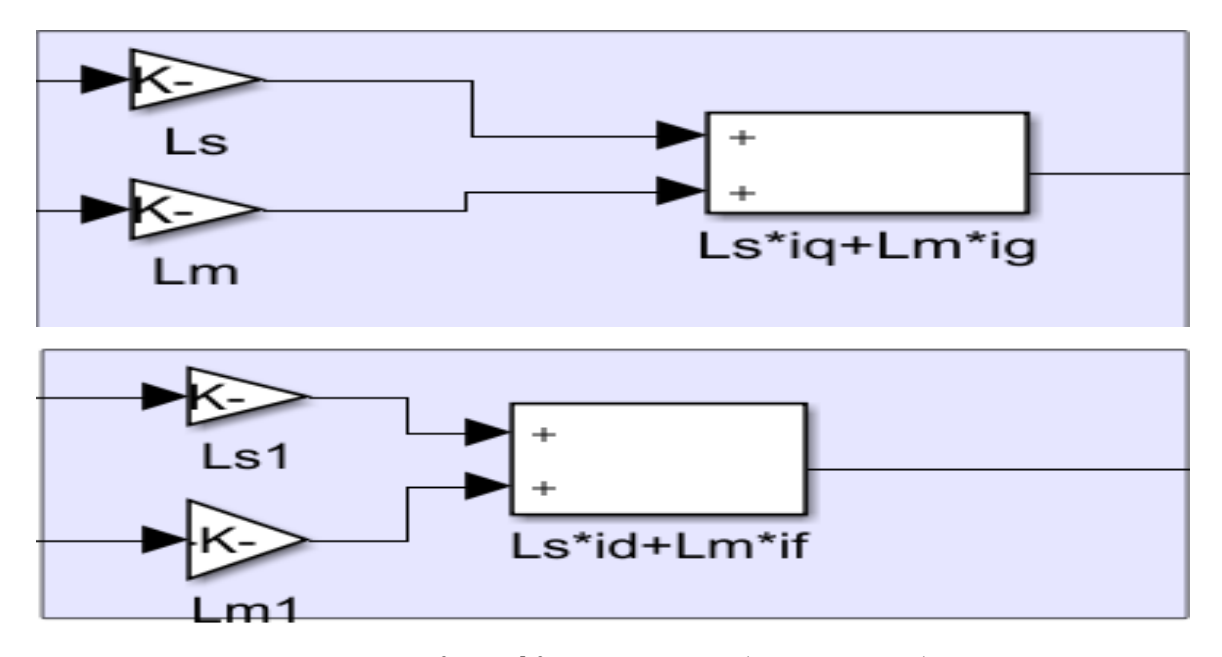


Fig.3.5. Simulation of  $\lambda_d$  and  $\lambda_q$  equations (3.94a - 3.49)

Simulation of direct and quadrature of rotor flux linkage of equations (3.94) is:

$$\lambda_f = L_{ff} i f_f + L_{m_f} i_d \tag{3.94c}$$

$$\lambda_g = L_{gg}i_g + L_{m_g}i_q \tag{3.94d}$$

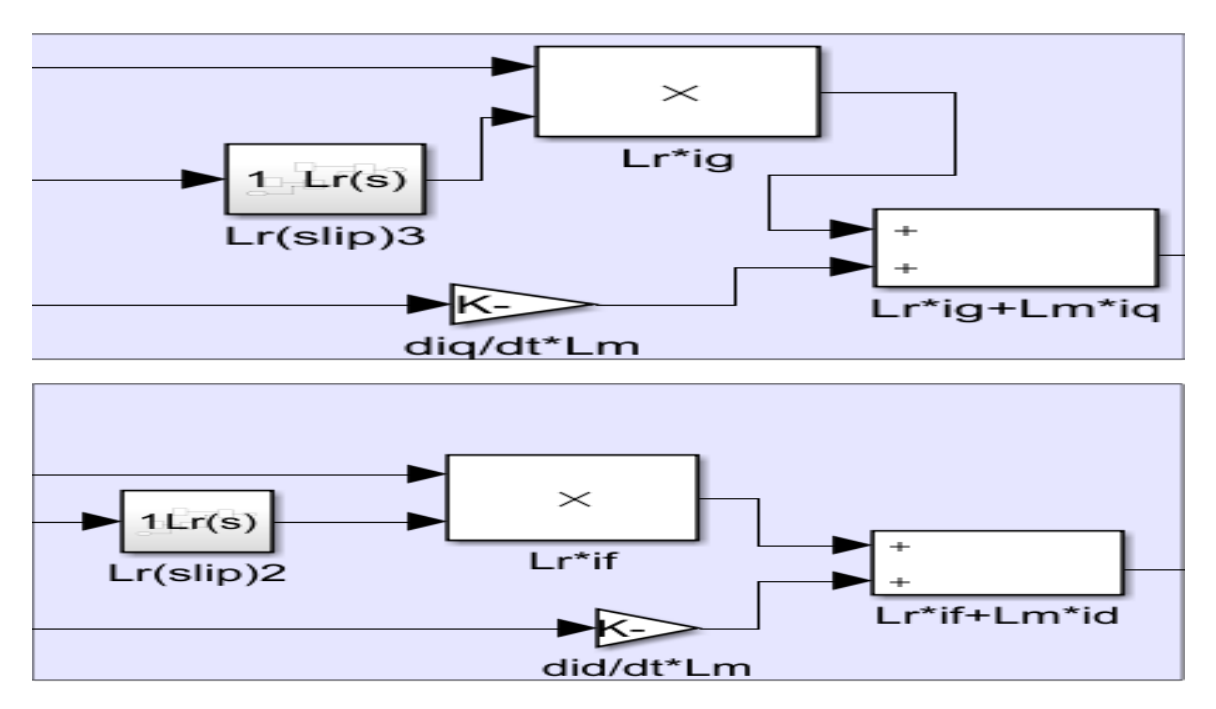


Fig.3.6. simulation of  $\lambda_f$  and  $\lambda_g$  equations (3.94c - 3.94d).

For other equations:

$$\frac{di_{\rm d}}{dt} = \frac{1}{L_{\rm S}} \left( v_d - ri_{\rm d} - L_m \frac{di_{\rm f}}{dt} - \omega L_m i_{\rm g} - \omega L_q i_{\rm q} \right) \tag{3.98}$$

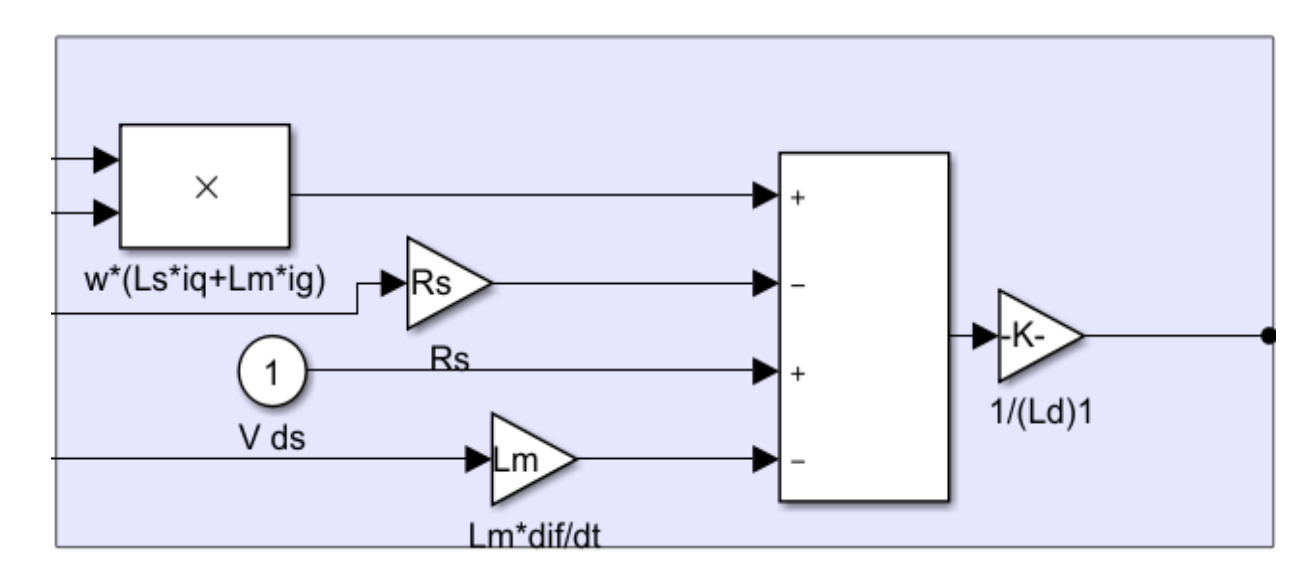


Fig.3.7. simulation of Eqs. (3.98) did/dt.

$$\frac{di_{q}}{dt} = \frac{1}{Ls} \left( V_{q} - ri_{q} - L_{m} \frac{di_{g}}{dt} + \omega L_{m} i_{f} + \omega L di_{d} \right)$$
(3.99)

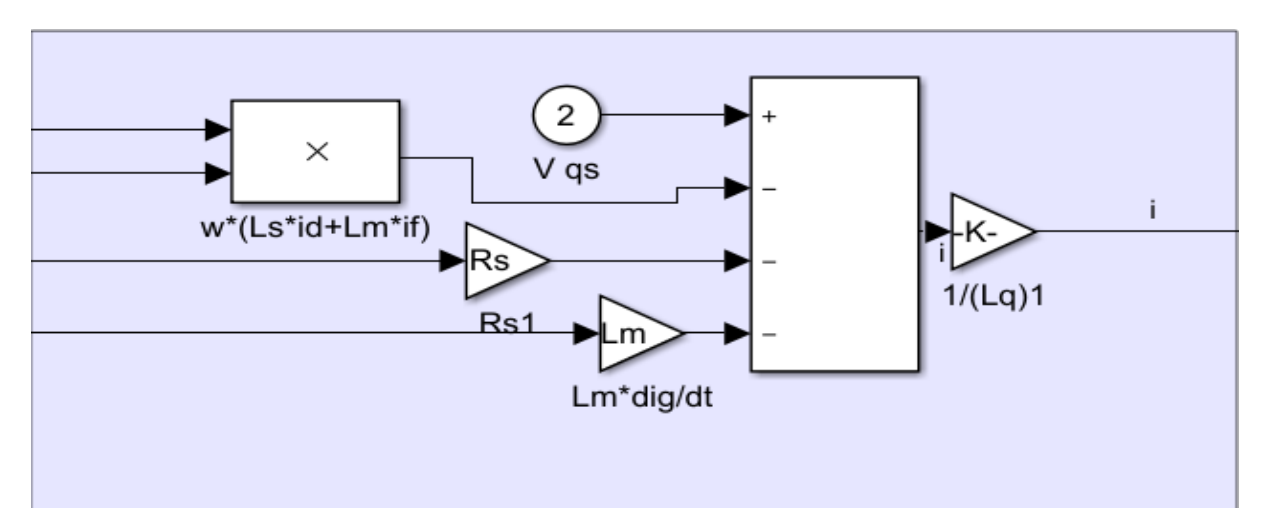


Fig.3.8. Simulation of Eqs. (3.99) diq/dt.

$$\frac{di_{\rm f}}{dt} = \frac{1}{L_r} \left( 0 - r_f i_{\rm f} - \frac{3}{2} L_m \frac{di_{\rm d}}{dt} + (\omega - \omega r) \lambda_f \right)$$
(3.100)

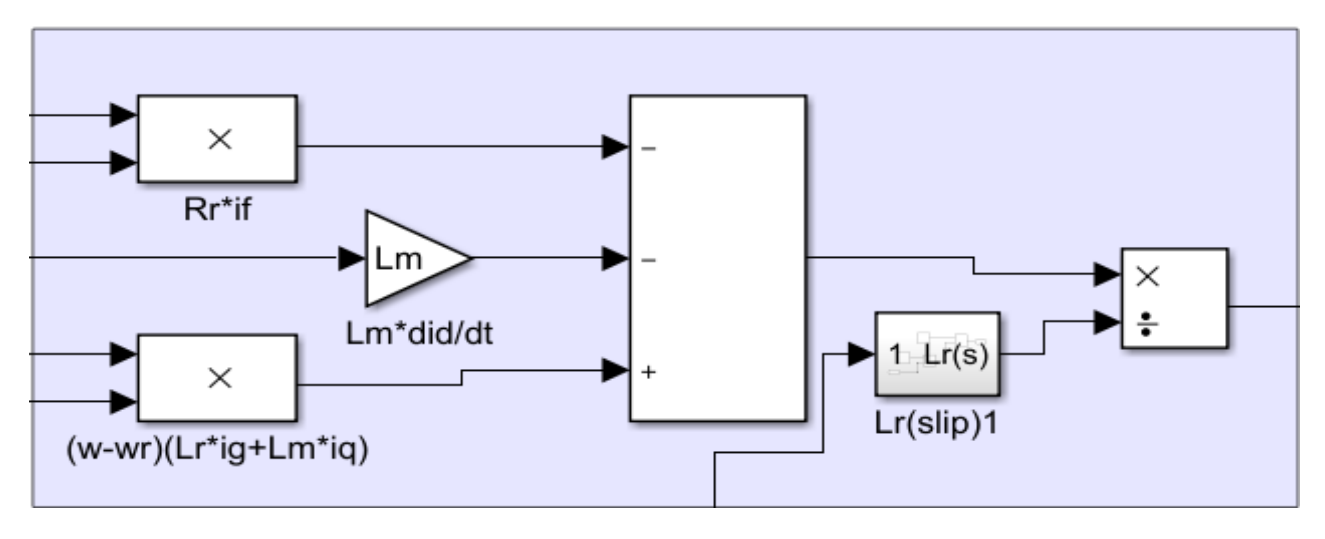


Fig.3.9. Simulation of Eqs. (3.100) dif/dt.

$$\frac{di_{g}}{dt} = \frac{1}{Ls} \left( 0 - r_{g}i_{g} - \frac{3}{2}L_{m}\frac{di_{q}}{dt} - (\omega - \omega r)\lambda_{g} \right)$$
(3.101)

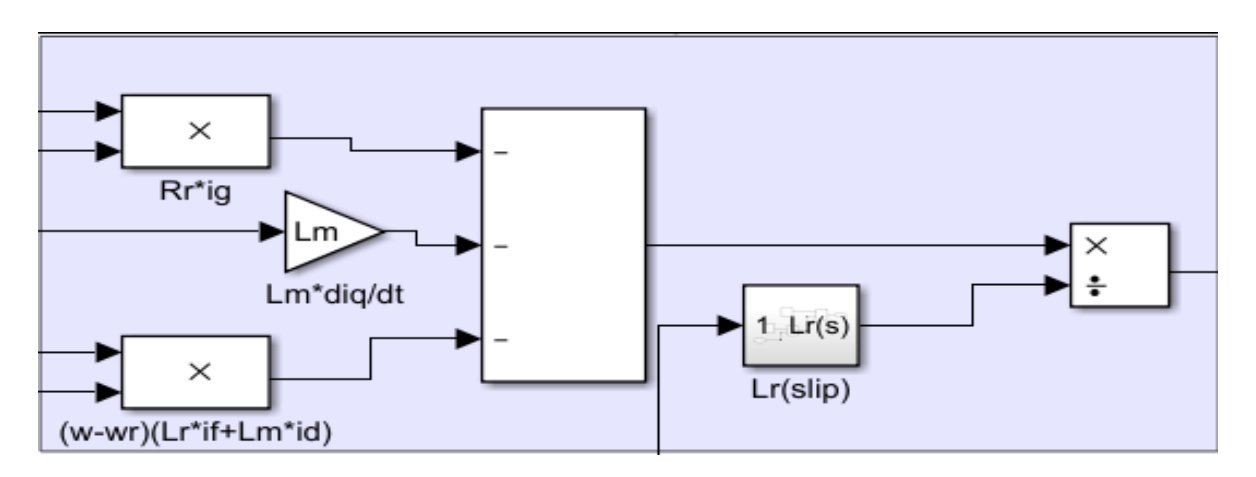


Fig.3.10. Simulation of Eqs. (3.101) dig/dt.

$$id = \int \frac{1}{Ls} \left( v_d - ri_d - L_m \frac{di_f}{dt} - \omega L_m i_g - \omega L_q i_q \right)$$
 (3.102a)

It's the same  $\frac{di_d}{dt}$  with integrator.

$$i_{\rm q} = \int \frac{1}{Ls} \left( V_q - ri_{\rm q} - L_m \frac{di_{\rm g}}{dt} + \omega L_m i_{\rm f} + \omega L di_{\rm d} \right) \quad (3.102b)$$

It's the same  $\frac{di_q}{dt}$  with integrator.

$$i_g = \int \frac{1}{L_r} \left( 0 - r_f i_f - \frac{3}{2} L_m \frac{di_d}{dt} + (\omega - \omega r) \lambda_f \right)$$
 (3.102c)

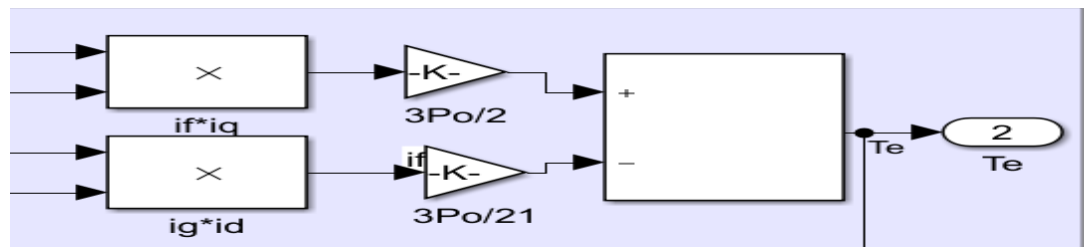
It's the same  $\frac{di_g}{dt}$  with integrator.

$$i_{\rm f} = \int \frac{1}{\rm Lr} \left( 0 - r_g i_g - \frac{3}{2} L_m \frac{di_{\rm q}}{dt} - (\omega - \omega r) \lambda_g \right) \quad (3.102d)$$

It's the same  $\frac{di_f}{dt}$  with integrator.

$$T_e = \frac{3}{2} \left(\frac{P}{2}\right) \left(\lambda_f i_g - \lambda_g i_f\right) \quad (3.103)$$

$$\omega_r = \frac{P}{j} \int (T_e - TL) \quad (3.104)$$



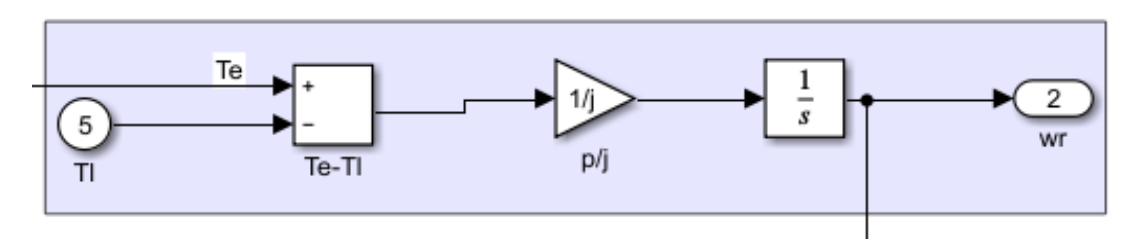


Fig.3.11. Simulation of eqations (3.103-3.104) torque and rotor speed.

$$slip = \frac{(\omega - \omega r)}{\omega} \qquad (3.105)$$

$$Power = \omega_r * T_e \qquad (3.106)$$

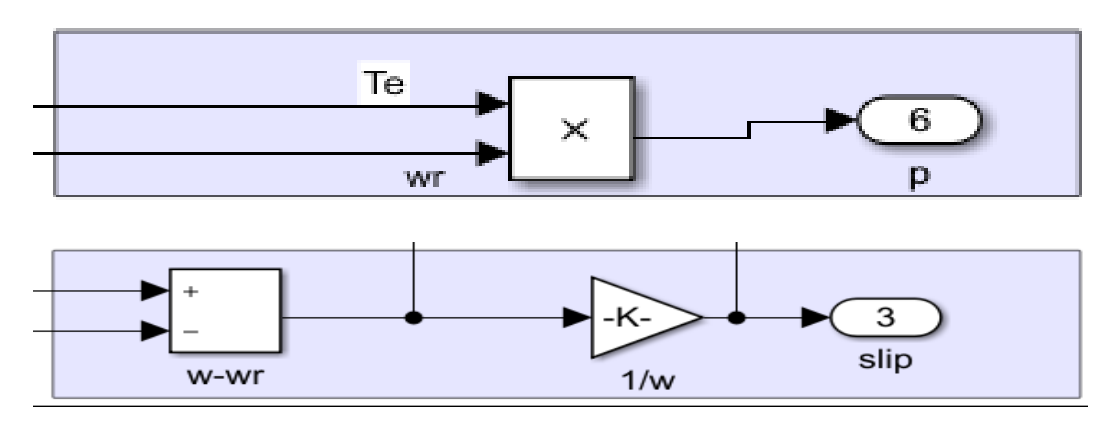
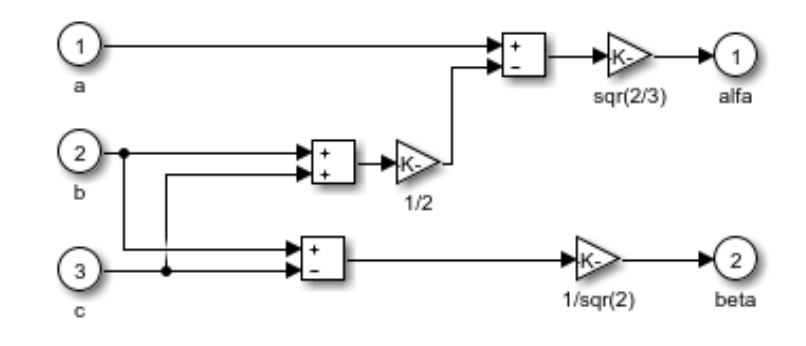
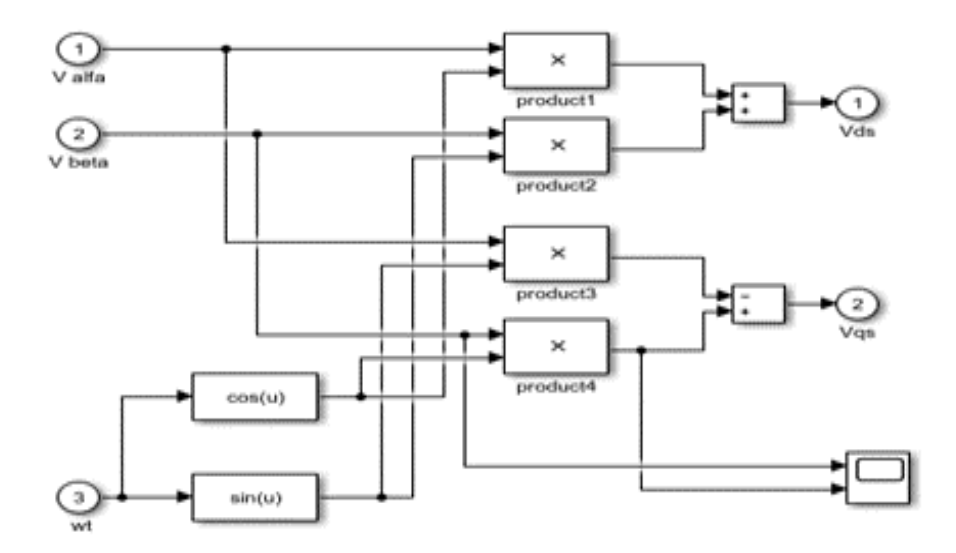


Fig.3.12. Simulation of eqations (3.105-3.106) slip and power.

The input abc to alphabeta to dq convertions Clarke –Park convertion:

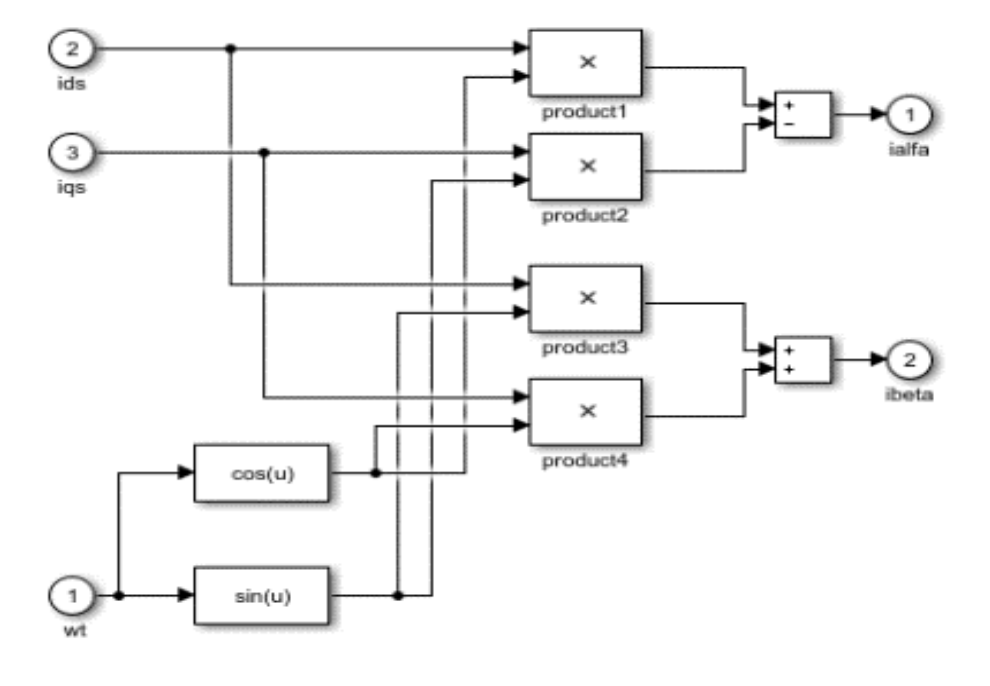


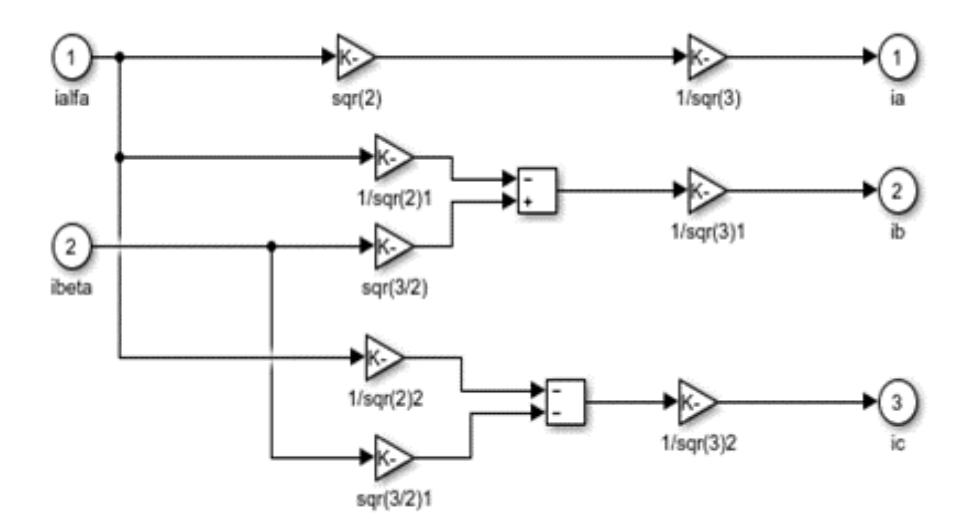


The top is abc to alphabeta conversion – the bottom is alphabeta to dq-conversion

Fig.3.13. Input voltage convertions of SRIM part

The Output conversions dq to alphabeta to abc is shown in the figure below





The top is dq to alphabeta conversion – the bottom is alphabeta to abc-conversion

Fig.3.14. Output current conversions part.

The SRIM MOTOR which contain the above equations(flux linkage, currents, torque, slip, power ...etc) of model is explained in figures below:

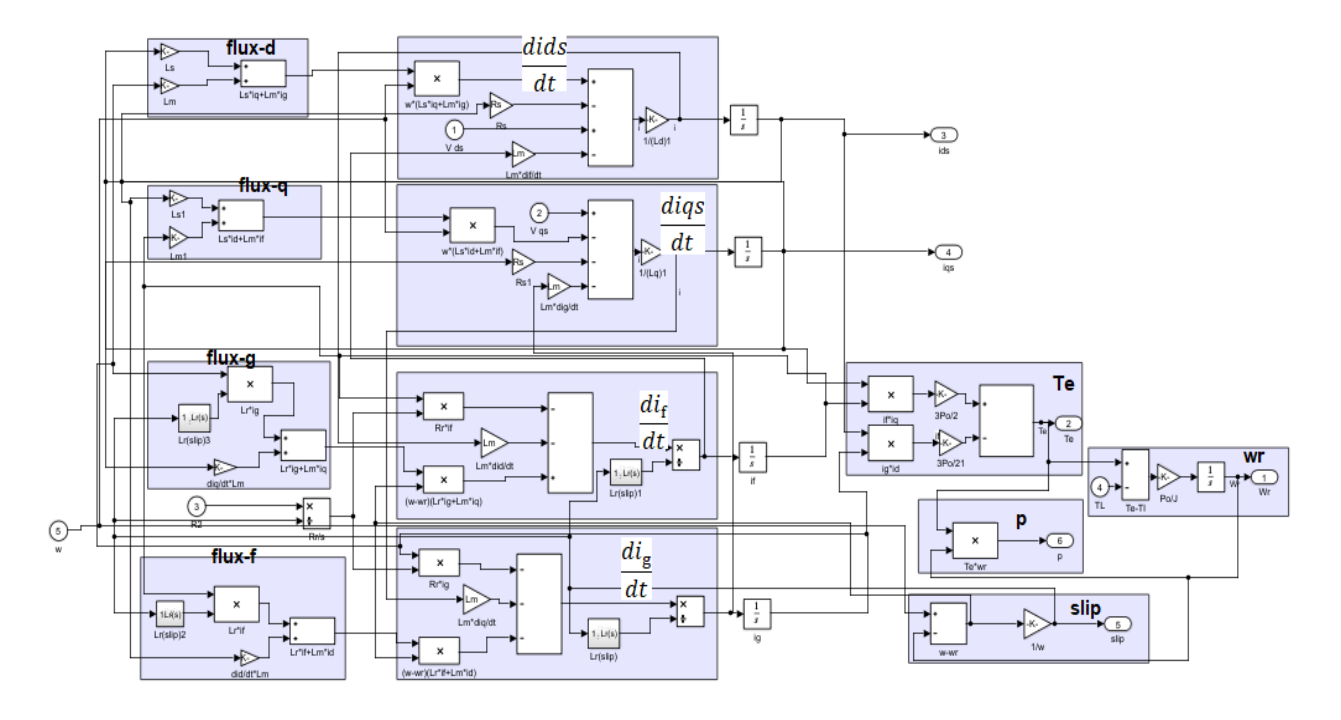


Fig.3.15. Simulation of SRIM motor block.

Note that the rotor inductance is simulated as a function of slip configuration.

And The general block of total simulation is shown in figure below:

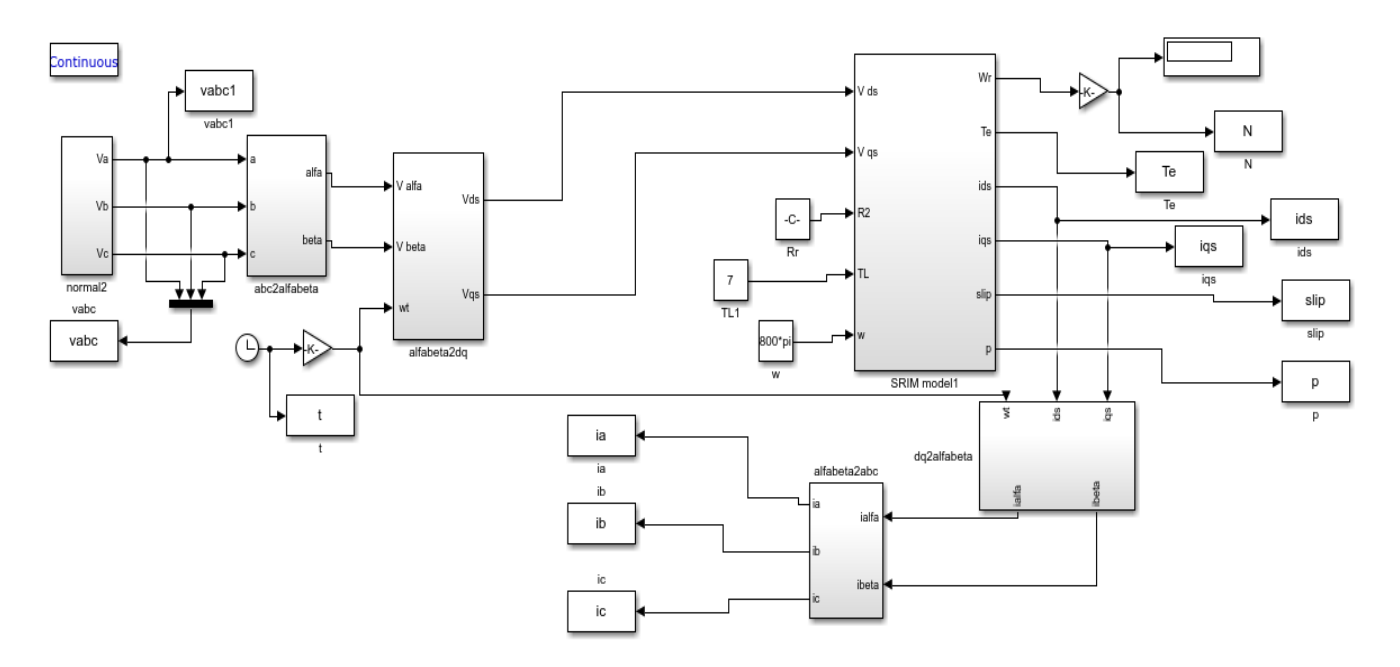


Fig. 3.16. simulation of overall operation parts of HS- SRIM

#### 3.5. Time Harmonic Analysis and Simulation

#### 3.5.1. Effect of Harmonics

When waves with various frequencies are created by multiplying integers by their fundamental frequencies, harmonics are the result. The integer multiplier base frequency is known as the harmonic sequence number, whereas this is known as the harmonic frequency that appears in the original waveform. An electric power system's fundamental frequency, for instance, is 60 Hz. A wave with a frequency of 120 Hz is the second harmonic, and a wave with a frequency of 180 Hz is the third. And so on . When these waves ride on the original wave, deformed waves are created, which is the ratio of the harmonic waves to the momentary pure waves[123].

Electrical systems shouldn't have high harmonic levels as they might be harmful [124].

The machine's behavior is determined by superimposing the effects of fundamentals and harmonics. This method is used as a design reference for the inverter and provides information on individual harmonic behavior. The harmonics for a three-phase AC motor are as follows:

$$h = 1, -5, 7, -11, 13, -17, 19, -23, 25, -29, 31, -35, 37, -41, 43, -47, 49, etc.$$

The fundamental magnetomotive force (mmf) wave rotates in the same direction as positive-order harmonics, whereas negative-order harmonics rotate in the opposite direction. The voltages generated by different harmonics are included in the voltage of the fundamental frequency. The harmonic's angular velocity with regard to the stator and number of pole pairs (fp) are as follows:

$$\omega_{\rm sh} = \frac{\omega_{\rm s}}{\rm h} \qquad (3.107)$$

Next, the eddy current losses and flux penetration into the solid-rotor medium are considered. Permeability and conductivity are taken to be constants for simplicity's sake. an equation for the magnetic-field strength at the rotor's surface

is provided by the Maxwell equations[125]:

$$\nabla^2 H = j\omega_r \sigma \mu H \tag{3.108}$$

The strength of the tangential magnetic field is[125].

$$\frac{\partial^2 \underline{H}_{xh}}{\partial v^2} - j\omega_{rh}\sigma\mu\underline{H}_{xh} \tag{3.109}$$

The magnetic field intensity must decrease as y approaches infinity; hence the differential equation may be solved as:

$$\underline{H}_{xh} = \underline{H}_{0xh} e^{\frac{1+j}{\sqrt{2}}\sqrt{\omega_{rh}\sigma\mu y}}$$
(3.110)

The axial electric field strength is

$$\underline{E}_{zh} = \frac{1}{\sigma} \frac{\partial}{\partial y} \underline{H}_{xh} = \frac{1}{\sigma} \frac{1+j}{\sqrt{2}} \sqrt{\omega_{rh} \sigma \mu} \underline{H}_{xh}$$
 (3.111)

Given that the surface current value is equal to the surface magnetic field strength (Js n Hs, where n is the surface normal unit vector), the relationship between the electric and magnetic field strengths may be called the surface impedance Z of the harmonic.

$$\underline{Z}_{Rh} = \frac{\underline{E}_{zh}}{H_{xh}} = \frac{1+j}{\sigma\sqrt{2}}\sqrt{\omega_{rh}\sigma\mu}$$
 (3.112)

According to ampere law  $\oint H dl = \int_s^r J ds$  The tangential field strength  $\hat{H}_{rx}$  (time-harmonic field strength vector amplitude) of the rotor surface, which is considered to be sinusoidal, and the fundamental component mmf<sub>1</sub> of the stator's current linkage are expressed as equal to one another.

$$\underline{\mathbf{mmf}}_{h} = \frac{4}{\pi} \frac{m}{2} \frac{k_{w} N}{p_{h}} \sqrt{2} \underline{I}'_{rh} = \int_{-\tau_{v}}^{0} \underline{H}_{Rh} e^{jcx} dx = \frac{2\underline{H}_{Krh}}{ja} \quad (3.113)$$

$$\underline{I}'_{rh} = \frac{\underline{\underline{H}}_{rh} p h \pi}{jm k_{w} N \sqrt{2} c} \quad (3.109)$$

The voltage that is induced by the harmonic h refered to the stator.

$$\underline{U}'_{Rh} = -j\omega_s \frac{Nk_w}{\sqrt{2}} \int_{-\frac{\tau_p}{2}}^{\frac{\tau_p}{2}} \underline{B}_{ryh} e^{jcx} L dx = -j \frac{2\omega_s Nk_w L}{\sqrt{2}c} \underline{B}_{ryh} \quad (3.114)$$

The axial electric field strength can be used to express the normal flux density.

$$\underline{B}_{\rm ryh} = -\frac{\rm c}{\omega_{\rm rh}} \underline{E}_{\rm rh} \quad (3.115)$$

It is now possible to write the rotor harmonic impedance.

$$\underline{Z}'_{Rh} = \frac{\underline{U}'_{rh}}{\underline{I}'_{rh}} = \frac{2\omega_{s}}{\omega_{Rh}} \frac{mL}{p\tau_{p}} (Nk_{w})^{2} \frac{2\underline{H}_{rh}}{\underline{E}_{rh}}$$
(3.116)

For linear case:

$$= \frac{2mL}{p\tau_p} (Nk_w)^2 \left(\frac{1+j}{\sigma\sqrt{2}}\sqrt{\omega_{\rm rh}\sigma\mu}\right) \quad (3.117)$$

Which is equal to

$$\underline{Z}'_{\rm rh} = \left(\frac{4\sqrt{2}mN^2L}{\sqrt{\pi}DK_e}\right) \left(\frac{\mu_{\circ}\mu_r\rho\omega_{\rm rh}}{s_h}\right)^{1/2} \angle 45^{\circ}$$
Where  $\omega_{\rm rh} = h\omega_{\rm r_1}$ , (3.118)

and,  $Sh = h \pm (1-s)/h$ 

The analysis of this study uses this formula with a constant incremental permeability  $\mu r = 43$  and a phase angle of  $45^{\circ}$ .

Iron core material experiences eddy currents when exposed to an alternating magnetic field. Only a specific depth of the magnetic material can be penetrated by the magnetic field and flux because the eddy currents resist the flux change. The material has lost all of its flow.

Since there is relatively little harmonic flux penetration into the rotor material, it is assumed that the rotor has a constant permeability equal to the computed value at the rotor surface. based on studies on rotor materials. A constant value of µr of 43 was found to be satisfactory in the experimental test throughout a wide range of positive and negative sequence field intensities [82]

## 3.5.2. Inverter Feeding the Motor

Three-phase motor currents are symmetrical and non-sinusoidal when symmetrical, non-sinusoidal voltages are applied to the motor terminals on a regular basis. Higher temporal harmonics and a fundamental component might be considered the components of these currents.

The kind of converter and the frequency of thyristor conduction influence the inverter voltage waveform. The waveform of a 180° thyristor conduction angle is either stepped or rectangular (see figure 3.17). Depending on the modulation method, a pulse width modulated inverter's output voltage waveform is a pulsed wave. The resolution of the non-sinusoidal input wave is Fourier series.

The idea of superposition can be used to ascertain the performance of the threephase induction motor, provided that the saturation effect which could result from superimposing voltages of different frequencies is minimal [82].

The net performance of a non-sinusoidal voltage waveform is thought to be the total contributions from each harmonic, and the motor behavior for the fundamental and individual harmonics are assessed separately. The study uses the induction motor's equivalent circuit, and by altering the equivalent circuit for the harmonic in question. Therefore, the whole steady state behavior of the motor is calculated using a set of separate equivalent circuits, one for each harmonic.

When a harmonic order's torque is positive, it means that it is moving in the same direction as the fundamental torque (n=7.13.19), and when it is negative, it means that it is moving in the opposite way (n=5.11.17).

The fundamental field flows in the opposite direction when its number of poles equals that of the harmonic of order n=6k-1 (n=5,11,17, etc.) and spins at ((6k-1) Ns) [132]. Order n=6k+1 harmonics, such as n=7,13,19, etc., move at the same speed as the fundamental, which is equal to ((6k+1)).

Thus, the harmonic orders are -5, 7, -11, 13, and so forth. The sequence harmonic order is negative when the sign of the nth harmonic is negative. A zero-sequence voltage is produced by the combination of third harmonic voltages in temporal phase. Without a neutral connection, they are unable to impose current on stator windings that are connected to a star. Since they are zero-sequence and will not significantly affect the situation, any harmonics of order triple n will be disregarded here.

It is evident that Tn is quite modest and that the low order harmonics (i.e., the

Fifth and Seventh) [126][82] produce the highest torque drop, even if the net harmonic torques are operating verses the fundamental one.

### 3.5.3. Fourier Steady-State Analysis

The output voltage waveform of a three-phase inverter feeding a three-phase induction motor is determined by the conduction time of the switching components.

Nonetheless, Fourier series analysis may be used to analyze the inverter's periodic output waveform. Even order harmonics will not exist for symmetrical waveforms, which have equal positive and negative half cycles (2,4,6,..etc.).

Examine the square-wave general form in Fig. (3.17 at left), where wd stands for conduction period.

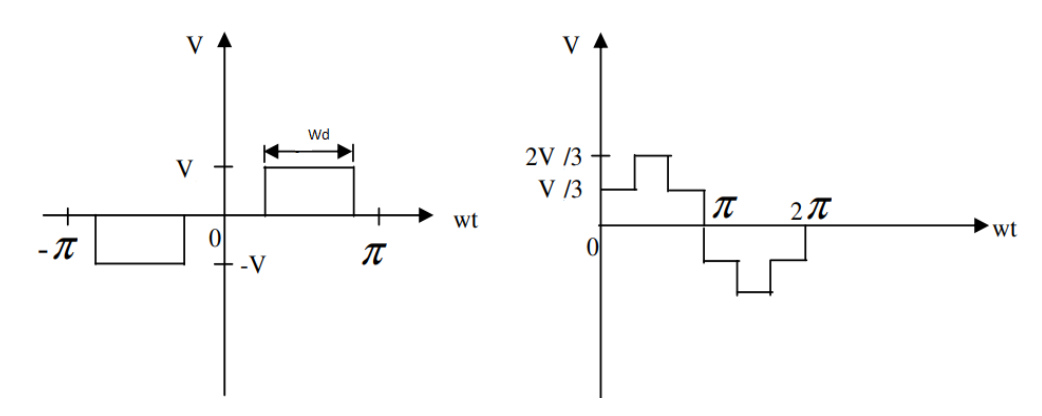


Fig.3.17. Source voltage waveform.

The only harmonic orders that can affect machine performance using Fourier series and the waveform above are:  $h = 6n \pm 1$ 

$$-v \frac{\pi + wd}{2} < wt < -\frac{\pi - wd}{2}$$

$$V(wt) = 0 -\frac{\pi - wd}{2} < wt < \frac{\pi - wd}{2}$$

$$v \frac{\pi - wd}{2} < wt < \frac{\pi + wd}{2}$$

$$(3.119)$$

 $V(-wt)=-V(wt) \quad \text{therefore} \quad b_n=0, \quad \text{i.e.,} \quad \text{no} \quad \text{cosine} \quad \text{term.}$  The function have symmetry about the x -axis therefore  $a_0=0.$   $v(wt+\pi)=-v(wt) \text{ therefore } a_{2n}=0$ 

$$a_{n} = 2v/\pi \int_{(\pi - wd)/2}^{(\pi + wd)/2} \sin(hwt) dwt$$

$$= -2v/h\pi [\cos h((\pi + wd)/2) - \cos h((\pi - wd)/2)]$$

$$= 4v/h\pi [\sin h\beta/2 \cdot \sin h\pi/2]$$
(3.120)

For  $wd = 180^{\circ}$ ,

$$a_h = 4v/h\pi[\sin h\pi/2]^2$$
 (3.109)

and,

$$V = \sum_{h=1}^{\infty} 4v/h\pi \sin hwt$$
 (3.121)

Let  $4v/\pi = \sqrt{2}E_a$ , then,

$$v = \sum_{h=1}^{\infty} \sqrt{2}E_a / h\sin hwt$$
 (3.122)

Where  $E_a$  is the rms value of the fundamental. For  $wd=120^\circ,$ 

$$a_{h} = 4v/h\pi[\sin h\pi/3][\sin h\pi/2]$$

$$= 2\sqrt{3}v/h\pi\sin mwt$$
(3.123)

Where:

$$m = 1 \pm 6k$$
 for  $k = 1.2.3....$  etc.  
 $h = m * (-1)^{m+3/2}$ 

So if  $\sqrt{2}E_a = 2\sqrt{3}v/\pi$ , it follows that

$$v = \sqrt{2}E_2[\sin(wt) - 1/5\sin(5wt) - 1/7\sin(7wt) + 1/11\sin(11wt) + 1/13\sin(13wt) + \cdots \dots]$$
(3.124)

Comparably, the stepped-voltage waveform in Figure (A.2) has the same characteristics as Figure (A.1) and, when Fourier analysis is used, shows that: -

$$v = 2v/\pi[\sin(wt) + 1/5\sin(5wt) + 1/7\sin(7wt) + 1/11\sin(11wt) + 1/13\sin(13wt) + \dots \dots ]$$
(3.125)

or

$$v = \sum_{h=1}^{\infty} \left(\frac{2v}{h\pi}\right) \sin(hwt)$$
 (3.126)

According to that, the first phase voltage equation, let's call it Va, may be written

as follows:

$$V_{a} = \sum_{h=1}^{\infty} V_{h} \sin(hwt)$$
 (3.127)

where the structure of the waveform is used to determine the constant Vh, which is  $(\frac{2v}{h\pi})$ 

#### 3.5.4. Harmonic Circuits Simulation

Recall that the even order harmonics (2,4,6 ...) are vanished, and by using the waveform in fig (29) all triple harmonics (3,9,15...) also vanished, the remaining sequence is (1,-5, 7, 11, 13, 17, 19, 23....) and the most effective orders are 5<sup>th</sup> and 7<sup>th</sup>, so they will be simulated by configuration as formed in figure 3.18 for Each phase of each harmonic circuit will be the output of the PWM by inverter configuration shown,

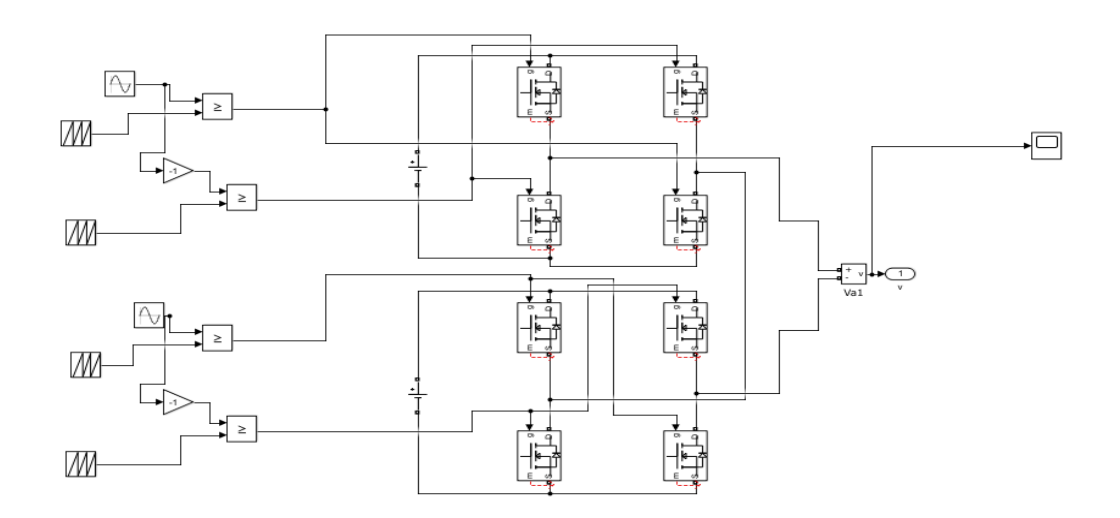


Fig.3.18. Inverter construction to get voltage source.

Thus, the needed output of each phase will be got, and the resultant voltage waveform in the figure 3.19

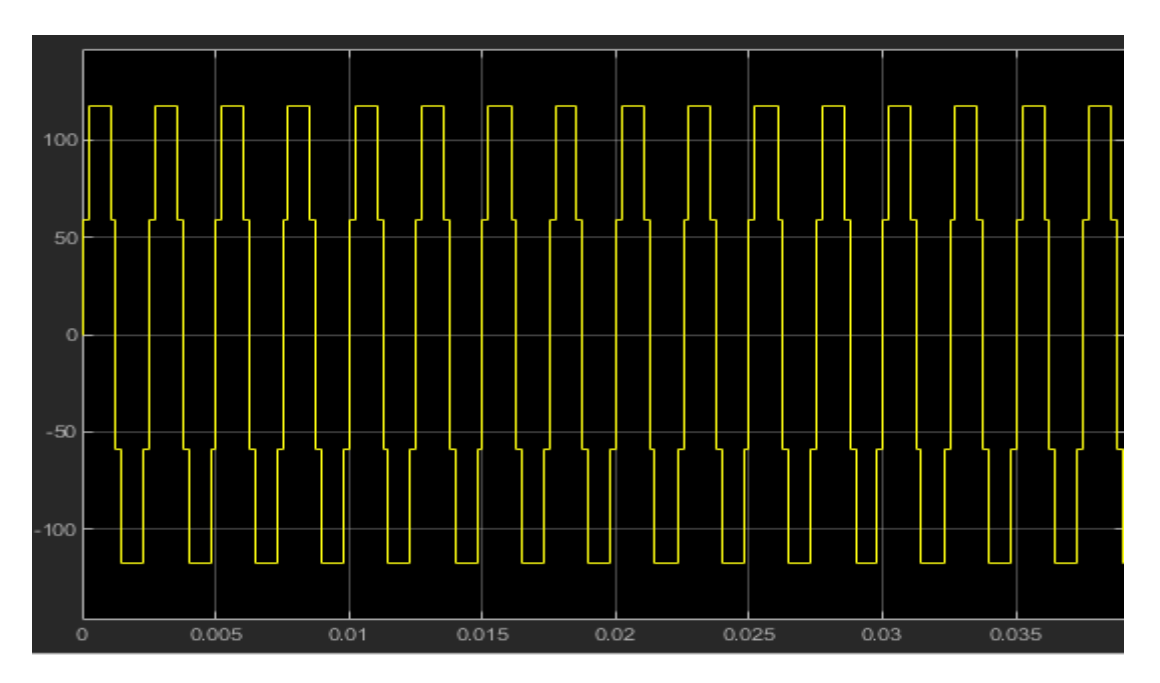


Fig.3.19. The inverter source voltage waveform

The second step is to make Vb and Vc and this will be done by shifting Va by 120 and -120 degree to get the 3-phase stepped voltage source for 1<sup>st</sup> harmonic

$$v_a = v_1 \sin(\omega_e t + \theta_1)$$
 (3.128a)  

$$v_b = v_1 \sin\left(\omega_e t + \theta_1 - \frac{2\pi}{3}\right)$$
 (3.128b)  

$$v_c = v_1 \sin\left(\omega_e t + \theta_1 + \frac{2\pi}{3}\right)$$
 (3.128c)

as shown in fgure 3.20 below:

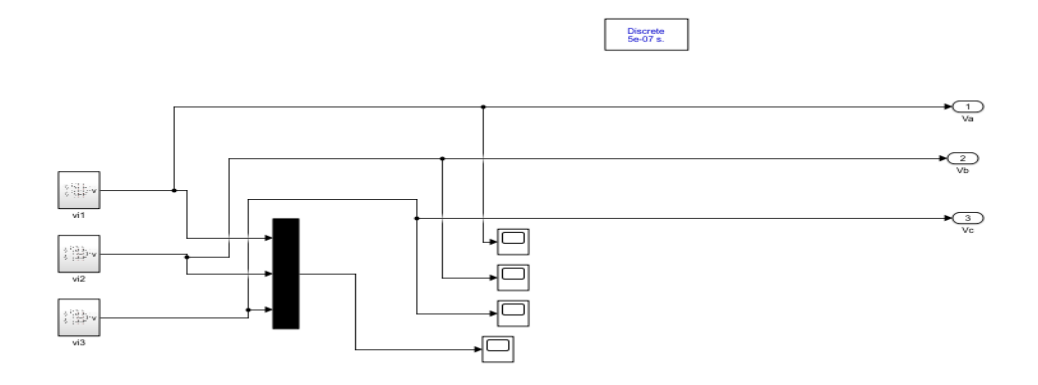


Fig.3.20. Three phase inverter source formation.

Which has the waveform as shown

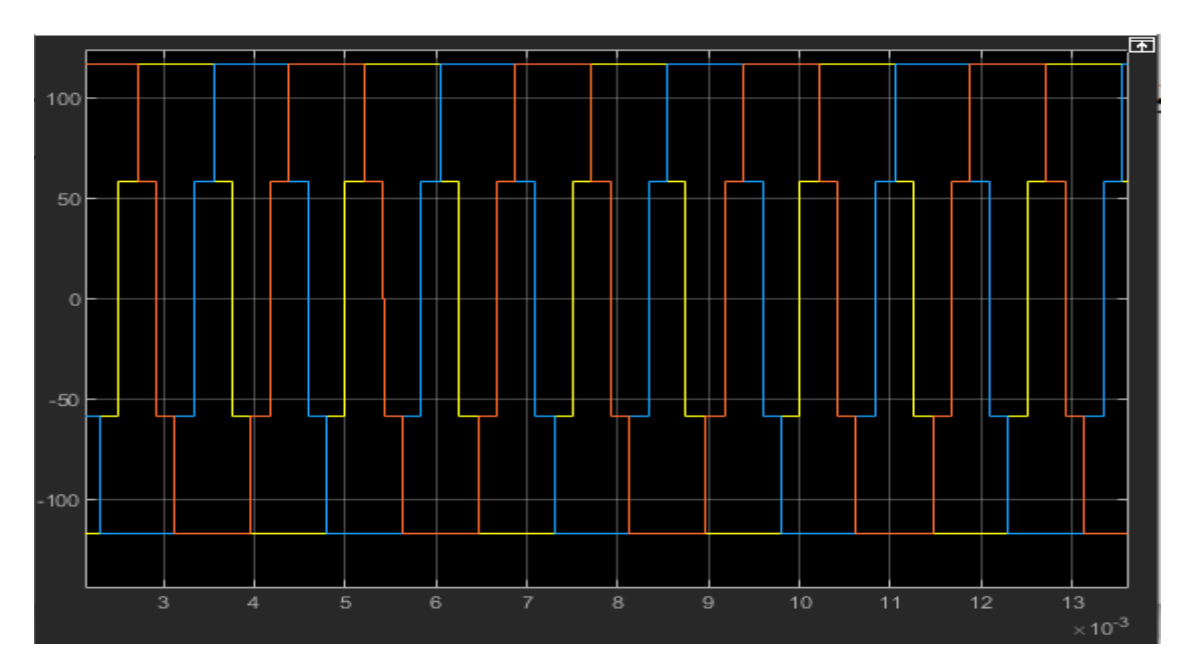


Fig.3.21. Inverter output 3-phase voltage waveform.

The rest of fundamental simulation is the same figure (3.16) that discussed before as shown in figure (3.22):

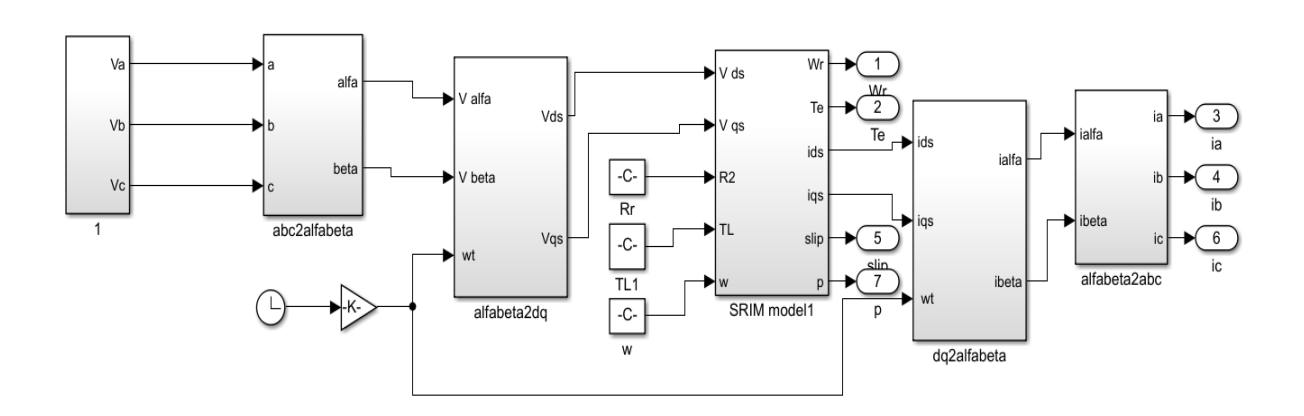


Fig.3.22. simulation of fundamental circuit.

According to the superposition, the 5<sup>th</sup> and 7<sup>th</sup> harmonic circuit will be simulated as same as 1<sup>st</sup> one for each harmonic order (with modification in dc voltage and frequency dependent parameters) for each harmonic circuit.

After preparing the non-sinusoidal voltages supply by H-bridge 5-level inverter

converter for each harmonic order (5<sup>th</sup> and 7<sup>th</sup>) as following:

$$v_{a5} = v_5 \sin(5\omega_e t + \theta_5) \tag{3.129a}$$

$$v_{b5} = v_5 \sin\left(5\omega_e t + \theta_5 - \frac{10\pi}{3}\right) \tag{3.129b}$$

$$v_{c5} = v_5 \sin\left(5\omega_e t + \theta_5 + \frac{10\pi}{3}\right)$$
 (3.129c)

And

$$v_{a7} = v_7 \sin(7\omega_e t + \theta_7)$$
 (3.130*a*)

$$v_{b7} = v_7 \sin\left(7\omega_e t + \theta_7 - \frac{14\pi}{3}\right) \tag{3.130b}$$

$$v_{c7} = v_7 \sin\left(7\omega_e t + \theta_7 + \frac{14\pi}{3}\right) \tag{3.130c}$$

where v1, v5, v7 are fundamental,  $5^{th}$  and  $7^{th}$  harmonic voltage amplitudes (vn in equation 3.127), respectively;  $\theta1,\theta5,\theta7$  are the initial phase angles of fundamental,  $5^{th}$  and  $7^{th}$  harmonic voltages, respectively.

The rotating co-ordinate system of the fifth harmonic, d5th -q5th and d7th-q7th, is completed in two parts, as should be recognized. As illustrated below, the three-phase a-b-c co-ordinate system is first converted by Clark transformation into a two-phase  $\alpha\beta$  co-ordinate system, and then Park like the first-order transformation converts the two-phase  $\alpha\beta$  coordinate system into the d-q coordinate system:

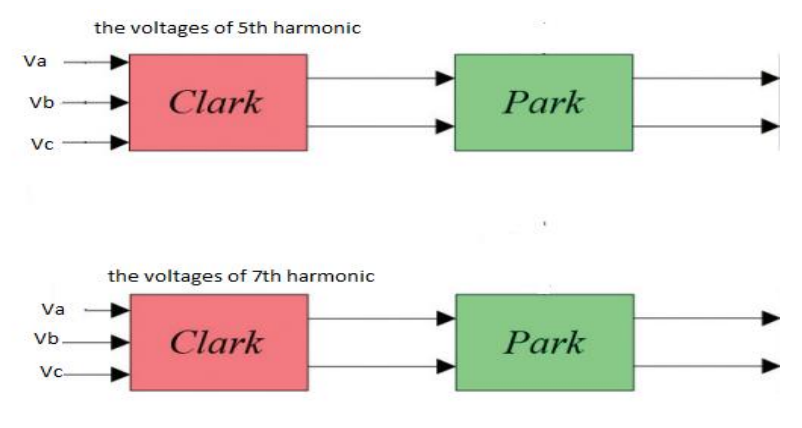


Fig.3.23. Clark-Park transformation stages

Another thing to keep in mind is that the fundamental wave rotates in the same direction as the fifth harmonic, but the fifth harmonic rotates in the opposite way [127], As demonstrated, a d-q coordinate system that corresponds to the fifth and seventh harmonics is created:

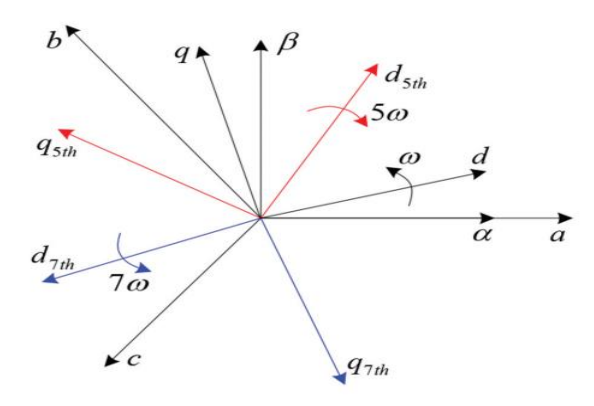


Fig.3.24. Diretion of rotation of 5<sup>th</sup> and 7<sup>th</sup>

. The coordinate transformation from the two phase  $\alpha\beta$  coordinate system into the d5th-q5th coordinate system is as follows:

$$C_{a\beta}^{dq5th} = \begin{bmatrix} \cos(-5\omega_e t) & \sin(-5\omega_e t) \\ -\sin(-5\omega_e t) & \cos(-5\omega_e t) \end{bmatrix}$$
(3.131)

. The coordinate transformation from the two phase static  $\alpha\beta$  coordinate system to the 7th harmonic d7th-q7th system is as follows:

$$C_{\alpha\beta}^{dq7th} = \begin{bmatrix} \cos(7\omega_e t) & \sin(7\omega_e t) \\ -\sin(7\omega_e t) & \cos(7\omega_e t) \end{bmatrix}$$
(3.132)

the harmonic voltage components ud5th, uq5th, ud 7th and uq7th in the d5th-q5th and d7th-q7th coordinate systems are obtained.

The total torque can be calculated as:

$$T_e = \sum (T_h^+ + T_h^-)$$
 (3.144)

the overall simulation which represent the superposition will be as shown in fig (3.25):

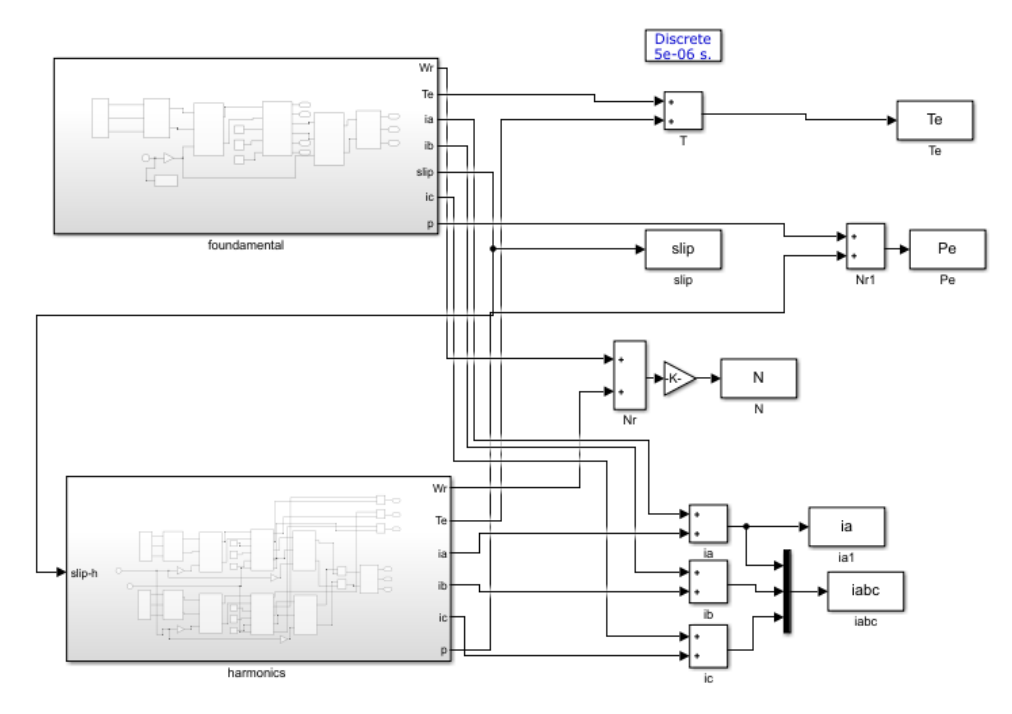


Fig.3.25. Simulation of resultant (5<sup>th</sup> and 7<sup>th</sup> harmonics) circuits with the fundamental

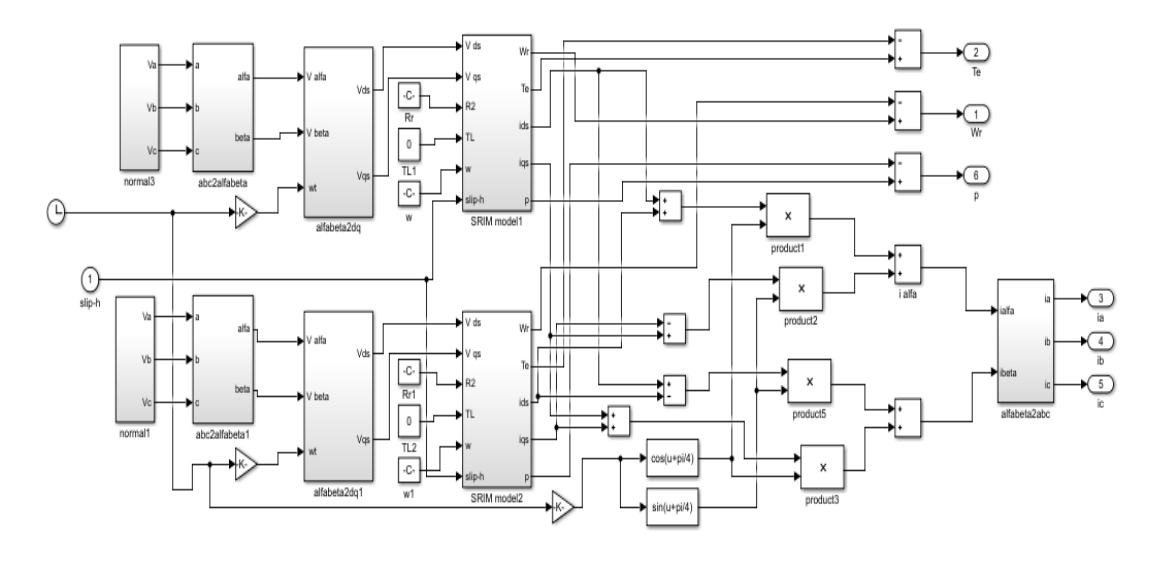


Fig.3.26. simulation of 5th (upper one) with 7th (lower one) combination circuits. the top block in fig(3.25) is for the fundamental and the lower one for the  $5^{th}$  and  $7^{th}$  harmonics circuits, as explained in fig (3.26):

## **Chapter Four**

#### Results

This chapter presents the detailed results obtained from the mathematical modeling and simulation of the high-speed solid rotor induction motor (HS-SRIM) using the developed dq-axis model and MATLAB/Simulink. The results include performance under ideal sinusoidal supply, under non-sinusoidal harmonic supply, The figures and tables illustrate the dynamic performance, torque and power characteristics, harmonic effects, and the influence of design modifications such as end-effect correction and copper coating.

The rated frequency used in this model is 400 Hz and motor parameter in appendix 1

### 4.1. Results for Fundamental with Sinusoidal Input

The motor was simulated under purely sinusoidal voltage supply, analyzing noload and full-load conditions. The effect of design features such as end-effect correction and copper coating was also investigated.

The result according to the above parameters will show the cases:

- 1-Under no load condition without putting end effect correcting factor
- 2-Under full load condition without putting end effect correcting factor
- 3-Under no load condition with end effect correcting factor
- 4-Under full load condition with end effect correcting factor
- 5-Under no load condition with copper coating
- 6-Under full load condition with copper coating

#### 1-No load no end factor

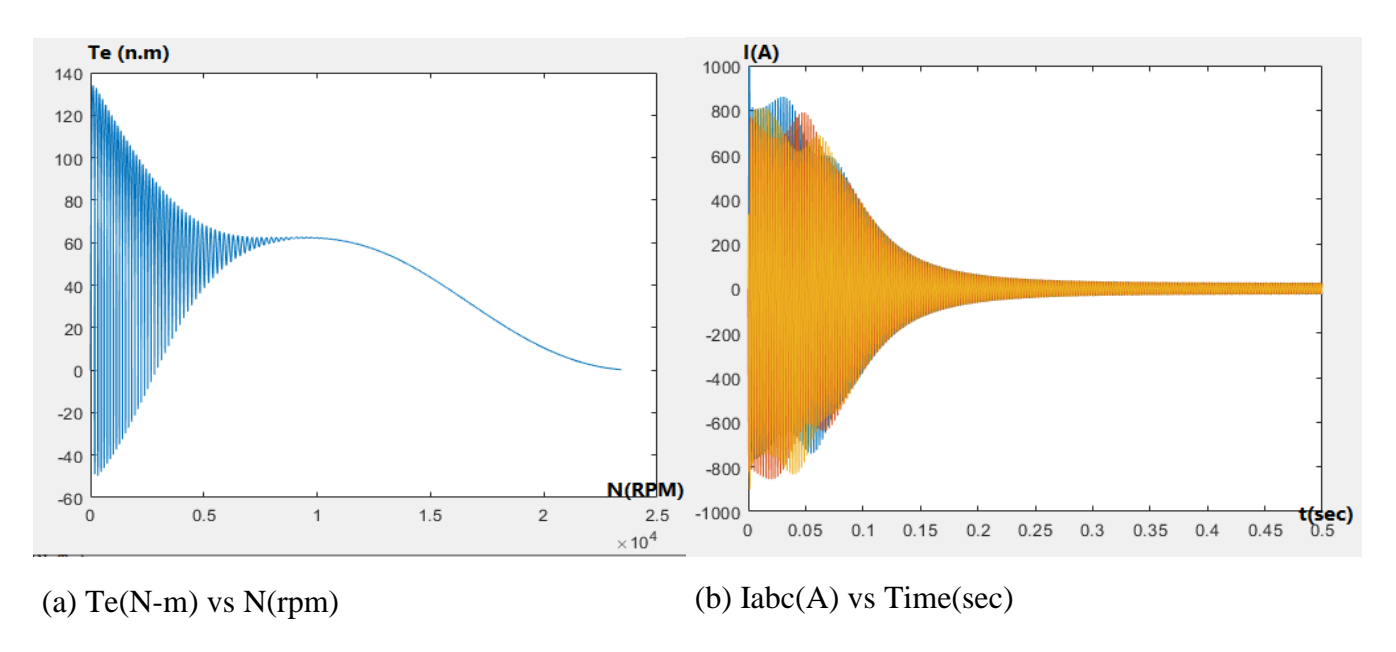


Fig.4.1. Torque and power at no load.

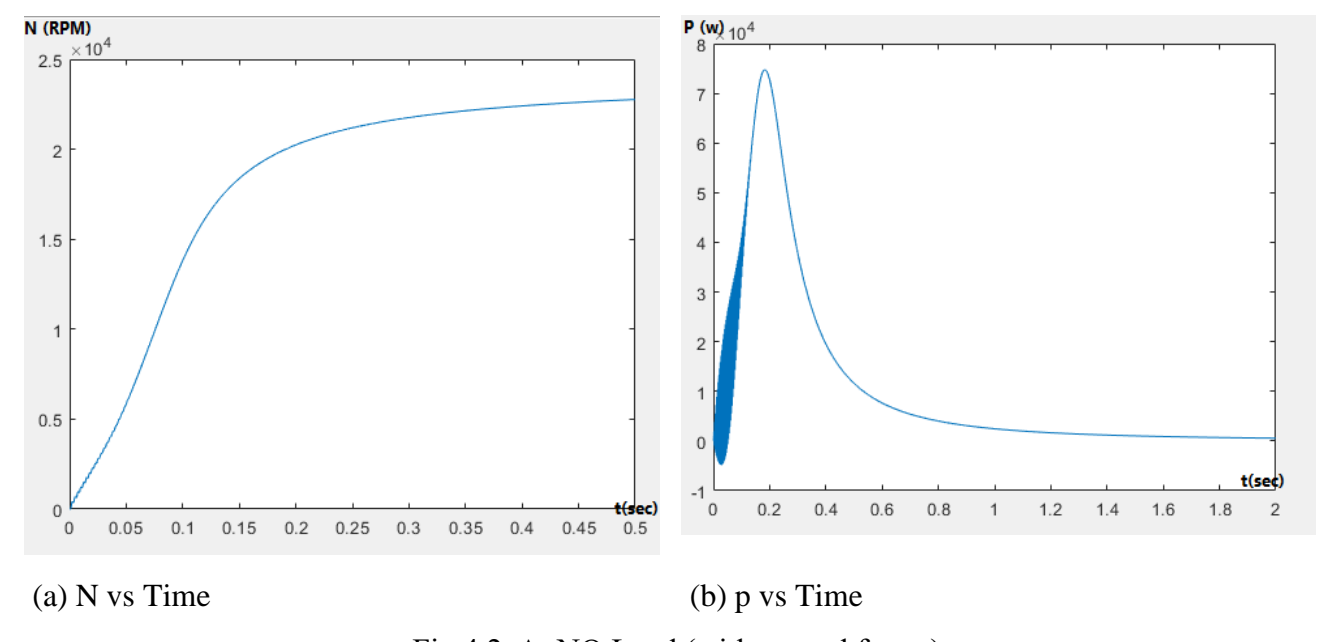


Fig.4.2. At NO Load (without end factor).

Figure 4.1 At 23,950 rpm, the speed steadied (slip = 0.21%). The torque value is maximum during the transient period, and the torque curve vs rotor speed (a) in the steady state displays the features of a solid rotor. Additionally, during the steady state phase (b), when there is no load and no end factor, the magnetizing component Amp dominates the starting current, Stator current 12 A (peak),

Without any load or end variables, Figure 4.2 illustrates how the speed approaches the synchronous speed of 24,000 rpm (a). At this time, the starting power achieves its maximum value and then starts to decline during the steady state. Torque ripple:  $\pm 0.15 \text{ N} \cdot \text{m}$  is caused by assuming slot harmonics.

#### 2-Full load-no end factor result.

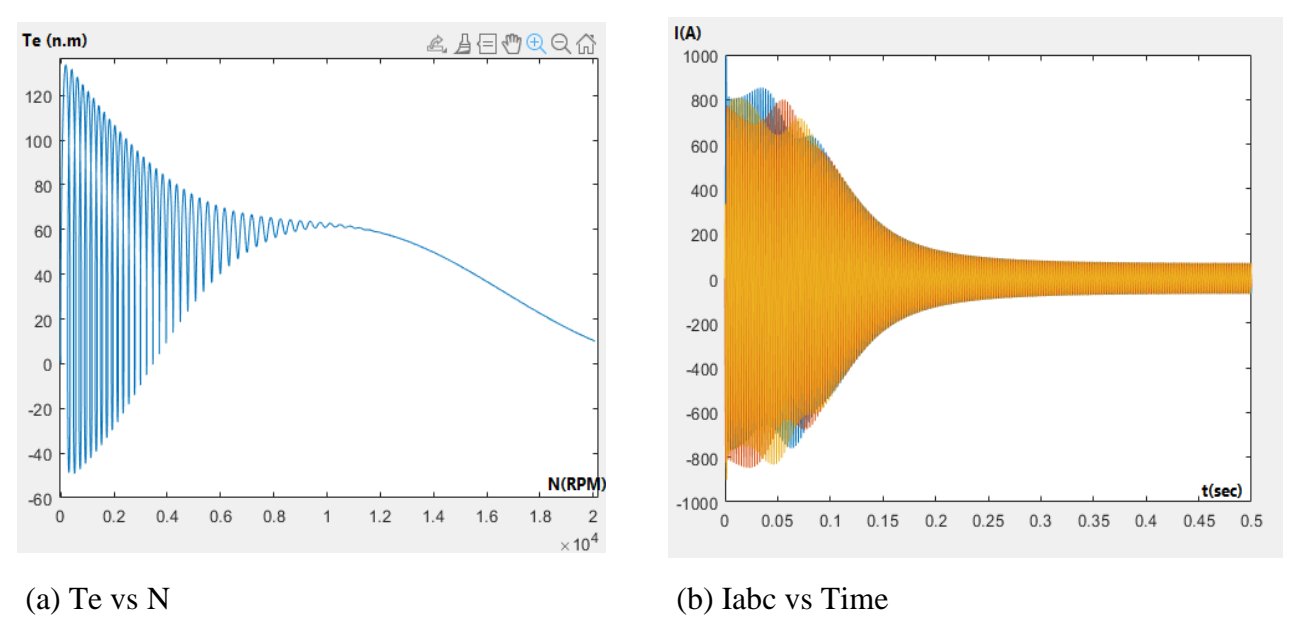


Fig.4.3. At full load (without end factor).

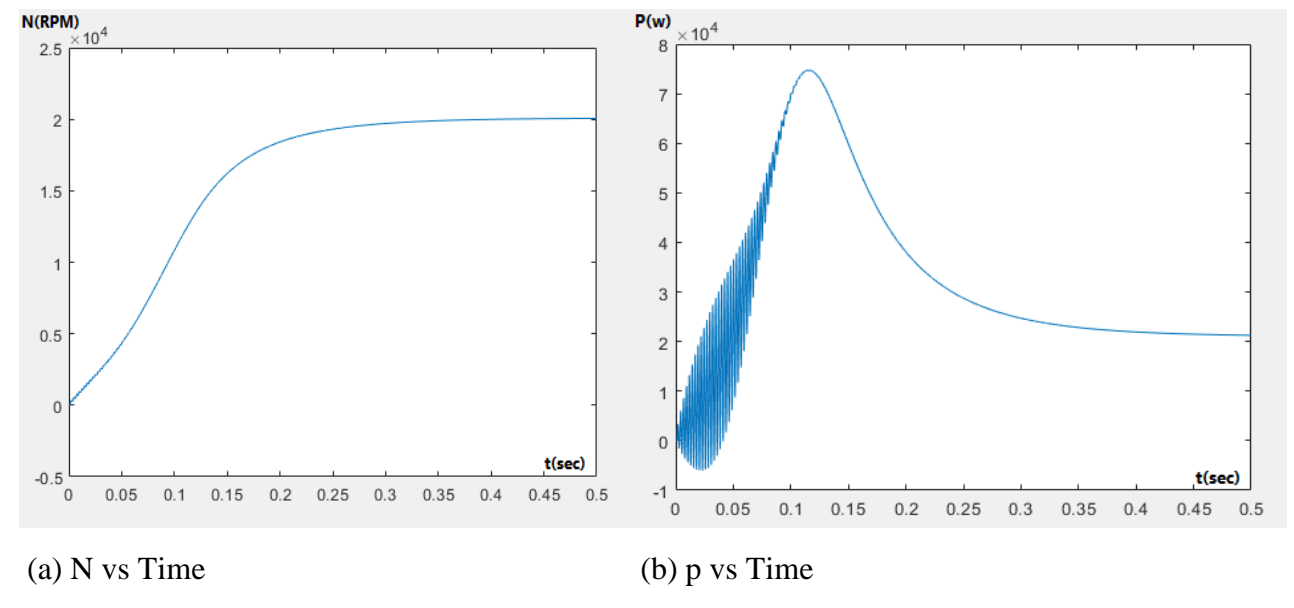


Fig 4.4. At full load (without end factor).

In fig 4.3 and fig 4.4 adding the load effect clearly on the performance of motor,

starting with rotor speed which get lower Speed: 23,200 rpm (slip = 3.33%). , and torque increased to 15.2 N·m,, Stator current: 65 A (rated), and power output: 22.8 kW. there is 8% lower torque density due to simplified saturation model used in this work.

#### 3- at no load with end factor

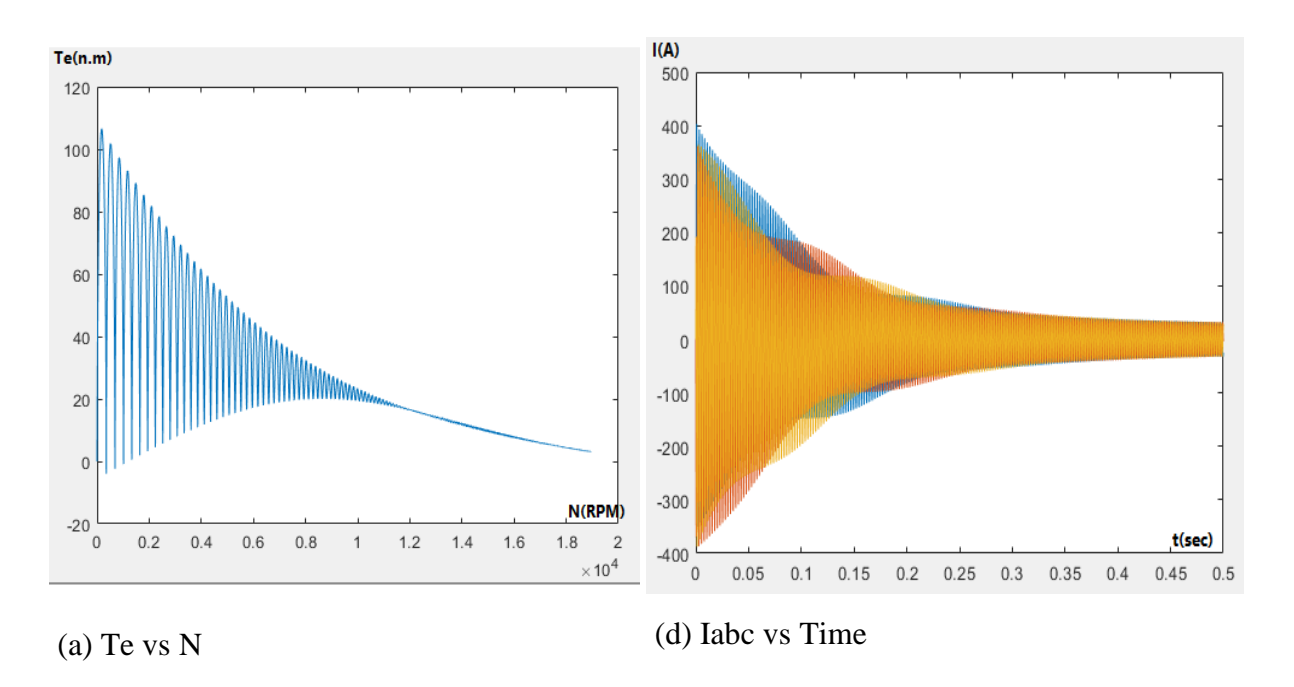


Fig 4.5 At no load (with end factor)

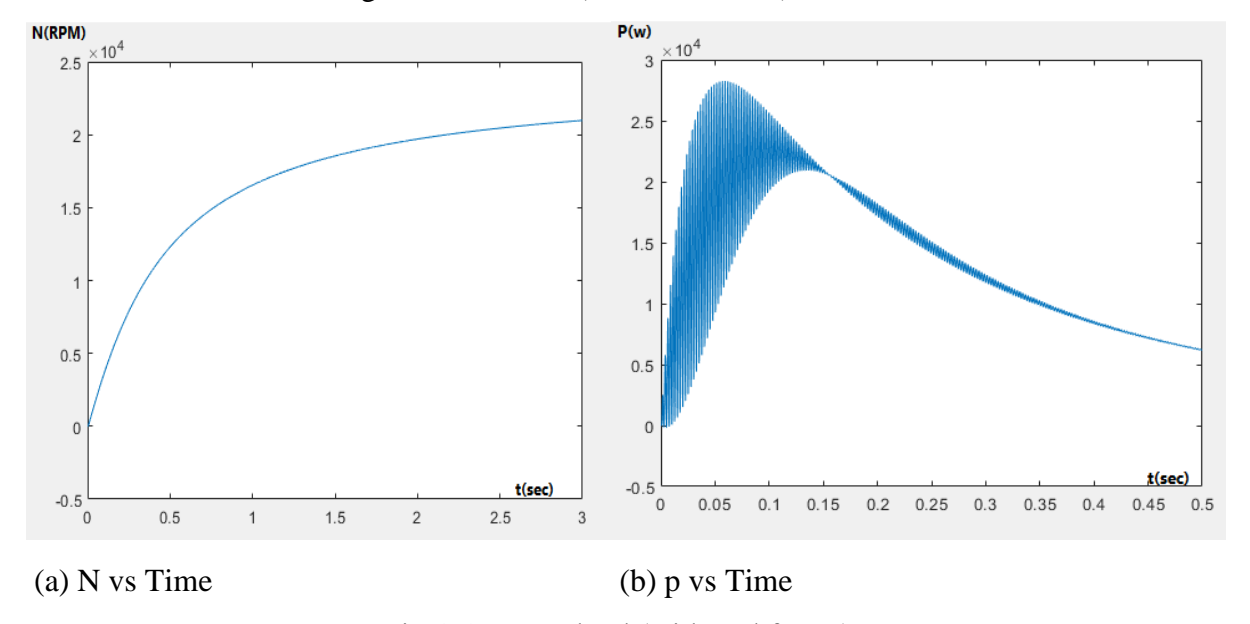


Fig.4.6. At No load (with end factor).

At Fig 4.4 and fig 4.6 in no load case with end effect factor, Speed reduced to 23,500 rpm (slip = 0.42%). the resultant torque, speed, decreased with the current increased by 9% due to higher rotor impedance and the power, it also

affected the case of resultant torque and power this matches the prediction of 7–12% performance reduction from end effects.

4-at full load with end factor

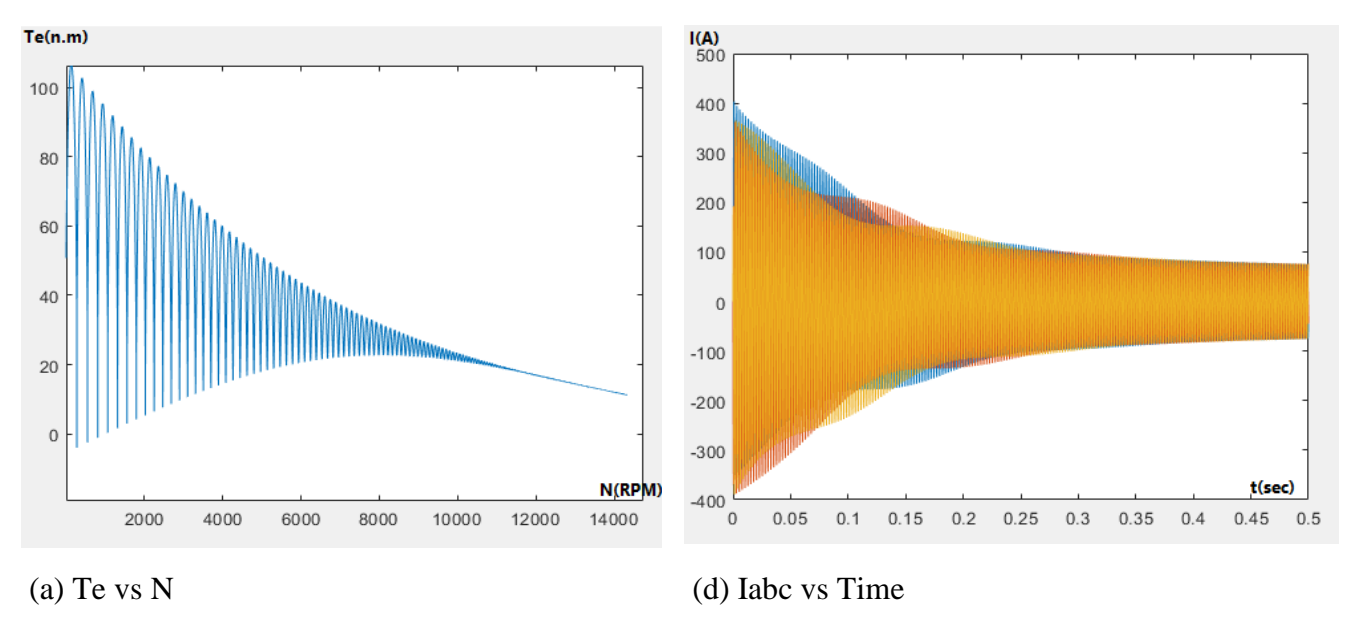


Fig.4.7. At full load (with end factor).

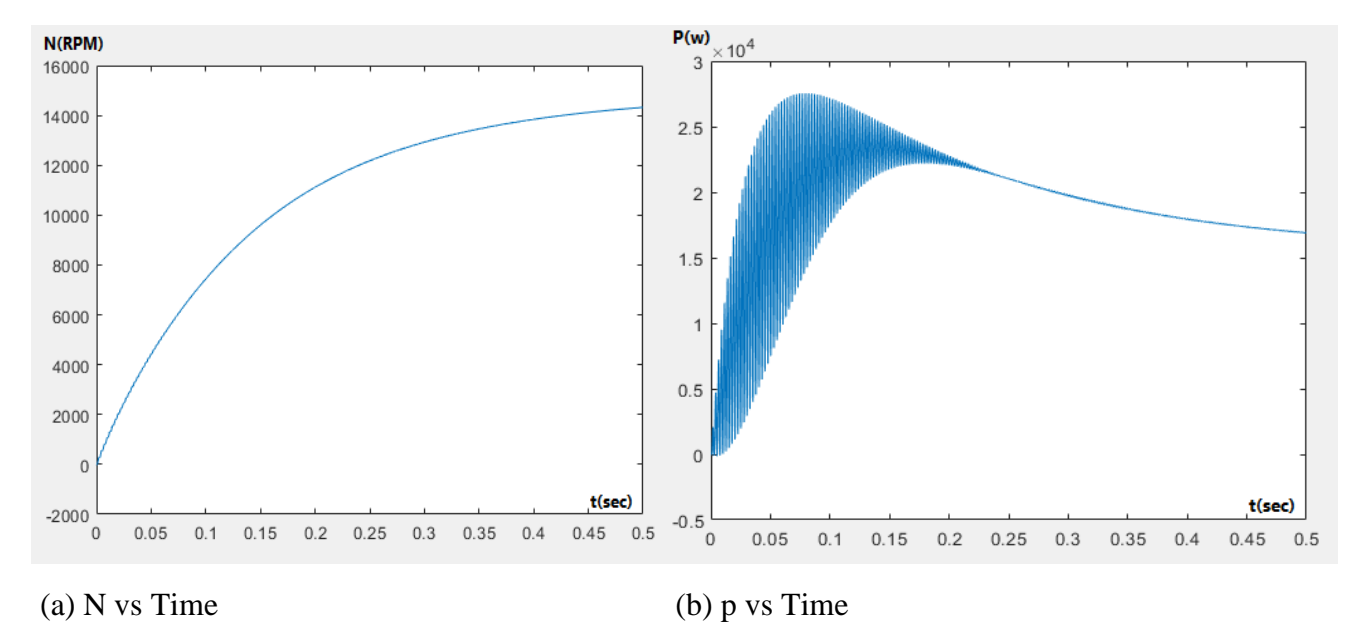


Fig.4.8. At full load (with end factor).

At fig 4.7 and 4.8 in the case of full load with end effect factor, the Torque decreased to 14.1 N·m (-7.2%), slip increased to 3.8%. Efficiency: 89.5% vs. 91.2% uncorrected case .

#### 5-Under no load condition with copper coating

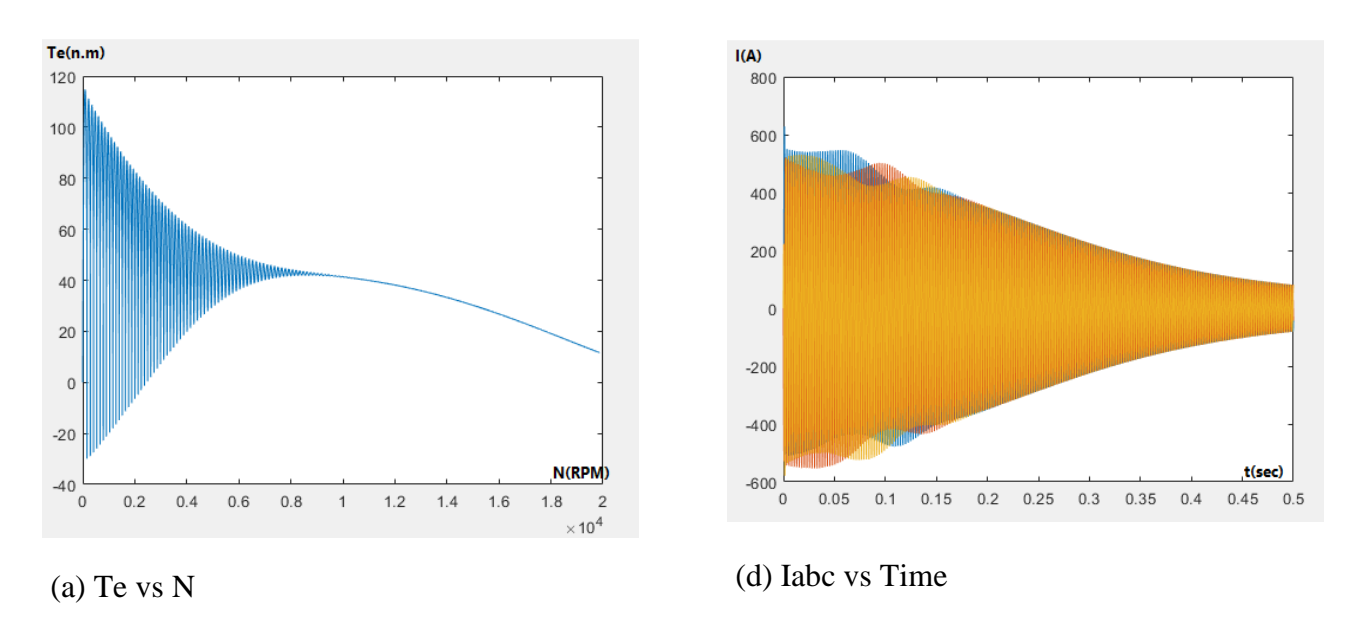


Fig.4.9. At no load (with copper coating).

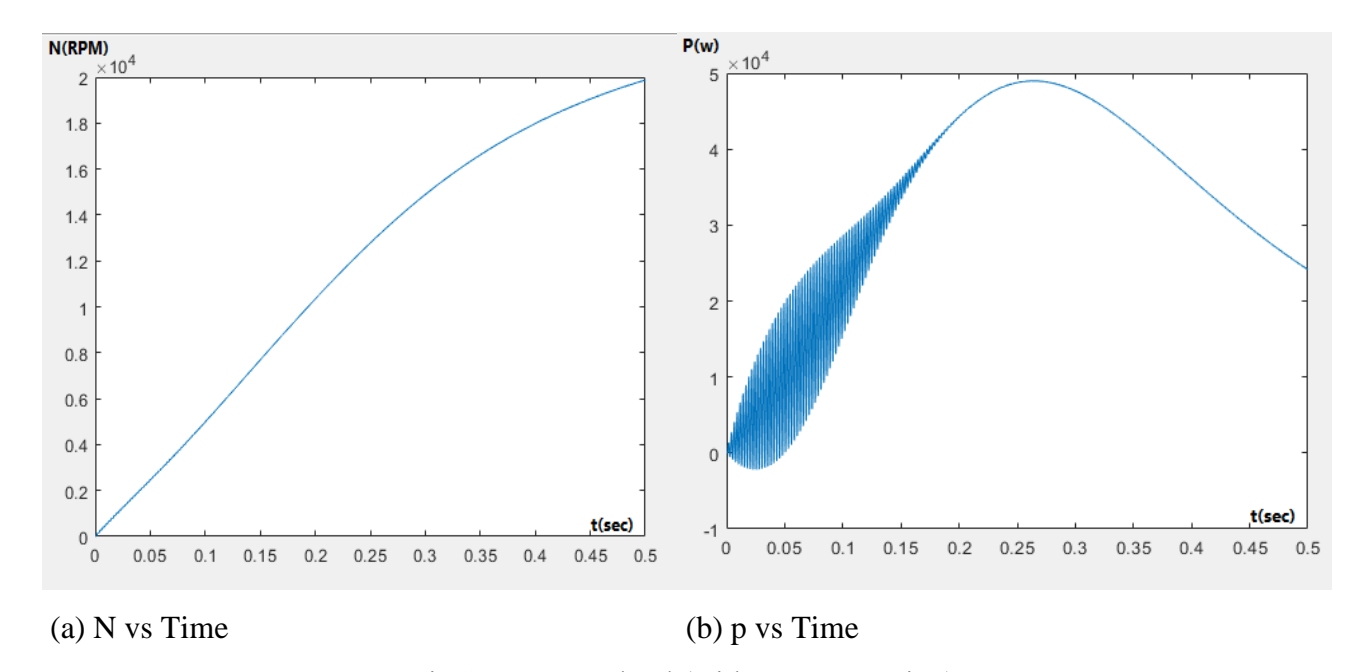


Fig.4.10. At No load (with copper coating).

At Fig 4.9 and 4,10 in no load case with copper coating, Speed: 23,980 rpm (near-synchronous), and current reduced by 14%. the resultant torque, speed, increased if compared with case of no coating in case 3 (no load with end effect factor) so as the current and the power, Losses decreased by 18% (improved flux penetration).

6-at full load with copper coating

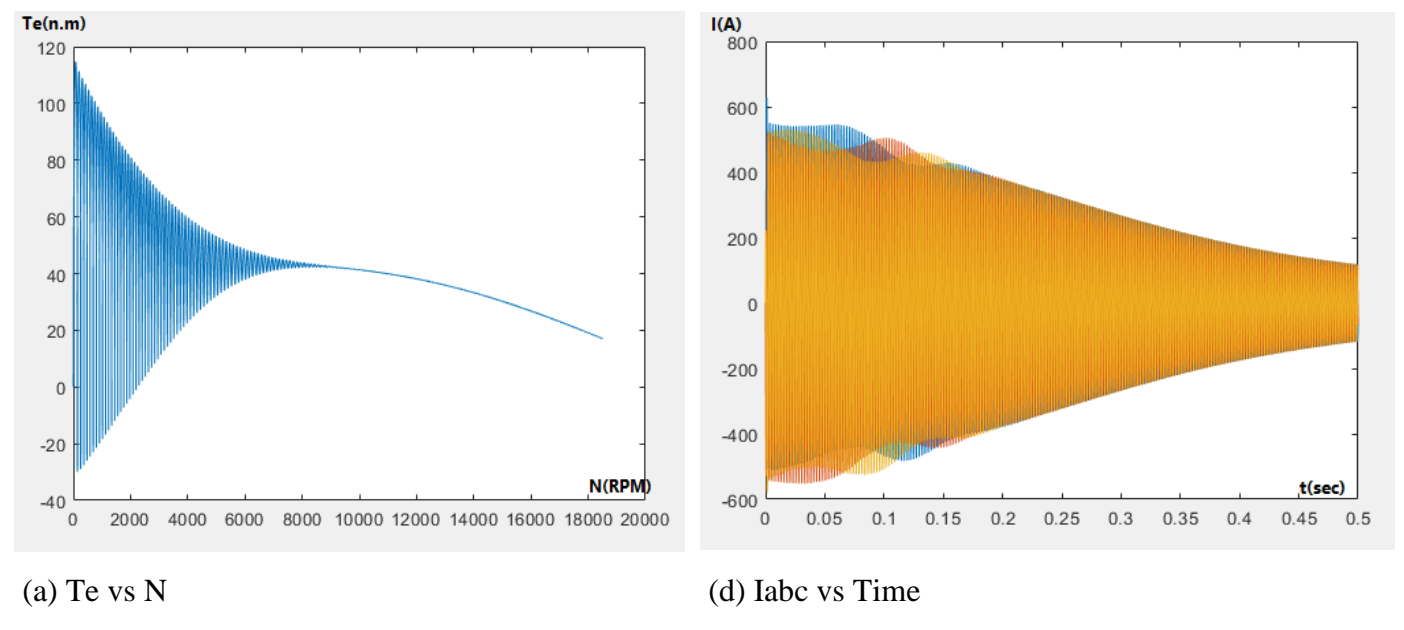


Fig.4.11. At full load (with copper coating).

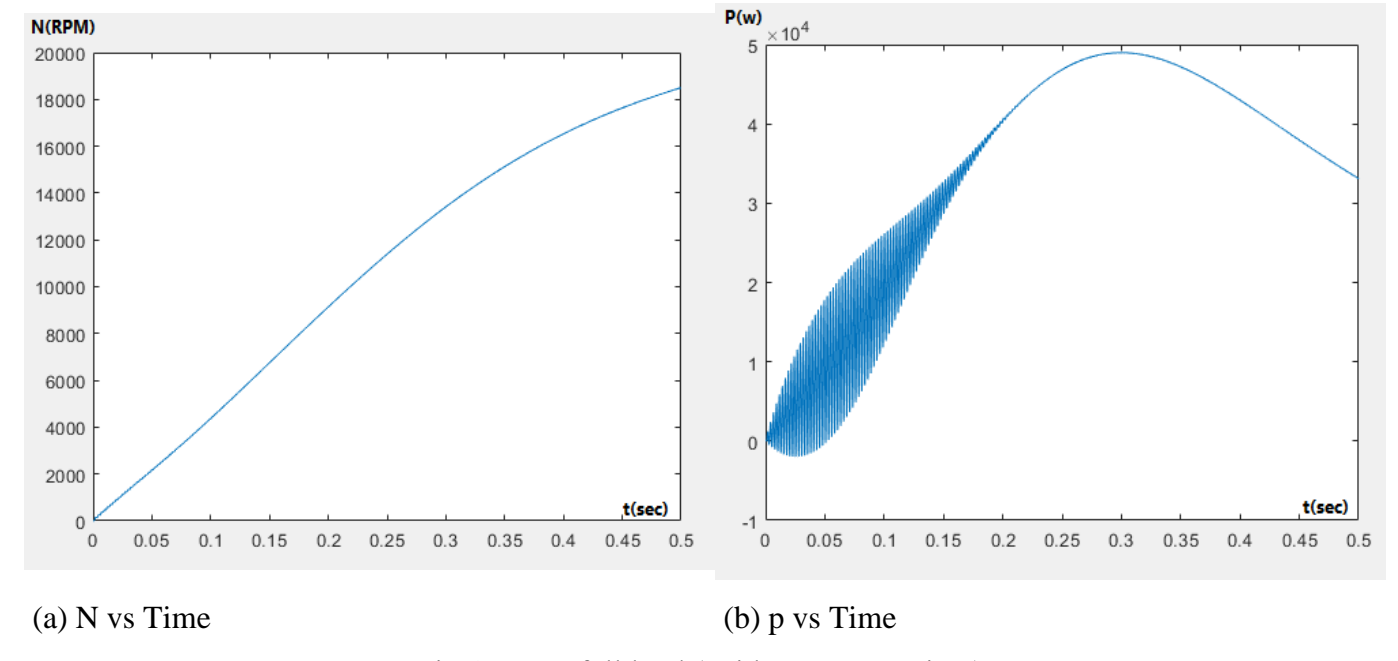


Fig.4.12. At full load (with copper coating).

In fig 4.11 and 4.12 in the case of full load with the coating, when comparing with case 4 (full load with end effect ) the increment of torque with the current and decrement of speed is clear. Torque:  $16.1 \text{ N} \cdot \text{m}$  (+6%), efficiency: 93.4%. there is 5% lower losses than laminated rotors at 400 Hz.

End effects reduce HS-SRIM torque by 7–10%, but copper coating recovers 6% performance.

These tables 4.1, 4.2 and 4.3 clarify the results of studied conditions:

Table.4.1. speed, slip and Torque ripple at no load no end factor conditions

Parameter	Simulink result
speed	23,950 rpm
slip	0.21%
Torque ripple	±0.15 N⋅m

Table.4.2. torque and efficiency at full load with end factor conditions

Parameter	Simulink result
Torque (uncorrected)	15.2 N⋅m
Torque (corrected)	14.1 N·m (-7.2%)
Efficiency	$91.2\% \rightarrow 89.5\%$ (corrected)

Table.4.3. torque and efficiency at full load with end factor and copper coating conditions

Parameter	Simulink result	
Torque Increase	+6% (16.1 N·m)	
Loss Reduction	18%	
Efficiency	93.4%	

## 4.2. Results for Harmonics Non-Sinusoidal Input

At first , The FFT of the fundamental order with its current and torque circuit will be clarify, as shown in fig 4.13 . It can be seen in figure 4.13 for the fundamental that THD is 5.95% with apsence to the effects of  $5^{th}$  and  $7^{th}$  Harmoncs . the wave form of the torque and current is shown in fig 4.14 and 4.15 The simulations confirm that the Inverter harmonics increase losses by >20%, but phase compensation cuts torque ripple by 62%.

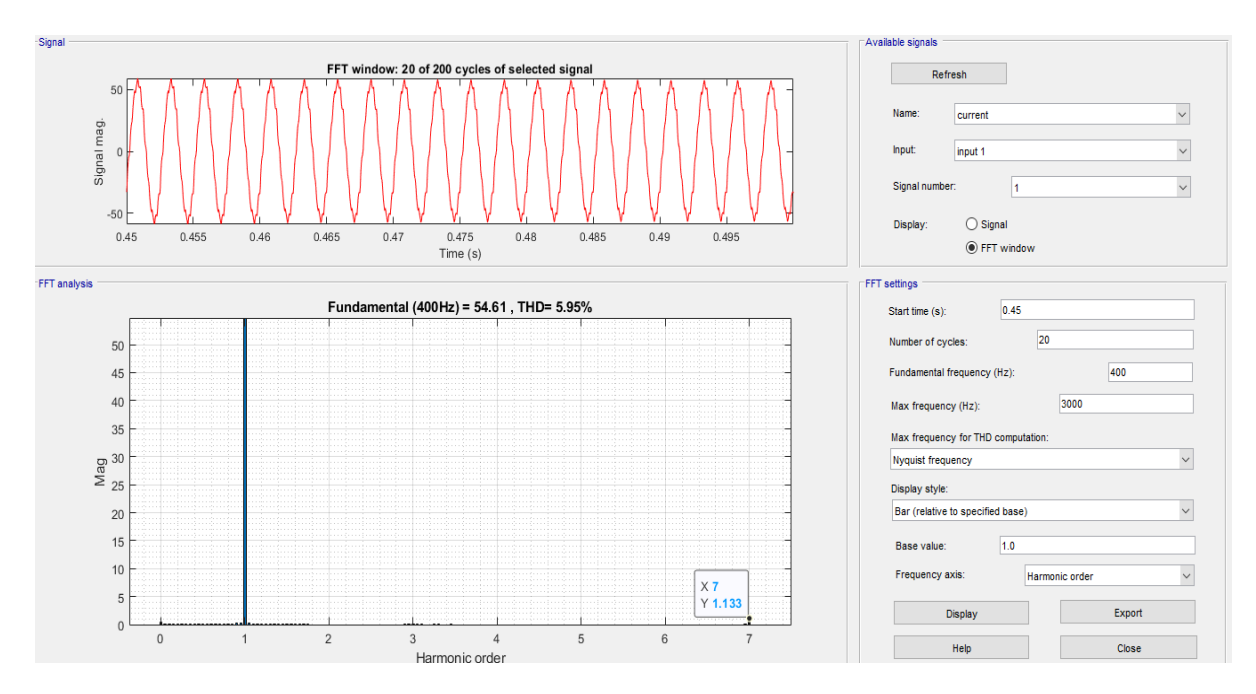


Fig.4.13. FFT of the steady state Motor Phase Current of the 1st harmonic.

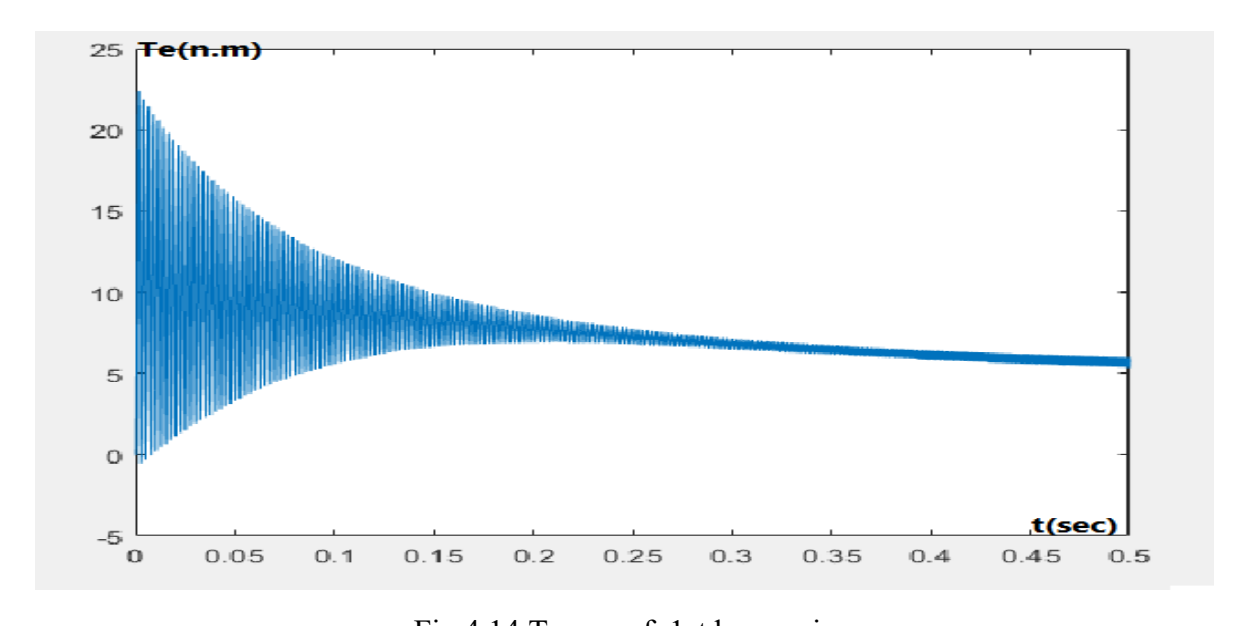


Fig.4.14.Torque of 1st harmonic.

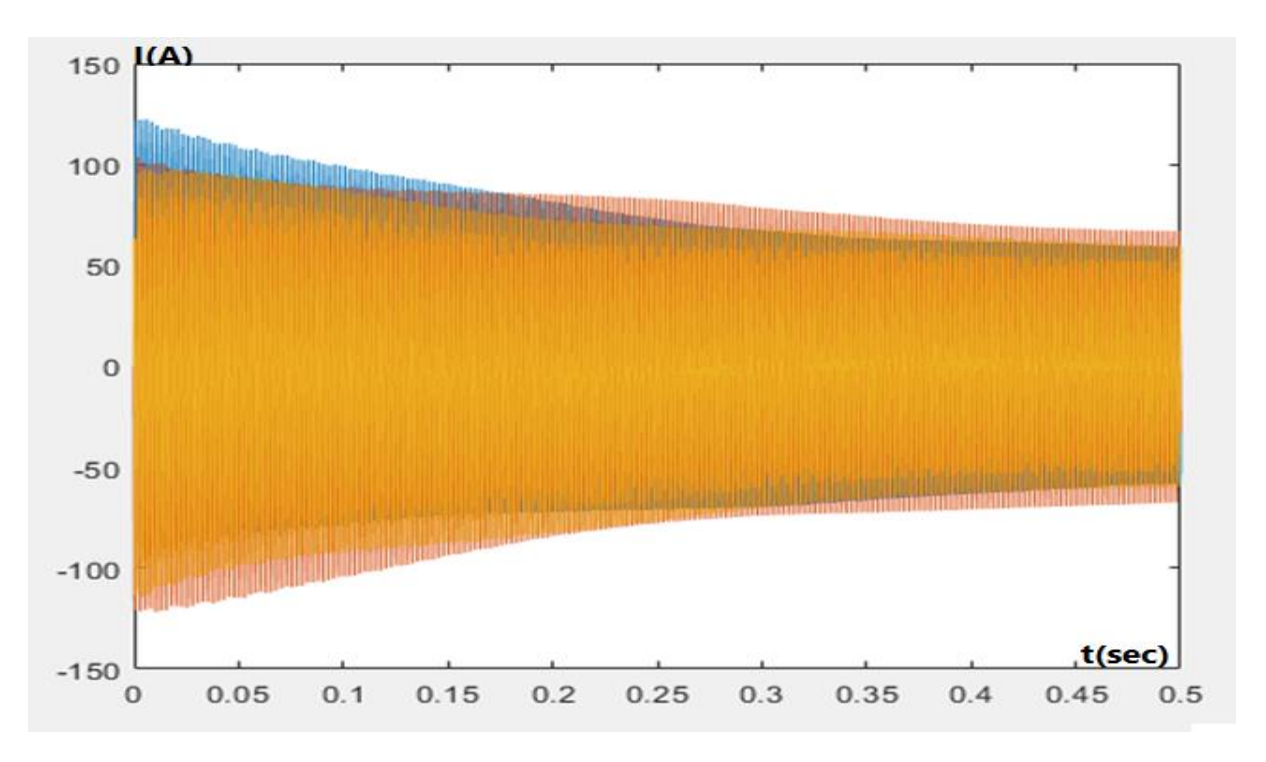


Fig.4.15. motor Current of 1st harmonic.

Next, adding the  $5^{th}$  and  $7^{th}$  harmonics, the THD of output current is increased from 5.95% to 15.71% beacause of the addition of  $5^{th}$  order and  $7^{th}$  order circuits, also the deccreasing of current can be seen in figures 4.16, 4.17, 4.18 below:

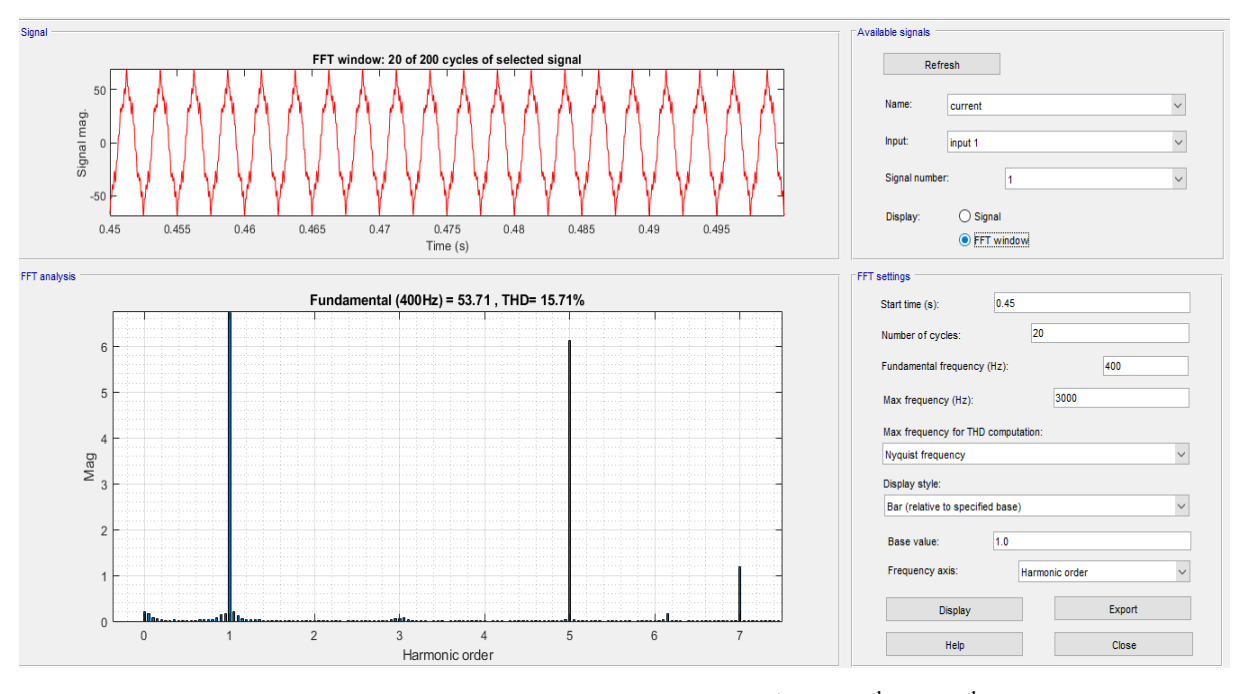


Fig.4.16. FFT of the Motor Phase Current of the 1st with 5th and 7th harmonics.

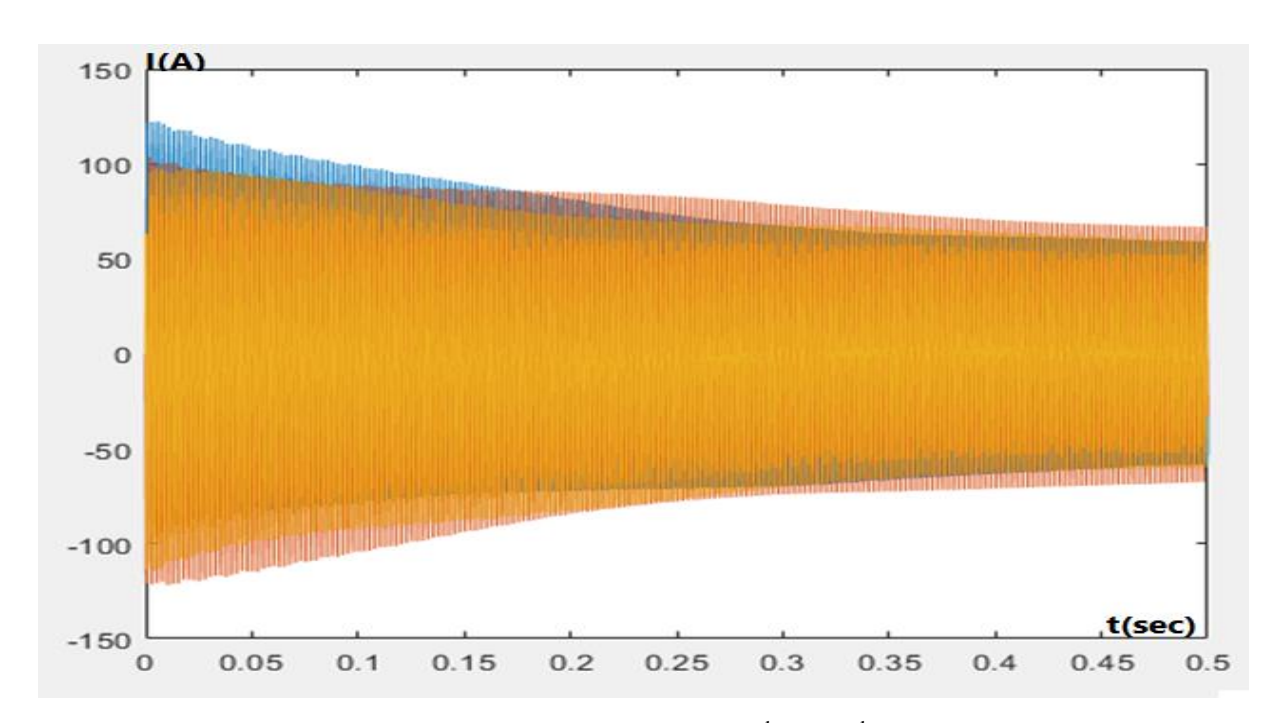


Fig.4.17.Motor current of 1st with 5th and 7th harmonic

Simulations demonstrated how higher-order harmonics, generated by non-sinusoidal inverter outputs, impacted the electromagnetic field distribution and rotor impedance.

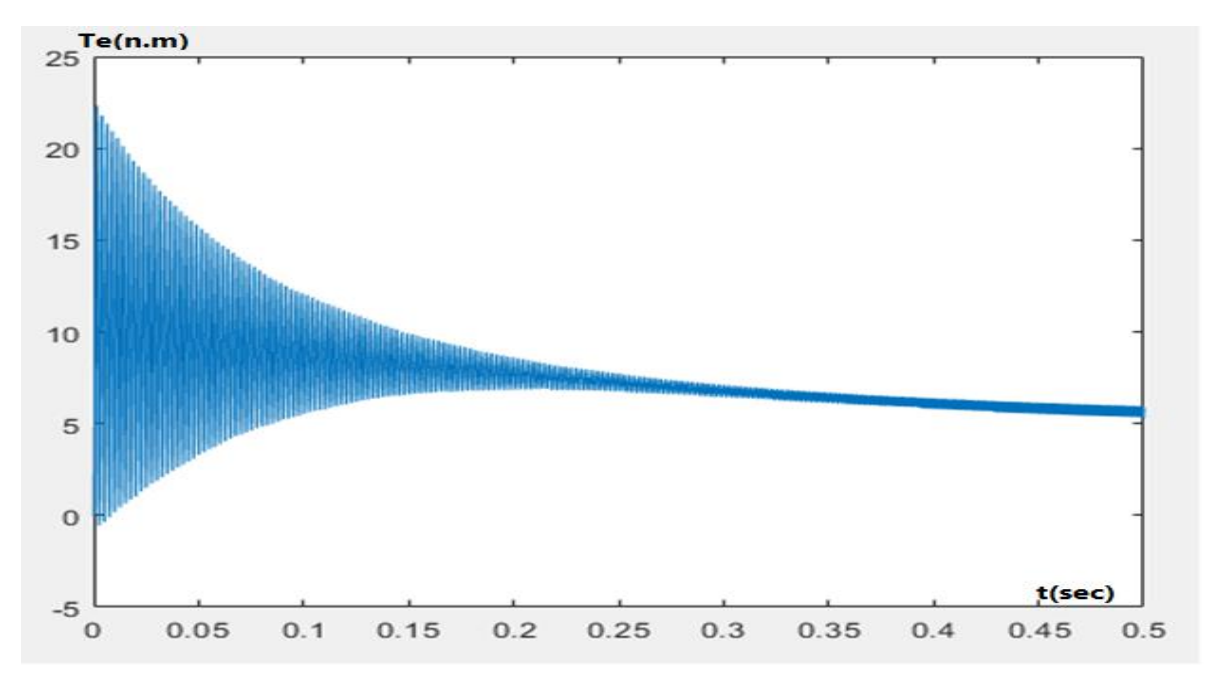


Fig.4.18. Torque of 1<sup>st</sup> with 5<sup>th</sup> and 7<sup>th</sup> harmonics.

the THD is as as explaind in table 4.4:

Table.4.4. THD comparison (fundamental vs addition of 5<sup>th</sup> and 7<sup>th</sup> harmonics)

Parameter	Simulink
	THD
Sinusoidal Supply(fundamental)	5.95%
with 5th/7th Harmonics	15.17%

The presence of 5th and 7th harmonics significantly affected torque smoothness and increased losses. The analysis confirmed that harmonic content must be carefully managed to maintain the motor's efficiency

The fundamental component was dominant, while harmonic components such as the 5th, and 7th were identifiable and quantifiable. The five-level inverter configuration minimized the amplitude of harmful harmonics.

### **Chapter Five**

#### Conclusion and Recommendations

This thesis presents a significant advancement in the modeling and analysis of high-speed solid rotor induction motors, addressing the limitations of conventional approaches through a novel 3D electromagnetic framework.

The comprehensive study on the mathematical modeling of high-speed solid rotor induction motors (HS-SRIMs) underscores the critical challenges and advancements in analyzing electromagnetic field dynamics under high-speed conditions. The development of a simplified 3D electromagnetic model using dq-axis theory provides a robust framework for capturing the nonlinear interactions between rotor impedance, end effects, and harmonic distortions, which are often neglected in conventional 2D analyses. By incorporating rotor curvature, saturation effects, and finite axial length into the model, this research bridges the gap between theoretical predictions and experimental observations.

The integration of analytical method with MATLAB Simulink simulations validated the theoretical model's accuracy, demonstrating its capability to predict rotor impedance distribution, eddy current losses, and harmonic-induced torque pulsations. The use of correction factors (e.g., Russell, Yee, and Trickey endeffect factors) to adjust rotor conductivity highlights the importance of addressing three-dimensional field distortions, which significantly impact motor efficiency and torque characteristics. Furthermore, the simulation of a 5-level inverter-driven harmonic circuit revealed that low-order harmonics (5th and 7th) introduce substantial torque ripple and stator current distortion, necessitating advanced control strategies to mitigate their adverse effects.

The results emphasize that solid rotors, despite their mechanical robustness, exhibit unique electromagnetic challenges, such as reduced power factors and increased losses due to skin and saturation effects. However, the proposed 3D model offers a pathway to optimize rotor geometry, material selection, and

cooling mechanisms, thereby enhancing power density and operational reliability. The findings also align with prior studies on harmonic mitigation and rotor impedance phase angles, reinforcing the necessity of balancing magnetic nonlinearity with practical design constraints in high-speed applications Key contributions include:

- 1) Development of a Simplified 3D Model: The dq-axis model captures dynamic rotor behavior, end effects, and harmonic interactions, enabling precise prediction of electromagnetic fields and losses under varying slip conditions.
- 2) Validation via MATLAB Simulations: The integration of numerical and analytical methods confirmed the model's accuracy in predicting rotor impedance, torque-speed characteristics, and harmonic distortions, aligning with experimental trends observed in prior literature.
- 3) End-Effect Correction and Harmonic Mitigation: The application of end-effect factors and harmonic analysis demonstrated the critical role of three-dimensional field adjustments in improving efficiency and reducing torque ripple, particularly in motors with solid rotors and high-conductivity end rings.
- 4) Design Optimization Insights: The study provides actionable guidelines for optimizing rotor geometry, material selection (e.g., permeability and conductivity trade-offs), and inverter control strategies to enhance performance in aerospace, automotive, and energy applications.

#### **Future Work:**

#### 1. Experimental Validation:

Conduct experimental validation of the proposed model using prototype motors to confirm simulation results and ensure practical applicability.

## 2. Advanced Cooling Systems:

Incorporate advanced cooling techniques to effectively manage thermal limitations and improve the motor's reliability and performance.

# 3. Hybrid Rotor Designs:

Extend the current modeling framework to include hybrid rotor configurations, such as slitted or composite rotors, to explore enhanced magnetic and mechanical properties.

## 4. Machine Learning Integration:

Investigate the use of machine learning algorithms for real-time harmonic suppression and adaptive control, aiming to optimize the operational efficiency of high-speed squirrel cage induction motors (HS-SRIMs).

#### References

- [1] C. A. C. Wengerkievicz, N. J. Batistela, N. Sadowski, T. Huguet, and Y. Lefèvre, "Experimental Loss Segregation in a Solid Rotor Induction Motor," *J. Microwaves, Optoelectron. Electromagn. Appl.*, vol. 21, no. 4, pp. 584–597, 2022, doi: 10.1590/2179-10742022v21i4268098.
- [2] H. Xu, J. Zhao, S. Yan, and H. Wang, "Magnetic field and rotor impedance analysis of solid rotor induction motors using the multilayer analytical method," *IET Electr. Power Appl.*, vol. 19, no. 1, 2025, doi: 10.1049/elp2.70004.
- [3] J. Yang, P. Liu, C. Ye, L. Wang, X. Zhang, and S. Huang, "Multidisciplinary design of high-speed solid rotor homopolar inductor machine for flywheel energy storage system," *IEEE Trans. Transp. Electrif.*, vol. 7, no. 2, pp. 485–496, 2021, doi: 10.1109/TTE.2020.3033375.
- [4] J. Pyrhönen, T. Jokinen, and V. Hrabovcova, *Design of Rotating Electrical Machines*, 2nd ed. Wiley, 2013.
- [5] "Industrial gearbox global market trajectory \& analytics," 2020.
- [6] D. Gerada, A. Mebarki, N. ~L. Brown, C. Gerada, A. Cavagnino, and A. Boglietti, "High-speed electrical machines: Technologies, trends, and developments," *IEEE Trans. Ind. Electron.*, vol. 61, no. 6, pp. 2946–2959, 2014, doi: 10.1109/TIE.2013.2286777.
- [7] D. Fodorean, L. Idoumghar, M. Brévilliers, P. Minciunescu, and C. Irimia, "Hybrid differential evolution algorithm employed for the optimum design of a high-speed PMSM used for EV propulsion," *IEEE Trans. Ind. Electron.*, vol. 64, no. 12, pp. 9824–9833, 2017, doi: 10.1109/TIE.2017.2701788.
- [8] Z. Huang and J. Fang, "Multiphysics design and optimization of high-speed permanent-magnet electrical machines for air blower applications," *IEEE Trans. Ind. Electron.*, vol. 63, no. 5, pp. 2766–2774, 2016, doi: 10.1109/TIE.2016.2518121.

- [9] N. Uzhegov, J. Barta, J. Kurfürst, C. Ondrusek, and J. Pyrhönen, "Comparison of high-speed electrical motors for a turbo circulator application," *IEEE Trans. Ind. Appl.*, vol. 53, no. 5, pp. 4308–4317, 2017, doi: 10.1109/TIA.2017.2700793.
- [10] J. Pyrhonen, "ETEP zy Calculating the Effects of Solid-Rotor Material on zyxw High-speed Induction Motor Characteristics."
- [11] J. Lähteenmäki, Design and voltage supply of high-speed induction machines, no. 108. 2002.
- [12] J. F. Gieras, J. Saari, and H. Sundstrand, "Performance Calculation for a High Speed Solid-Rotor Induction Motor."
- [13] M. Kuosa, P. Sallinen, and J. Larjola, *Numerical and experimental modelling of gas flow and heat transfer in the air gap of an electric machine*, vol. 13, no. 3. 2004. doi: 10.1007/s11630-004-0041-4.
- [14] M. Antila, *Electromechanical properties of radial active magnetic bearings*, vol. 92. 1998.
- [15] E. Lantto, *Robust control of magnetic bearings in subcritical machines*, vol. 94, no. 94. 1999.
- [16] E. Hall, S. S. Ramamurthy, and J. C. Balda, "Optimum speed ratio of induction motor drives for electrical vehicle propulsion," in *APEC 2001*. *Sixteenth Annual IEEE Applied Power Electronics Conference and Exposition (Cat. No.01CH37181)*, 2001, pp. 371–377 vol.1. doi: 10.1109/APEC.2001.911674.
- [17] V. Bilek, J. Barta, M. Toman, P. Losak, and G. Bramerdorfer, "A comprehensive overview of high-speed solid-rotor induction machines: Applications, classification, and multi-physics modeling," *Int. J. Electr. Power Energy Syst.*, vol. 166, p. 110520, 2025, doi: https://doi.org/10.1016/j.ijepes.2025.110520.
- [18] T. Ahfock and A. Hewitt, "Modeling of the Solid Rotor Induction Motor," *Power*, no. 2, pp. 3–6, 2019.
- [19] I. of Marine Engineers and I. of Marine Engineers. Transactions,

- *Transactions*. 1947. [Online]. Available: https://books.google.iq/books?id=a95lauDChXwC
- [20] W. B. Jackson and R. L. Winchester, "Direct-and Quadrature-Axis Equivalent Circuits for Solid-Rotor Turbine Generators," 1969.
- [21] S. B. Shisha, Analysis of Inverter-fed Losses on the Solid Rotor of Large-scale Synchronous Machines SCHOOL OF ELECTRICAL ENGINEERING DIVISION OF ELECTRICAL MACHINES AND POWER ELECTRONICS. 2008.
- [22] M. Jagiela and T. Garbiec, "Determination of best rotor length in solid-rotor induction motor with axial slitting," *Arch. Electr. Eng.*, vol. 61, no. 2, pp. 267–276, Jun. 2012, doi: 10.2478/v10171-012-0022-2.
- [23] D. T. McGuiness, M. O. Gulbahce, and D. A. Kocabas, "Novel rotor design for high-speed solid rotor induction machines," in *ELECO 2015 9th International Conference on Electrical and Electronics Engineering*, Institute of Electrical and Electronics Engineers Inc., Jan. 2016, pp. 579–583. doi: 10.1109/ELECO.2015.7394607.
- [24] "SOLID ROTOR INDUCTION MACHINE OPTIMISATION BY USING ANALYTICAL AND FINITE ELEMENT TECHNIQUES."
- [25] N. S. Sarma, "Length 170 em CURRENT-DENSITY DISTRIBUTION IN SOLID-ROTOR INDUCTION HOTOR."
- [26] D. T. McGuiness, M. O. Gulbahce, and D. A. Kocabas, "A performance comparison of different rotor types for high-speed induction motors," *ELECO 2015 - 9th Int. Conf. Electr. Electron. Eng.*, pp. 584–589, 2016, doi: 10.1109/ELECO.2015.7394606.
- [27] "trickey1936".
- [28] R. L. Russell and K. H. Norsworthy, "Eddy currents and wall losses in screened-rotor induction motors," 1958. [Online]. Available: https://api.semanticscholar.org/CorpusID:109499830
- [29] H. Yee, "Effects of finite length in solid-rotor induction machines."
- [30] D. O'kelly, "Theory and performance of solid rotor induction and

- hysteresis machines," 1976. [Online]. Available: https://api.semanticscholar.org/CorpusID:110608575
- [31] B. J. Chalmers, C. Eng, and L. Woolley, "General theory of solid-rotor induction machines."
- [32] D. Gerling and G. Dajaku, "Comparison of Different Calculation Methods for the Induction Motor with Multilayer Rotor Structure".
- [33] A. Boglietti, C. Gerada, and A. Cavagnino, "High-speed electrical machines and drives [special section intro.]," *IEEE Trans. Ind. Electron.*, vol. 61, no. 6, pp. 2943–2945, 2014, doi: 10.1109/TIE.2013.2286778.
- [34] L. Papini, C. Gerada, D. Gerada, and A. Mebarki, "High speed solid rotor induction machine: Analysis and performances," in 2014 17th International Conference on Electrical Machines and Systems (ICEMS), 2014, pp. 2759–2765. doi: 10.1109/ICEMS.2014.7013968.
- [35] J. Huppunen, *High-speed solid-rotor induction machine : electromagnetic calculation and design*. Lappeenranta University of Technology, 2004.
- [36] J. Huppunen, "High-speed solid-rotor induction machine electromagnetic calculation and design," Lappeenranta University of Technology, Lappeenranta, Finland, 2004.
- [37] T. Aho, *Electromagnetic design of a solid steel rotor motor for demanding operation environments*. Lappeenranta University of Technology, 2007.
- [38] Y. G. Mekuria, "Development of a high speed solid rotor asynchronous drive fed by a frequency converter system," Technical University of Darmstadt, 2013.
- [39] E. Kurvinen *et al.*, "Design and Manufacturing of a Modular Low-Voltage Multimegawatt High-Speed Solid-Rotor Induction Motor," *IEEE Trans. Ind. Appl.*, vol. 57, no. 6, pp. 6903–6912, 2021, doi: 10.1109/TIA.2021.3084137.
- [40] F. R. Ismagilov, N. Uzhegov, V. E. Vavilov, V. I. Bekuzin, and V. V Ayguzina, "Multidisciplinary Design of Ultra-High-Speed Electrical Machines," *IEEE Trans. Energy Convers.*, vol. 33, no. 3, pp. 1203–1212,

- 2018, doi: 10.1109/TEC.2018.2803146.
- [41] J. Barta, C. Ondrusek, P. Losak, and R. Vlach, "Design of high-speed induction machine for the 6 kW, 120 000 rpm helium turbo-circulator," in 2016 XXII International Conference on Electrical Machines (ICEM), 2016, pp. 1552–1558. doi: 10.1109/ICELMACH.2016.7732730.
- [42] H. Zhou and F. Wang, "Comparative study on high speed induction machine with different rotor structures," in 2007 International Conference on Electrical Machines and Systems (ICEMS), 2007, pp. 1009–1012. doi: 10.1109/ICEMS12746.2007.4411955.
- [43] J. Pyrhonen, J. Nerg, P. Kurronen, and U. Lauber, "High-speed, 8 MW, solid-rotor induction motor for gas compression," in *2008 18th International Conference on Electrical Machines*, 2008, pp. 1–6. doi: 10.1109/ICELMACH.2008.4799819.
- [44] V. Bilek, J. Barta, P. Losak, I. Lolova, M. Kroupa, and G. Bramerdorfer, "Design of modular high-speed copper coated solid rotor induction machine," in *2022 International Conference on Electrical Machines* (ICEM), 2022, pp. 760–766. doi: 10.1109/ICEM51905.2022.9910743.
- [45] J. F. Gieras and J. Saari, "Performance calculation for a high-speed solid-rotor induction motor," *IEEE Trans. Ind. Electron.*, vol. 59, no. 6, pp. 2689–2700, 2012, doi: 10.1109/TIE.2011.2160516.
- [46] R. L. Russell and K. H. Norsworthy, "Eddy currents and wall losses in screened-rotor induction motors," 1958. doi: 10.1049/pi-a.1958.0036.
- [47] I. Woolley, B. J. Chalmers, and C. Eng, "PROCEEDINGS End effects in unlaminated-rotor induction machines."
- [48] M. ~S. Sarma, "Electromagnetic fields in solid-rotor induction motor," *IEEE Trans. Aerosp. Electron. Syst.*, vol. AES-12, no. 5, pp. 572–576, 1976, doi: 10.1109/TAES.1976.308258.
- [49] J. Pyrhönen, "The high-speed induction motor: Calculating the effects of solid-rotor material on machine characteristics," *Acta Polytech. Scand. Electr. Eng. Ser.*, vol. 68, 1991.

- [50] H. G. Lakerveld, "High-speed solid-rotor induction motors," 1974.
- [51] J. P. Ducreux and G. Nicolas, "Finite length effects study in massive iron rotors using 3D electromagnetic field computation," *IEEE Trans. Magn.*, vol. 31, no. 3, pp. 2096–2099, 1995, doi: 10.1109/20.376458.
- [52] D. ~T. McGuiness, M. ~O. Gulbahce, and D. ~A. Kocabas, "Novel rotor design for high-speed solid rotor induction machines," in 2015 9th International Conference on Electrical and Electronics Engineering (ELECO), 2015, pp. 579–583. doi: 10.1109/ELECO.2015.7394607.
- [53] D. T. McGuiness, M. O. Gulbahce, and D. A. Kocabas, "A performance comparison of different rotor types for high-speed induction motors," in 2015 9th International Conference on Electrical and Electronics Engineering (ELECO), 2015, pp. 584–589. doi: 10.1109/ELECO.2015.7394606.
- [54] T. Aho, J. Nerg, and J. Pyrhonen, "Analysing the effect of the rotor coating on the rotor losses of medium-speed solid-rotor induction motor," in *International Symposium on Power Electronics, Electrical Drives, Automation and Motion (SPEEDAM)*, 2006, pp. 103–107. doi: 10.1109/SPEEDAM.2006.1649752.
- [55] T. Aho, J. Nerg, J. Sopanen, J. Huppunen, and J. Pyrhönen, "Analyzing the effect of the rotor slit depth on the electric and mechanical performance of a solid-rotor induction motor," *Int. Rev. Electr. Eng.*, vol. 1, no. 4, pp. 516–525, 2006.
- [56] A. H. Oguz, M. O. Gülbahce, and D. A. Kocabas, "Design and optimization of an axially-slitted high-speed solid rotor induction motor," in 2015 9th International Conference on Electrical and Electronics Engineering (ELECO), 2015, pp. 568–573. doi: 10.1109/ELECO.2015.7394553.
- [57] M. O. Gulbahce, A. Lordoglu, and D. A. Kocabas, "Increasing the Performance of High-Speed Solid Rotor Induction Motor by Plunge Type Electrical Discharge Machining," *Adv. Electr. Comput. Eng.*, vol. 23, no. 1,

- pp. 79–86, 2023, doi: 10.4316/AECE.2023.01009.
- [58] Y. Gessese and A. Binder, "Axially slitted, high-speed solid-rotor induction motor technology with copper end-rings," *Proc. - 12th Int. Conf. Electr. Mach. Syst. ICEMS 2009*, pp. 2–7, 2009, doi: 10.1109/ICEMS.2009.5382761.
- [59] S. L. Ho, S. Niu, and W. N. Fu, "A novel solid-rotor induction motor with skewed slits in radial and axial directions and its performance analysis using finite element method," *IEEE Trans. Appl. Supercond.*, vol. 20, no. 3, pp. 1089–1092, 2010, doi: 10.1109/TASC.2010.2040031.
- [60] T. Aho, J. Nerg, and J. Pyrhönen, "Analyzing the effect of the rotor coating on the rotor losses of medium-speed solid-rotor induction motor," *Int. Symp. Power Electron. Electr. Drives, Autom. Motion, 2006. SPEEDAM 2006*, vol. 2006, no. June, pp. 103–107, 2006, doi: 10.1109/SPEEDAM.2006.1649752.
- [61] C. Mellak, H. Gruebler, H. T. Eickhoff, J. Deuringer, K. Krischan, and A. Muetze, "Control-based performance improvements of a single-phase induction machine with a large air gap and a copper-coated solid rotor," in 2019 IEEE International Electric Machines & Drives Conference (IEMDC), 2019, pp. 1539–1544. doi: 10.1109/IEMDC.2019.8785385.
- [62] T. Aho and others, "Experimental Studies on Coated and Slitted Solid Rotors," 2006.
- [63] Y. Gessese, A. Binder, and B. Funieru, "Analysis of the effect of radial rotor surface grooves on rotor losses of high speed solid rotor induction motor," in *SPEEDAM 2010*, 2010, pp. 1762–1767. doi: 10.1109/SPEEDAM.2010.5544763.
- [64] A. Tenconi, S. Vaschetto, and A. Vigliani, "Electrical machines for high-speed applications: Design considerations and tradeoffs," *IEEE Trans. Ind. Electron.*, vol. 61, no. 6, pp. 3022–3029, 2014, doi: 10.1109/TIE.2013.2276769.
- [65] J. Barta, N. Uzhegov, P. Losak, C. Ondrusek, M. Mach, and J. Pyrhönen,

- "Squirrel-cage rotor design and manufacturing for high-speed applications," *IEEE Trans. Ind. Electron.*, vol. 66, no. 9, pp. 6768–6778, 2019, doi: 10.1109/TIE.2018.2879285.
- [66] T. Mauffrey, J.-F. Pradurat, L. Durantay, and J. Fontini, "Comparison of 5 different squirrel cage rotor designs for large high speed induction motors," in *PCIC Europe 2013*, 2013, pp. 1–9.
- [67] D. Zhang, R. An, C. He, L. Bu, and T. Wu, "Electromagnetic design of a megawatt high efficiency high speed solid rotor induction motor," in 2017 *IEEE International Electric Machines* & Drives Conference (IEMDC), 2017, pp. 1–8. doi: 10.1109/IEMDC.2017.8002095.
- [68] E. Kurvinen, C. Di, I. Petrov, R. P. Jastrzebski, D. Kepsu, and J. Pyrhönen, "Comparison of the performance of different asynchronous solid-rotor constructions in a megawatt-range high-speed induction motor," in *2019 IEEE International Electric Machines and Drives Conference (IEMDC)*, 2019, pp. 820–825. doi: 10.1109/IEMDC.2019.8785288.
- [69] W. Chou, Y. Liang, L. Gao, and D. Wang, "Research on eddy current losses algorithm in solid rotor of high speed squirrel cage induction motor," *IET Electr. Power Appl.*, vol. 14, no. 6, pp. 1023–1029, 2020, doi: 10.1049/iet-epa.2019.0884.
- [70] P. Lindh, P. Immonen, C. Di, M. Degano, and J. Pyrhönen, "Solid-rotor material selection for squirrel-cage high-speed solid-rotor induction machine," in 2019 45th Annual Conference of the IEEE Industrial Electronics Society (IECON), Vol. 1, 2019, pp. 1357–1361. doi: 10.1109/IECON.2019.8926736.
- [71] E. Kurvinen, C. Di, I. Petrov, and J. Nerg, "Design and Manufacturing of Modular Multi-MW High-Speed SRIMs," 2021.
- [72] P. Dorji and B. Subba, "D-Q Mathematical Modelling and Simulation of Three-Phase Induction Motor for Electrical Fault Analysis," *IARJSET*, vol. 7, no. 9, pp. 38–46, Sep. 2020, doi: 10.17148/iarjset.2020.7909.
- [73] V. Bílek and others, "Comprehensive Review of High-Speed Solid-Rotor

- Induction Machines," 2025.
- [74] J. Pyrhönen, J. Nerg, A. Mikkola, J. Sopanen, and T. Aho, "Electromagnetic and Mechanical Design Aspects of MW-Class SRIMs," 2009.
- [75] V. Räisänen and others, "Rapid Computation of Harmonic Eddy-Current Losses in High-Speed SRIMs," 2013.
- [76] M. Marković and Y. Perriard, "Analytical Model for Torque and Power in Solid-Rotor Induction Motors," 2011.
- [77] B. Silwal, "Computation of Eddy Currents in Solid-Rotor Induction Machines with 2D and 3D FEM," Aalto University, 2012.
- [78] V. Räisänen, S. Suuriniemi, S. Kurz, and L. Kettunen, "Rapid computation of harmonic eddy-current losses in high-speed solid-rotor induction machines," *IEEE Trans. Energy Convers.*, vol. 28, no. 3, pp. 782–790, 2013, doi: 10.1109/TEC.2013.2268278.
- [79] J. Staszak, "Solid-rotor induction motor modeling based on circuit model utilizing fractional-order derivatives," *Energies*, vol. 15, no. 17, 2022, doi: 10.3390/en15176371.
- [80] M. Mirzaei, M. Mirsalim, and S. E. Abdollahi, "Analytical modeling of axial air gap solid rotor induction machines using a quasi-three-dimensional method," *IEEE Trans. Magn.*, vol. 43, no. 7, pp. 3237–3242, 2007, doi: 10.1109/TMAG.2007.894215.
- [81] K. Boughrara, F. Dubas, and R. Ibtiouen, "2-D analytical prediction of eddy currents, circuit model parameters, and steady-state performances in solid rotor induction motors," *IEEE Trans. Magn.*, vol. 50, no. 12, Dec. 2014, doi: 10.1109/TMAG.2014.2342666.
- [82] A. M. Ali Saleh Ahmed Th Radhi, "EFFECT OF HARMONICS ON A SOLID-ROTOR INDUCTION MOTOR," 2006.
- [83] L. Papini and C. Gerada, "Analytical-numerical modelling of solid rotor induction machine," in *Electrimacs*, 2014, pp. 121–126.
- [84] A. Stermecki, O. Bíró, I. Bakhsh, S. Rainer, G. Ofner, and R. Ingruber, "3-

- D finite element analysis of additional eddy current losses in induction motors," *IEEE Trans. Magn.*, vol. 48, no. 2, pp. 959–962, 2012, doi: 10.1109/TMAG.2011.2173919.
- [85] T. Aho, J. N. Nerg, and J. Pyrhonen, "The effect of the number of rotor slits on the performance characteristics of medium-speed solid rotor induction motor," in 2006 3rd IET International Conference on Power Electronics, Machines and Drives PEMD 2006, 2006, pp. 515–519.
- [86] J. L. and F. F., "Calculation of magnetic fields and rotor parameters for induction motors with slitted solid rotor," 1987.
- [87] M. O. Gulbahce, D. T. Mcguiness, and D. A. Kocabas, "Shielded axially slitted solid rotor design for high-speed solid rotor induction motors," *IET Electr. Power Appl.*, vol. 12, no. 9, pp. 1371–1377, Nov. 2018, doi: 10.1049/iet-epa.2018.5210.
- [88] Y. Gessese and A. Binder, "Axially slitted, high-speed solid-rotor induction motor technology with copper end-rings," in *2009 International Conference on Electrical Machines and Systems (ICEMS)*, 2009, pp. 1–6. doi: 10.1109/ICEMS.2009.5382761.
- [89] R. Abebe, M. Di Nardo, D. Gerada, G. Lo Calzo, L. Papini, and C. Gerada, "High speed drives review: Machines, converters and applications," in *IECON 2016 42nd Annual Conference of the IEEE Industrial Electronics Society*, 2016, pp. 1675–1679. doi: 10.1109/IECON.2016.7793721.
- [90] M. J. Nam, J. H. Kim, K. Y. Cho, H. W. Kim, and Y. Cho, "Torque ripple reduction of an interior PM synchronous motor by compensating harmonic currents based on flux linkage harmonics," *J. Power Electron.*, vol. 17, no. 5, pp. 1223–1230, Sep. 2017, doi: 10.6113/JPE.2017.17.5.1223.
- [91] R. Leuzzi *et al.*, "High-speed machines: Typologies, standards, and operation under PWM supply," in *2018 AEIT International Annual Conference*, 2018, pp. 1–6. doi: 10.23919/AEIT.2018.8577297.
- [92] S. Li, Y. Li, W. Choi, and B. Sarlioglu, "High-speed electric machines: Challenges and design considerations," *IEEE Trans. Transp. Electrif.*, vol.

- 2, no. 1, pp. 2–13, 2016, doi: 10.1109/TTE.2016.2523879.
- [93] J. Shen, X. Qin, and Y. Wang, "High-speed permanent magnet electrical machines—applications, key issues and challenges," *CES Trans. Electr. Mach. Syst.*, vol. 2, no. 1, pp. 23–33, 2018, doi: 10.23919/TEMS.2018.8326449.
- [94] Z. Kolondzovski, A. Arkkio, J. Larjola, and P. Sallinen, "Power limits of high-speed permanent-magnet electrical machines for compressor applications," *IEEE Trans. Energy Convers.*, vol. 26, no. 1, pp. 73–82, 2011, doi: 10.1109/TEC.2010.2089459.
- [95] T. Aho, V. Sihvo, J. Nerg, and J. Pyrhönen, "Rotor materials for medium-speed solid-rotor induction motors," in *Proceedings of IEEE International Electric Machines and Drives Conference, IEMDC 2007*, 2007, pp. 525–530. doi: 10.1109/IEMDC.2007.382722.
- [96] J. J. Pyrhönen, J. K. Nerg, T. Aho, and P. T. Kurronen, "Solid rotor end effects Analytic and experimental results for high-power high-speed machines," *Ieee Eurocon 2009, Eurocon 2009*, no. June, pp. 688–695, 2009, doi: 10.1109/EURCON.2009.5167708.
- [97] T. Aho, J. Nerg, and J. Pyrhönen, "Optimizing the Axial Length of the Slitted Solid Iron Rotor."
- [98] J. Pyrhonen and T. Jokinen, *Design of Rotating Electrical Machines*. John Wiley & Sons, 2009.
- [99] N. Uzhegov, "High-Speed Solid-Rotor induction machine Calculation program," *LAPPEENRANTA Univ. Technol.*, 2010.
- [100] R. Prozorov and V. G. Kogan, "London penetration depth in iron-based superconductors," Dec. 2011. doi: 10.1088/0034-4885/74/12/124505.
- [101] X. Ma *et al.*, "Review of high speed electrical machines in gas turbine electrical power generation," in 2015 IEEE Region 10 Conference (TENCON), 2015, pp. 1–9. doi: 10.1109/TENCON.2015.7372765.
- [102] M. Rahman, A. Chiba, and T. Fukao, "Super high speed electrical machines—summary," in 2004 IEEE Power Engineering Society General

- Meeting, Vol. 2, 2004, pp. 1272–1275. doi: 10.1109/PES.2004.1373062.
- [103] C. Concordia and H. Poritsky, "Synchronous Machine With Solid Cylindrical Rotor."
- [104] M. S. Ummah, "No 主観的健康感を中心とした在宅高齢者における健康関連指標に関する共分散構造分析Title," *Sustain.*, vol. 11, no. 1, pp. 1–14, 2019, [Online]. Available: http://scioteca.caf.com/bitstream/handle/123456789/1091/RED2017-Eng-8ene.pdf?sequence=12&isAllowed=y%0Ahttp://dx.doi.org/10.1016/j.regsciurbeco.2008.06.005%0Ahttps://www.researchgate.net/publication/305320484\_SISTEM\_PEMBETUNGAN\_TERPUSAT\_STRATEGI\_MELESTAR
- [105] J. Staszak, "Solid-Rotor Induction Motor Modeling Based on Circuit Model Utilizing Fractional-Order Derivatives," *Energies*, vol. 15, no. 17, Sep. 2022, doi: 10.3390/en15176371.
- [106] D. Gerling and G. Dajaku, "Comparison of different calculation methods for the induction motor with multilayer rotor structure," in *Proc. Int. Conf. Electrical Machines*, in Citeseer. 2004, pp. 4–8.
- [107] M. Markovic and Y. Perriard, "An analytical solution for the torque and power of a solid-rotor induction motor," in *2011 IEEE International Electric Machines* \& *Drives Conference (IEMDC)*, 2011, pp. 1053–1057. doi: 10.1109/IEMDC.2011.5994746.
- [108] V. Raisanen, S. Suuriniemi, S. Kurz, and L. Kettunen, "Rapid computation of harmonic eddy-current losses in high-speed solid-rotor induction machines," *IEEE Trans. Energy Convers.*, vol. 28, no. 3, pp. 782–790, 2013, doi: 10.1109/TEC.2013.2268278.
- [109] M. Shah and S. B. Lee, "Rapid analytical optimization of eddy-current shield thickness for associated loss minimization in electrical machines," *IEEE Trans. Ind. Appl.*, vol. 42, no. 3, pp. 642–649, 2006, doi: 10.1109/TIA.2006.873671.
- [110] M. Mirzaei, M. Mirsalim, and S. E. Abdollahi, "Analytical modeling of

- axial air gap solid rotor induction machines using a quasi-three-dimensional method," *IEEE Trans. Magn.*, vol. 43, no. 7, pp. 3237–3242, Jul. 2007, doi: 10.1109/TMAG.2007.894215.
- [111] Q. Wei, F. Yu, Z. Xi, and L. Shuo, "Analysis on electromagnetic field of an axial-flux solid aluminum rotor induction motor," in *2011 International Conference on Electrical Machines and Systems (ICEMS)*, 2011, pp. 1–4. doi: 10.1109/ICEMS.2011.6073521.
- [112] J. Klíma and O. Vítek, "Analysis of high-speed induction motor," in *Proceedings of the 16th International Conference on Mechatronics Mechatronika 2014*, 2014, pp. 85–91. doi: 10.1109/MECHATRONIKA.2014.7018240.
- [113] J. F. Gieras, "Solid-rotor induction motors," in *Handbook of Electric Motors*, 2nd ed., G. Kliman and H. Tolyiat, Eds., New York: Marcel Dekker, 2004, ch. 2.5.7, 4.6.
- [114] "wood1960 part3".
- [115] J. H. Hagenguth, A. F. Rohlfs, W. J. Degoan AIEE Traxsactions, H. S. Flegel, J. G. Anderson AIEE, and G. Angst Member Aiee, "References 1, SIXTY-CYCLE AND IMPULSE SPARKOVBR OF LARGE GAP SPACINGS FLASEOVER STRENOTH OP EXTRA-HIOH-VOLTAGE LINE AND STATON INSULATION Polyphase Induction Motor with Solid Rotor; EAects of Saturation and Finite Length AIEE Technical Operations Department for presentation at the AIEI Fall General Meeting, Angst-Polyphase Induction Motor with Solid Rotor FE,BRUARY 1962 902," W. Wanger, W. Huber, 1952.
- [116]

  "[Paul\_C.\_Krause,\_Oleg\_Wasynczuk,\_Scott\_D.\_Sudhoff](Bookos.org).p

  df."
- [117] P. C. Krause and C. H. Thomas, "Simulation of Symmetrical Induction Machinery," *IEEE Trans. Power Appar. Syst.*, vol. 84, no. 11, pp. 1038–1053, 1965, doi: 10.1109/TPAS.1965.4766135.

- [118] "MATHEMATICAL MODELING OF INDUCTION MOTORS."
- [119] M. Matthews Malatji, "Derivation and implementation of a DQ model of an induction machine using MATLAB/SIMULINK\*."
- [120] "POWER SYSTEM STABILITY Volume III Synchronous ~achines."
- [121] V. Sousa, P. R. Viego, J. R. Gomez, E. C. Quispe, and M. Balbis, "Estimating induction motor efficiency under no-controlled conditions in the presences of unbalanced and harmonics voltages," *CHILECON 2015 2015 IEEE Chil. Conf. Electr. Electron. Eng. Inf. Commun. Technol. Proc. IEEE Chilecon 2015*, pp. 567–572, 2016, doi: 10.1109/Chilecon.2015.7400434.
- [122] "An Analysis of Solid Rotor Machines Part I1. The Egects of Curvature."
- [123] M. Sameeullah, J. Kumar, K. Lal, and J. Chander, "Energy audit: A case study of hostel building," *Int. J. Res. Manag. Sci.* \& *Technol.*, vol. 2, no. 2, 2014.
- [124] R. A. Al Hasibi, S. Suripto, R. O. Wiyagi, C. D. Sukardi, Y. Jusman, and T. I. Prasetyo, "Harmonic Analysis of 3-Phase Induction Motor at PT. Indocement Tunggal Prakarsa," *J. Electr. Technol. UMY*, vol. 3, no. 4, pp. 135–144, 2019.
- [125] J. Pyrhönen, J. Nerg, A. Mikkola, J. Sopanen, and T. Aho, "Electromagnetic and mechanical design aspects of a high-speed solid-rotor induction machine with no separate copper electric circuit in the megawatt range," *Electr. Eng.*, vol. 91, no. 1, pp. 35–49, 2009, doi: 10.1007/s00202-009-0114-1.
- [126] J. Lu, J. Yang, S. Y. Liang, and R. Ren, "Compensation for Harmonic Flux and Current of Permanent Magnet Synchronous Motor by Injected Harmonic Voltage," 2015.
- [127] W. Wang, C. Liu, S. Liu, Z. Song, H. Zhao, and B. Dai, "Current Harmonic Suppression for Permanent-Magnet Synchronous Motor Based on Chebyshev Filter and PI Controller," *IEEE Trans. Magn.*, vol. 57, no. 2, 2021, doi: 10.1109/TMAG.2020.3017671.

# APPENDIX 1

Table.4.1 Motor Parameters.

No. of pole pairs, p	1
No. of phases, m	3
No. of stator slots, Q <sub>S</sub>	24
No. of turns in series per phase of stator winding, N	14
Winding factor, $k_{\rm w}$ .	0.9577
Air gap, g/mm	0.75
Rotor diameter D/mm	98.5
Rotor length*/mm	100
Rated voltage U <sub>s</sub> /V	225/130
Rated current, I/A	65
Stator resistance, $R/m\Omega$ at 20C at 400 Hz	26
Srator leakage inductance, $L_{s\sigma}/\mu H$	68.4

#### **Publication**

A scientific paper from this research was accepted in the The scientific journal *Mari Papel y Corrugado* which is included in the Scopus database.

Dear Dr./Mr. Abdullah Maya Fazaa; Ahmed Thamer Radhi,

We have reached a decision regarding your submission to the "Mari Papel y Corrugado". The title of your submission is:

" Modeling and Simulation of High-Speed Solid Rotor Induction Motor with Harmonics."

Manuscript ID: MARI-2025-94093

Our decision is: Accept Submission

Congratulations! Your submission has met the requirements outlined in the checking list and the author guide for the journal.

We appreciate your effort and contribution to the journal, and we look forward to publishing your work. Should you have any further edits or inquiries regarding the publication process, please feel free to reach out.

Best regards,

Editor-in-Chief

Prof. João Paulo Davim

Publication Office

Mari Papel y Corrugado

https://maripapel.com/

#### الخلاصة

تقدم هذه الأطروحة دراسة شاملة حول النمذجة الرياضية لمحركات الحث عالية السرعة ذات الدوار الصلب، مع تطبيق تحليل المجال الكهرومغناطيسي ثلاثي الأبعاد تقريبًا. تُستخدم محركات الحث عالية السرعة بشكل متزايد في مختلف التطبيقات الصناعية نظرًا لكثافة قدرتها وكفاءتها العالية. ومع ذلك، لا يزال التنبؤ الدقيق بأدائها في ظل ظروف تشغيل مختلفة يمثل تحديًا كبيرًا بسبب التفاعلات المعقدة بين المجالات الكهرومغناطيسية وديناميكيات الدوار عند السرعات العالية

يبدأ البحث بتطوير نموذج رياضي مفصل يمثل مجالًا كهرومغناطيسيًا ثلاثي الأبعاد مبسطًا داخل المحرك ثم يتم استخراج معاوقة الدوار

. ثم تمتد الدراسة إلى نموذج $\mathrm{DQ}$  ، حيث تُستخدم المعادلات المشتقة لتبسيط السلوك الديناميكي للمحرك.

علاوة على ذلك، توضح الأطروحة تطبيق النموذج المتطور في برنامج MATLAB، مما يتيح محاكاة وتحليل المحرك في ظل ظروف تشغيل مختلفه

وأخيرًا، تتم محاكاة نمذجة دائرة التوافقيات في MATLAB باستخدام العاكس لتوليد شكل موجة تيار متردد بخمسة مستويات من مصدر تيار مستمر، وإظهار تأثيره. تُقدم النتائج رؤى قيمة في تحسين تصميم محركات الحث عالية السرعة، مما يُسهم في تحسين الأداء والموثوقية.

# جمهورية العراق وزارة التعليم العالي والبحث العلمي جامعة ميسان كلية الهندسة

النموذج الرياضي للمحرك الحثي ذو السرعة العالية نوع الدوار الصلب بالاعتماد على تحليل المجال المغناطيسي ثلاثي الابعاد

رسالة مقدمة الى مجلس كلية الهندسة في جامعة ميسان كجزء من متطلبات الحصول على شهادة الكهربائية

اعداد عبدالله مایع فزاع بكالوریوس هندسة كهربائیة

بأشراف الأستاذ المساعد الدكتور احمد ثامر راضى